Application of Multivalent Interactions for Recognition Imaging and Delivery of Therapeutics

by

Saikat Manna

A Dissertation Presented in Partial Fulfillment
of the Requirements for the Degree
Doctor of Philosophy

Approved June 2016 by the
Graduate Supervisory Committee:

Stuart Lindsay, Co-Chair
Peiming Zhang, Co-Chair
Ian Gould
Nicholas Stephanopoulos

ARIZONA STATE UNIVERSITY

August 2016

ABSTRACT

Multivalency is an important phenomenon that guides numerous biological interactions. It has been utilized in design of therapeutics and drug candidates. Hence, this study attempts to develop analytical tools to study multivalent interactions and design multivalent ligands for drug delivery and therapeutic applications.

Atomic Force Microscopy (AFM) has been envisioned as a means of nanodiagnostics due to its single molecule sensitivity. However, the AFM based recognition imaging lacks a multiplex capacity to detect multiple analytes in a single test. Also there is no user friendly wet chemistry to functionalize AFM tips. Hence, an uncatalyzed Click Chemistry protocol was developed to functionalize AFM tips. For multiplexed recognition imaging, recognition heads based on a C3 symmetrical three arm linker with azide functionalities at its ends were synthesized and the chemistry to attach them to AFM tips was developed, and these recognition heads were used in detecting multiple proteins simultaneously using AFM.

A bis-Angiopeptide-2 conjugate with this three-arm linker was synthesized and this was conjugated with anti-West Nile virus antibody E16 site specifically to target advanced West Nile virus infection in the Central Nervous System. The bis-Angiopeptide-2 conjugate of the antibody shows higher efficacy compared to a linear linker-Angiopeptide-2 conjugate of the antibody in in vitro studies and currently the efficacy of this antibody conjugate in studied in mice. Surface Plasmon Resonance imaging (SPRi) results indicate that the conjugation does not affect the antigen binding activity of the antibody very significantly.

A Y-shaped bisbiotin ligand was also prepared as a small sized antibody mimic. Compared to a monovalent biotin ligand, the y-Bisbiotin can cooperatively form a significantly more stable complex with streptavidin through intramolecular bivalent interactions, which were demonstrated by gel electrophoresis, SPR and AFM. Continuing on these lines, a four-arm linker was synthesized containing three single chain variable fragments (scFv) linked to the scaffold to form a tripod base, which would allow them to concomitantly interact with a trimeric Glycoprotein (GP) spike that has a “chalice” configuration. Meanwhile, a human IgG1 Fc is to be installed on the top of the tetrahedron, exerting effector functions of a monoclonal antibody.

ACKNOWLEDGMENTS

First and foremost I would like to express my deepest gratitude to my advisors Dr. Stuart Lindsay and Dr. Peiming Zhang for giving me the opportunity to work under their supervision. They have been outstanding mentors throughout the period of my graduate studies. Their expertise, understanding, generous guidance and support made it possible for me to work on research topics that were very interesting to me. I would also like to thank them for giving me the opportunity to work in synthetic chemistry as well as protein bioconjugation apart from using analytical tools like AFM and SPR. I am hopeful that the kind of expertise I have gained in this lab will help me further in my career. No words of gratitude is sufficient for Professor Ian Gould for his constant support from the very first day when I came here. I would also like to thank Dr. Nicholas Stephanopoulos for his helpful suggestions and supervision.

I would also like to extend my gratitude to Dr. Qiang Chen and Dr. Huafang Lai for collaborating with me on my projects. I would also like to thank Dr. Subhadip Senapati for mentoring me and teaching me how to use the AFM. I am also extremely grateful to Ian Shoemaker for assistance with SPRi experiments. I would also like to thank Brian Cherry for teaching me how use the NMR and Natalya Zolotova for HRMS sample analysis. I would like to thank my coworkers Dr. Sudipta Biswas, Dr. Sovan Biswas, Dr. Suman Sen, Dr. Jong-one Im, Dr. Yanan Zhao, Dr. Pei Pang and Dr. Brian Ashcroft for their helpful suggestions. It was fun working with you guys. I would like to express my sincerest gratitude to Margaret Black and Mike Dodson for their constant support over the years.

I would like to thank my parents, my brother and my friends in USA and in India for their constant support and assistance. Last but not the least, I would like to thank my beautiful girlfriend, Sampa Maiti for everything. Your love and support has been the greatest inspiration.

TABLE OF CONTENTS

Page

CHAPTER Page

CHAPTER Page

LIST OF TABLES

LIST OF FIGURES

Figure Page

Figure Page

LIST OF SCHEMES

Scheme Page

LIST OF ABBREVIATIONS

ADIBO	Aza-dibenzocycloctyne
AFM	Atomic Force Microscopy
ANGII	Angiopeptide-2
APS	1-(3-aminopropyl)silatrane
APTES	(3-aminopropyl)triethoxysilane
ARMs	Antibody –recruiting small molecules
BBB	Blood-Brain Barrier
BCN	(1R, 8S, 9R)-bicyclo[6.1.0]non-4-yn-9-ylmethanol
br	broad
CNS	Central Nervous System
δ	Chemical shift (ppm)
d	doublet
dd	doublet of doublet
DCM	Dichloromethane
DFT	Density Functional Theory
DMF	Dimethylformamide
DMSO	Dimethyl sulfoxide
DNA	Deoxyribonucleic Acid
EBOV	Ebola Virus
EDC	1-ethyl-3-(3-dimethylaminopropyl)carbodiimide
ELISA	Enzyme-linked Immunosorbent Assay

ELSD	Evaporative Light Scattering Detector
Fab	Fragment antigen-binding
Fc	Fragment crystallizable
FTIR	Fourier transform Infrared spectroscopy
GP	Glycoprotein
HIV	Human Immuno Deficiency Virus
HPLC	High Performance Liquid Chromatography
Hz	Hertz
ICA	4(5)-(2-mercaptoethyl)-H-imidazole-2-carboxamide
IgG	Immunoglobin G
kD	kilodaltons
LOD	Limit of detection
LRP	Lipoprotein receptor-related protein
m	multiplet
Mab	Monoclonal antibody
MALDI-MS	Matrix Assisted Laser Desorption/Ionization Mass Spectrometry
MALDI-TOF	Matrix Assisted Laser Desorption/Ionization-Time of Flight
mg	milligram
mL	milliliters
mM	millimolar
mmol	millimoles
mRI	Multiplex Recognition Imaging

mV	millivolts
m/z	mass to charge ratio
NFκβ	Nuclear factor Kappa-light-chain-enhancer of activated B cells
ng	nanograms
NHS	N-hydroxysuccinimide
nm	nanometer
nM	nanomlar
nN	nanonewton
N/m	Newtons per meter
NMR	Nuclear Magnetic Resonance
OEG	Oligo(ethyleneglycol)
PBS	Phosphate buffered saline
PDB	Protein Data Bank
PEG	Polyethylene glycol
pI	Isoelectric point
pN	piconewton
RI	Recognition Imaging
RNA	Ribonucleic Acid
ROI	region of interest
RP-HPLC	Reverse phase-High performance liquid chromatography
RT	Recognition Tunneling
RU	Response unit

s	singlet
ScFv	Single chain variable fragment
SEC	Size Exclusion Chromatography
SPRi	Surface Plasmon Resonance Imaging
STM	Scanning Tunneling Microscope
SyAm-Ps	Synthetic antibody mimics targeting prostrate cancer
t	triplet
TBA	Thombin binding aptamer
TCEP	Tris(2-carboxyethyl)phosphine
TCO	(E)-cyclooct-4-enol
TEAA	Triethylamino acetate
TFA	Trifluoroacetic acid
THF	Tetrahydrofuran
THPTA	tris(3-hydroxypropyltriazolylmethyl)amine
TLC	Thin layer chromatography
TLR	Toll-like receptor
TNF	Tumor Necrosis Factor
TREC	Simultaneous Topography and Recognition Imaging
μg	micrograms
μL	microliters
μM	micromole
UV	Ultra-violet

VEGF	Vascular endothelial growth factor
WLC	Worm Like Chain
WNV	West Nile Virus

CHAPTER 1

INTRODUCTION

1.1 Multivalent Biomolecular Interactions

Valency of a biological entity is defined as the number of structural units of the same or similar type that are connected to the entity.[1] The maximum valency of the biological entity that is threotically possible based on the number of ligands attached to the multivalent construct is known as structural valency while the valency employed during multivalent association is known as functional valency.

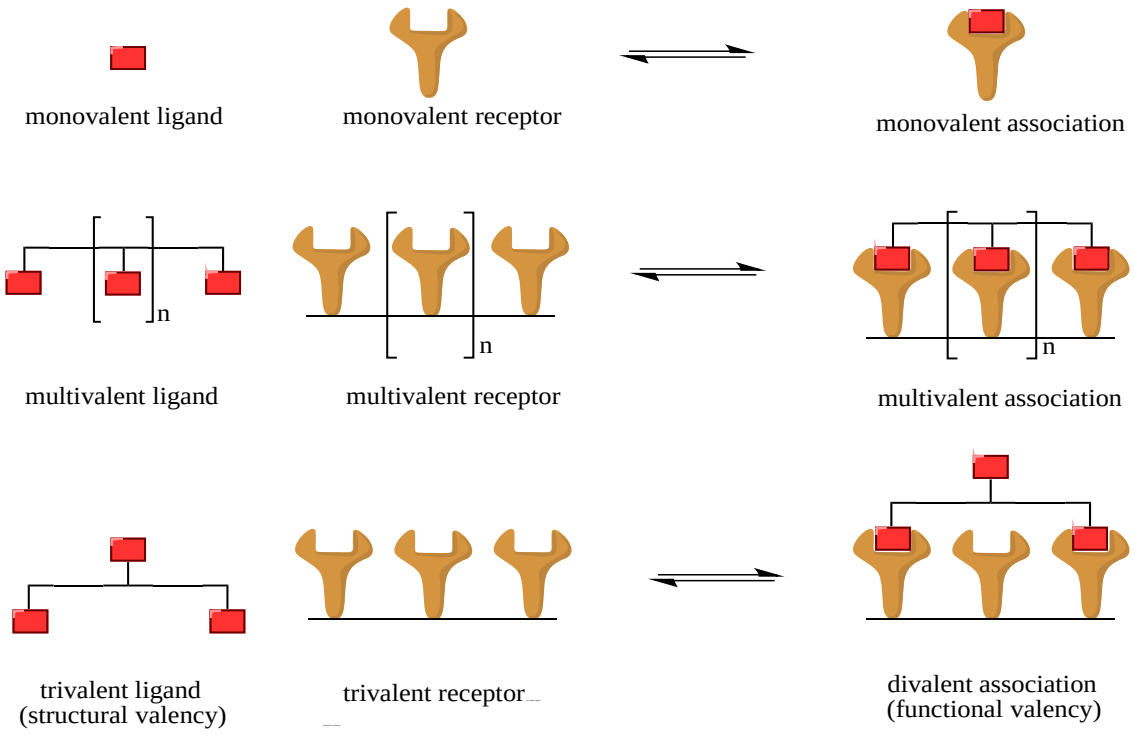

Figure 1. Structural and Functional valency. Adapted from reference (1) copyright 2000 John Wiley & Sons

Various biological ligands are known to display polyvalency as the unique collective property due to multiple simultaneous interactions is different from properties displayed by individual constituents.[2] There are various modes of multivalent binding such as statistical rebinding, chelation, clustering or subsite binding.[3]

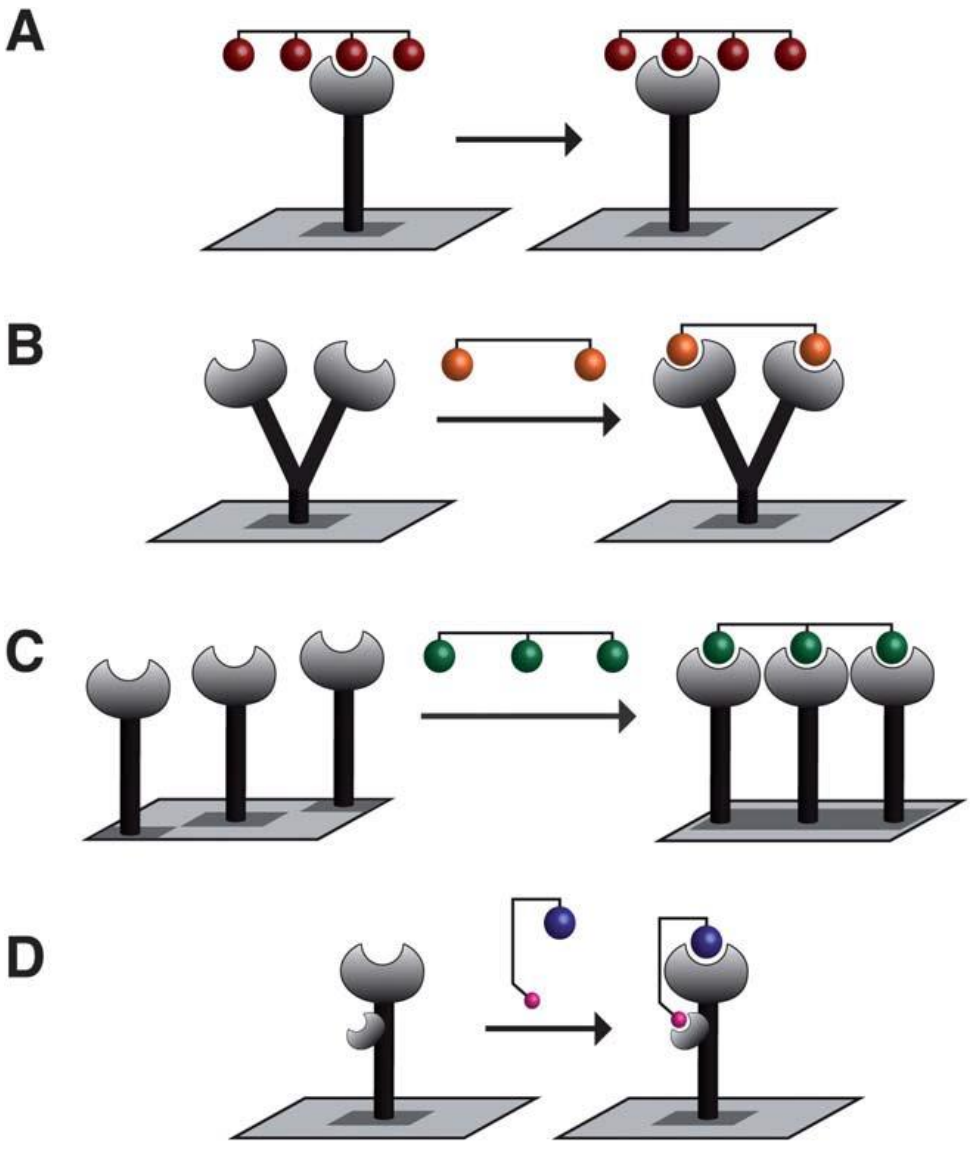

Figure 2. A. Statistical rebinding B. Chelation C. Clustering D. Subsite binding. Reproduced with permission from reference (3) copyright 2013 Royal Society of Chemistry

Multisite binding prevents dissociation due to transient unbinding events and hence serves to increase affinity.[3] There are various examples of application of multivalent interactions in natural biological ligands.

The influenza virus hemagglutinin binds trivalently to sialic acid on cell surfaces. The multivalent interaction involves tight binding while the monovalent interaction in weak.[1,2] This has been employed in designing multivalent sialic acid inhibitors to target influenza viruses.[4,5,6] Polymeric Vancomycin have been found to interact with multiple copies of D-Ala-D-Ala, a cell wall precursor present in the gram-positive bacteria more strongly compared to the monovalent ligand are known to exhibit more potent anti-bacterial properties.[7] Mannose binding plant lectins like Concanavalin A are known to assemble into higher order aggregates depending on the pH.[8, 9] A drug molecule has higher affinity and residence time to its target due to multivalent interaction.[10]

Hence, multivalency is an important phenomenon that guides most biological interactions.

1.2 Synthetic Multivalent Bio-molecules

Multivalency has been utilized in design of therapeutics and drug candidates. For instance, thermodynamically, if two ligands of a bivalent molecule are unstrained and independent, the change of enthalpy in the bivalent association (ΔH^{bi}) is two times as

much as that in the monovalent binding (ΔH^{mono}).[11] On the other hand, the structure should also have a minimal entropy loss when it binds to achieve the best outcome. In general, the entropy can be expressed as below:[12]

$$T\Delta S^{Bi} \approx T\Delta S^{mono}_{trans}(translational) + T\Delta S^{mono}_{Rot}(rotational) + T\Delta S^{Bi}_{Conf}(conformational, linker)$$

where ΔS^{Bi}_{Conf} takes into account all unfavorable entropic terms as a result of rotatable bonds becoming frozen when the bivalent ligand binds to its receptor. To achieve a highly positive cooperativity, the absolute value of ΔS^{Bi}_{Conf} should remain as small as possible. Also, it should be noted that a small difference in entropy results in a large change in the entropic term $T\Delta$S, creating significant impact on the binding energy; however, some of the entropy cost can be paid in advance by preorganization.[13] Hence, study of multivalent interactions and design of multivalent scaffolds and linkers is of utmost importance.

High affinity (avidity) in antibodies arise due to bivalent crosslinking by the two Fabs. Most anti-HIV-1 antibodies are known to bind monovalently due to low density of glycoprotein spikes present in the virus and hence have low potency.[14] However, two hetero Fabs connected together by a DNA linker can bind by intraspike cross-linking and are shown to have 2.5 fold increase in potency compared to its monovalently bound counterpart.[14]

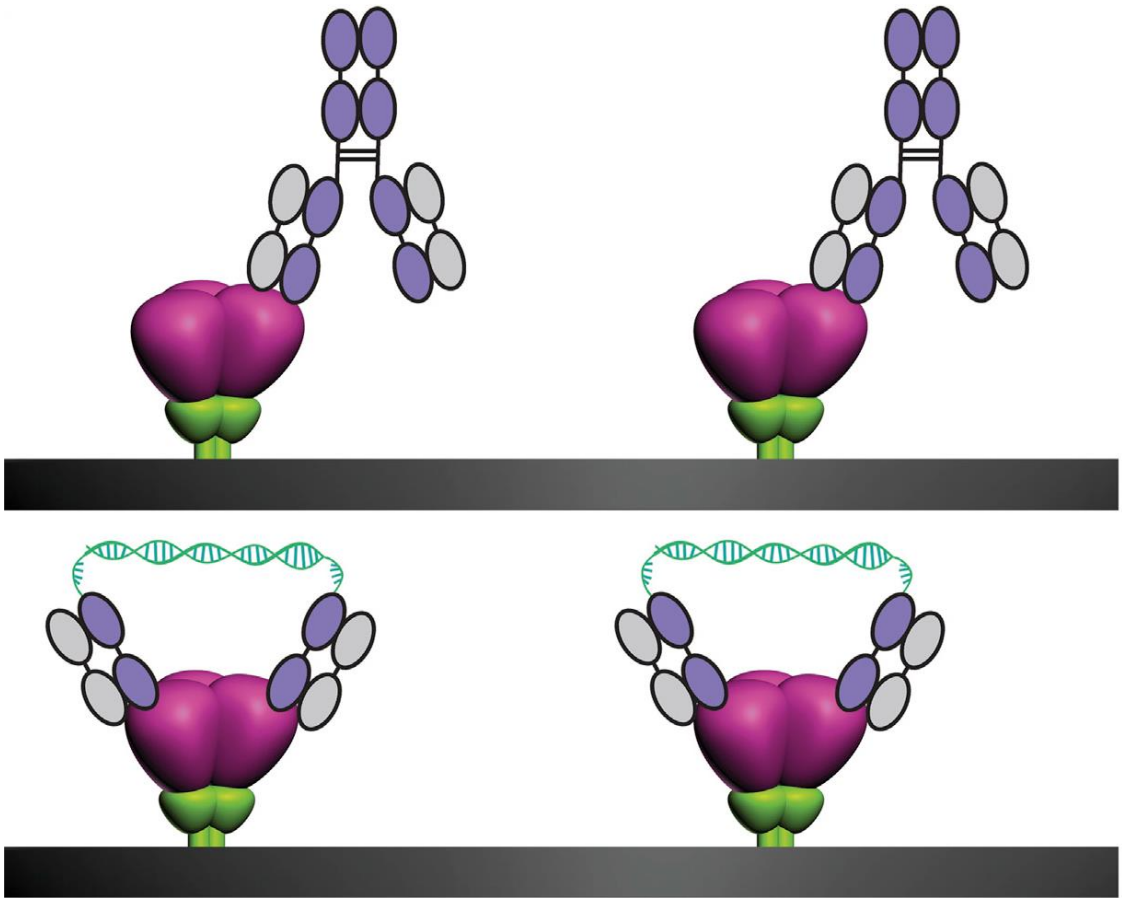

Figure 3. Intraspike cross-linking in di-Fabs. Reproduced with permission from reference (11) copyright 2015 Elsevier.

Bispecific CovX-Bodies generated by site-specifically attaching pharmacophore peptide heterodimers to a scaffold antibody shows high efficacy and is known to have long half-life.[15]

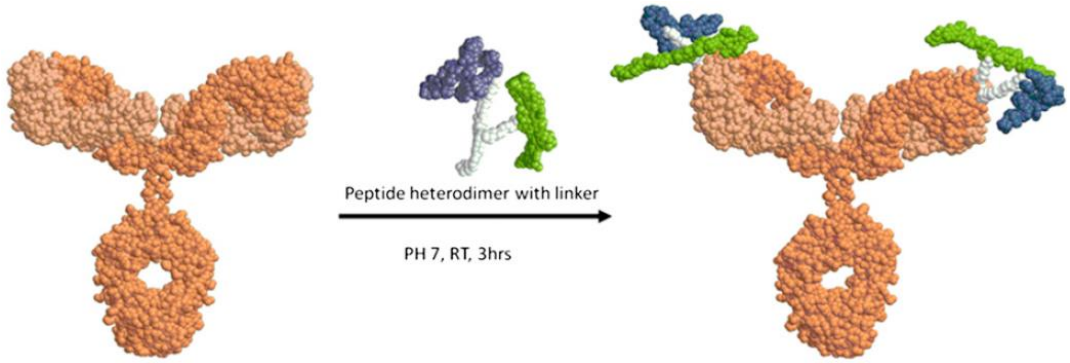

Figure 4. Bispecific CovX-body. Reproduced with permission from reference (12) copyright 2010 National Academy of Sciences, USA.

Esser-Kahn and coworkers designed combinations of di and tri-agonists of Toll-like receptors (TLR) and the linked agonists showed increased activation of transcription factor NFκβ and enhanced and directed immune related cytokine production and gene expression beyond cells treated with an unconjugated mixture of agonists.[16]

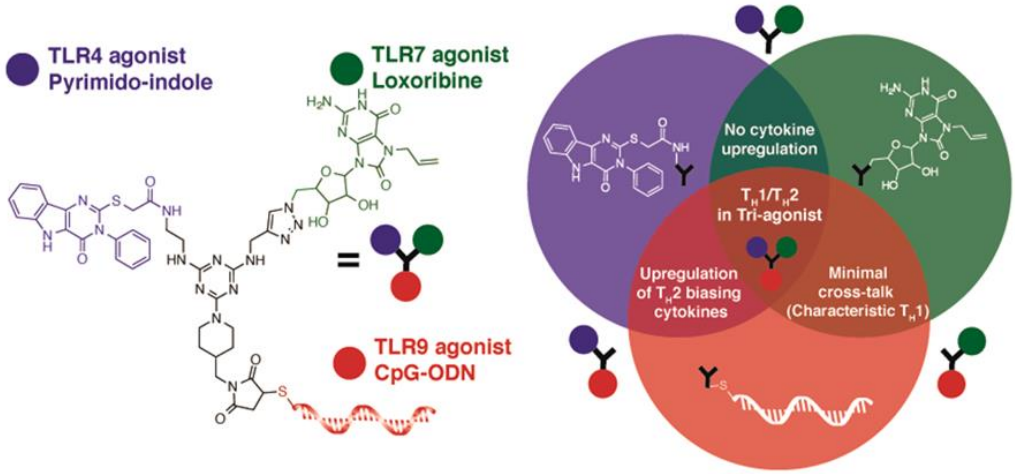

Figure 5. TLR Triagonist. Adapted from reference (13)

Antibody-recruiting small molecules (ARMs) containing Target-binding terminus and Antibody-binding terminus have been shown to enhance binding between antibodies and disease-related pathogens thus facilitating immune-mediated clearance.[17]

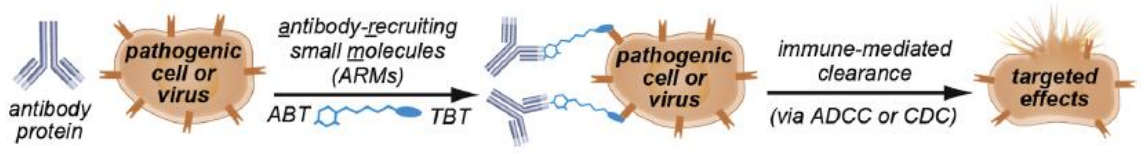

Figure 6. Antibody-recruiting small molecules (ARMs). Reproduced with permission from reference (14) copyright 2012 American Chemical Society.

Synthetic antibody molecules of intermediate size have been shown to simultaneously bind to target specific prostrate antigen and F_c gamma receptor I thus eliciting highly selective cancer cell phagocytosis.[18]

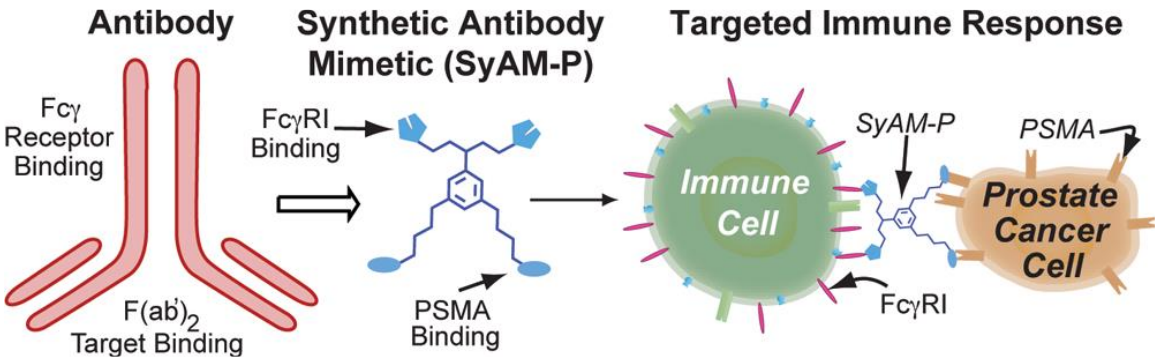

Figure 7. Synthetic antibody mimics targeting prostrate cancer (SyAM-Ps). Adapted from reference (15)

Thus synthetic multivalent biomolecules has been employed with increased efficacy for targeted delivery. The design of multivalent synthetic reagents that can illicit enhanced immune response or can deliver biologics site-specifically is emerging as an important field of study.

1.3 Delivery of Therapeutics to the Central Nervous System

All animals with a complex nervous system require a Blood-Brain Barrier (BBB). [19] Structurally the BBB is formed by endothelial cells having tight junctions known as Zona Occludens. They form the capillary of the brain and spinal cord. Because the main role of the BBB is to protect neurons from circulations cytotoxic agents, the endothelial cells along with specialized brain cells such as Astrocytes and Pericytes practically restrict any free diffusion of solutes across the BBB.[19, 20]

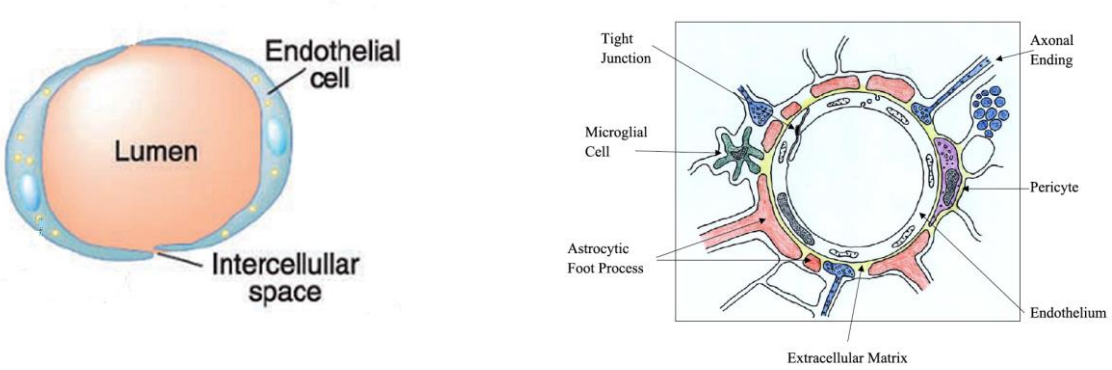

Capillary (in General) Blood-Brain Barrier (BBB)

Figure 8. A normal capillary and the Blood-Brain Barrier. Reproduced with permission from reference (16) copyright 2004 Elsevier. Adapted from reference (17)

In absence of free diffusion there are a few potential routes for transport of solutes across the BBB.

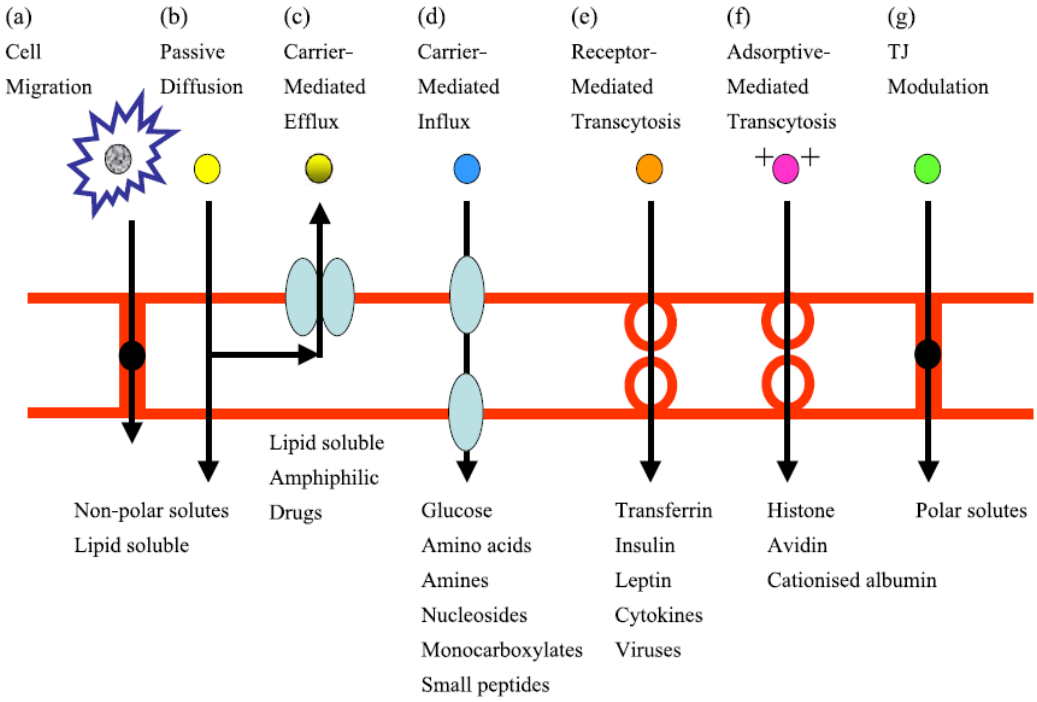

Figure 9. Potential routes for transport across the BBB. Reproduced with permission from reference (16) copyright 2004 Elsevier.

Leucocytes may cross the BBB by modifying tight junctions. While solutes may passively diffuse based on their lipid solubility, there are some active efflux carriers that intercept some of these passively penetrating solutes and transport them out of the endothelial cell. Polar substrates like glucose, amino acids and nucleosides may get transported by carrier-mediated influx. Most macromolecules are transported through receptor mediated transcytosis while negatively charged macromolecules may also be transported by Absorptive-Mediated Transcytosis. Some polar solutes may get transported by Tight junction modulation resulting in relaxation of the junctions. [19]

To transport therapeutics to the brain different strategies are employed: [21]

(i) Invasive or transcranial delivery,

(ii) Increasing Lipid solubility of the drug,

(iii) Reformulation of the drug to access endogenous BBB transporters.

While carrier mediated transporters have been successfully utilized to transport small molecule drugs conjugated with various essential analytes like glucose, amino acids, hexoses and vitamins that have carrier mediated transport systems embedded within the BBB, the most popular way to transport macromolecular drugs to the brain is by receptor mediated transcytosis by taking advantage of peptide specific receptor transporters located on the capillary endothelium.[21, 22] This has given rise to the Molecular Trojan Horse technology for delivery of therapeutics. A macromolecular drug or a non-viral plasmid DNA or a monoclonal antibody is attached to a vector that can access a specific catalyzed transport machinery leading to the transport of the drug across the BBB.[21-24] A radio-labelled recombinant lysosomal enzyme iduronate-2-sulfatase fused with a radiolabeled monoclonal antibody against human insulin receptor shows the penetration of the conjugate to all parts of the brain whereas iduronate-2-sulfatase does not cross the BBB. [25]

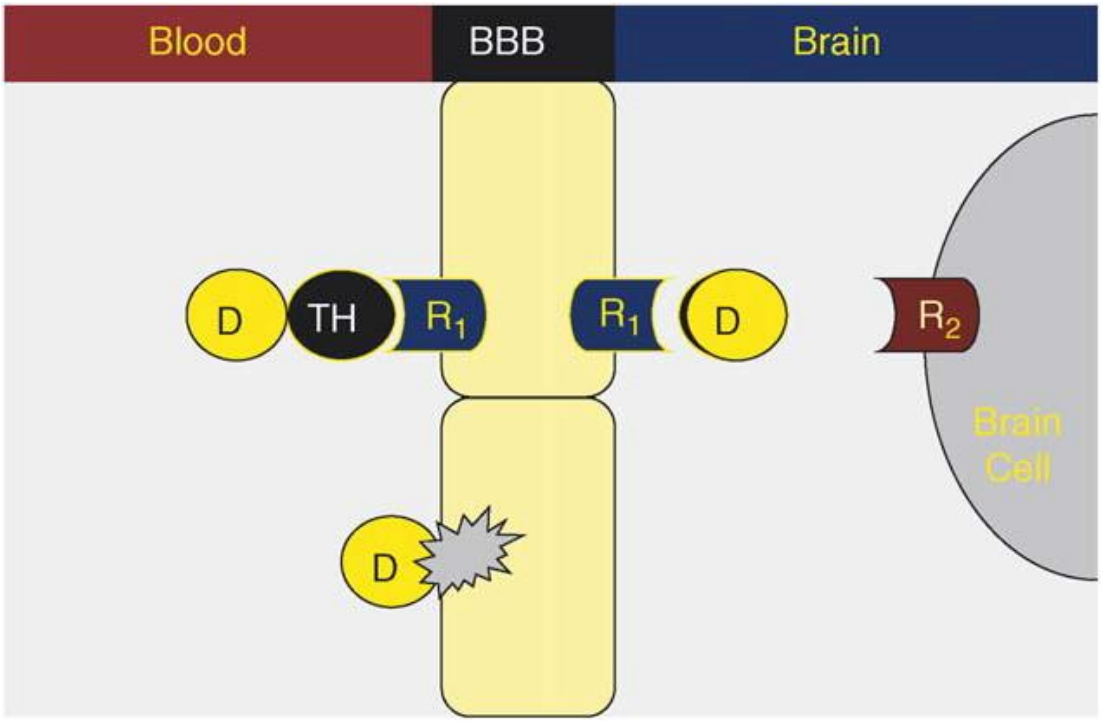

Figure 10. Molecular Trojan Horse technology. Reproduced with permission from reference (18) copyright 2006 Elsevier.

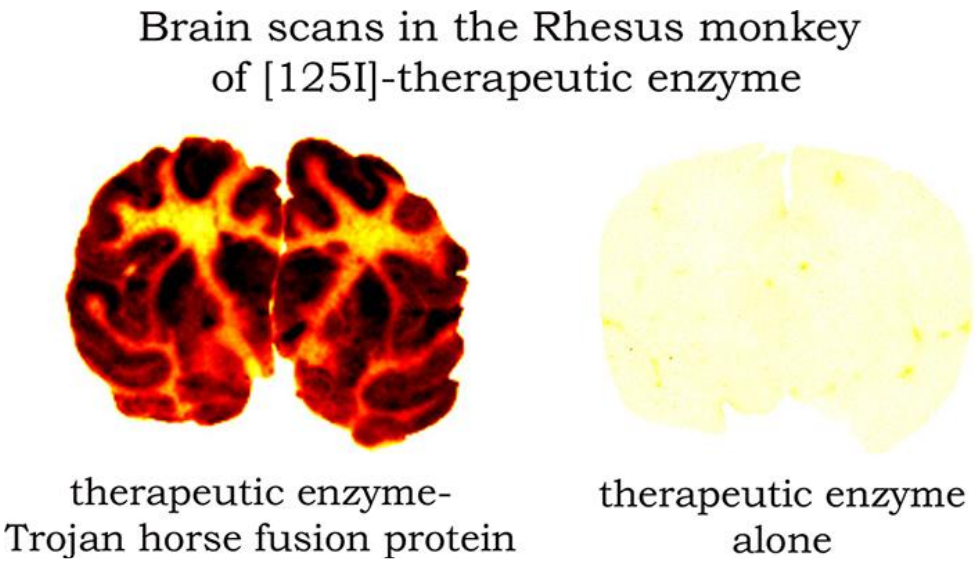

Figure 11. Radiolabeled enzyme-Trojan horse protein conjugate shows distribution to all parts of brain. Reproduced with permission from reference (22) copyright 2012 American Chemical Society.

1.4 Application of Atomic Force Microscopy as a Tool to Study Biomolecular Interactions

Understanding single molecular interactions forces is a challenging task in molecular and structural biology.[26] The advent of probe microscopes particularly the atomic force microscope (AFM) has revolutionized this field.[26-28] The AFM consists of a sharp tip mounted on top of a cantilever. The tip can scan over a surface in x-y direction to give rise to a topographic image of the sample and it can also be moved in the z direction, first downwards until it contacts the surface and then upwards till no interactions between the probe and the substrate are felt giving rise to a resulting plot (force curve) of the cantilever deflection versus the separation of the probe and the substrate.[26]

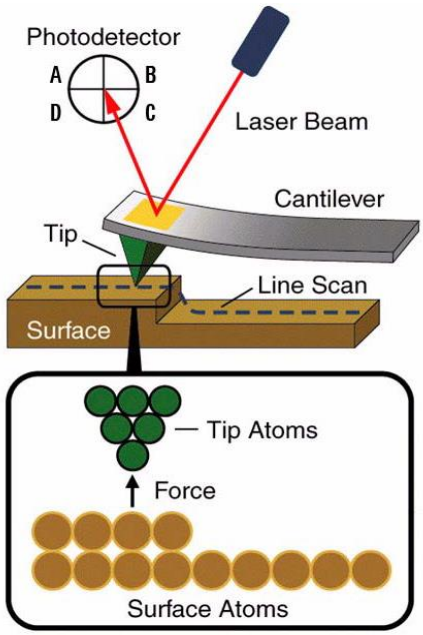

Figure 12. Basic AFM Principle. Adapted from Agilent 5500 manual.

There are two modes of AFM, the contact (static) mode in which the tip approaches the substrate and is the pushed into the substrate and finally retracted back and the dynamic mode in which the cantilever oscillates with a certain frequency. The dynamic mode can be operated in the acoustic mode in which the cantilever is oscillated above the surface near its resonance frequency and the magnetic mode in which a magnetically coated cantilever is oscillated using a magnetic ac field. Figure 12 shows the interactions between the scanning tip and the sample during different modes of AFM measurements.[29]

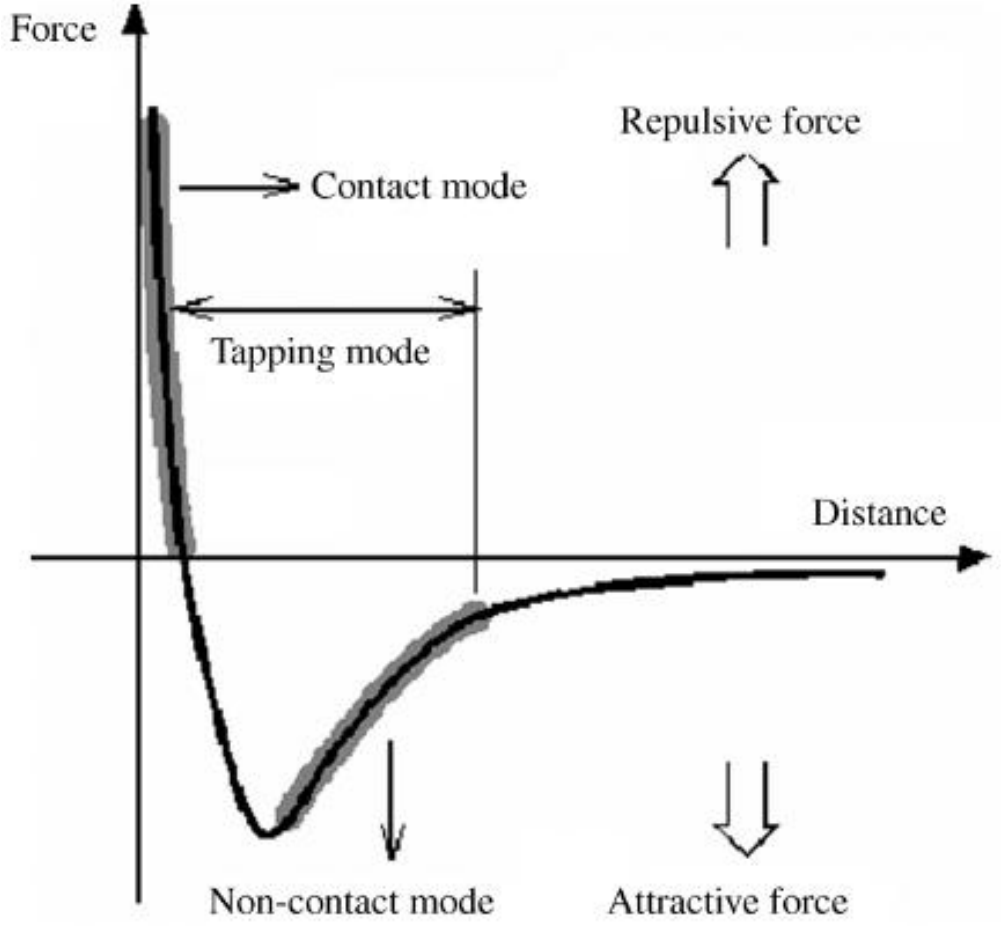

Figure 13. Interactions during AFM measurements. Adapted from reference (26).

In a further modification of the AFM, Lieber and coworkers developed the chemical force microscopy by which the probe tips can be molecularly functionalized to measure forces of interaction with organic monolayer functionalized surface.[30] This method has been employed in studying interactions between biomolecules and revolutionized our way understanding single molecule biomolecular interactions.[31] Some examples of biomolecular interactions studied using AFM include integrin binding to fibrinogen,[32-34] lectin binding to carbohydrates[35,36] aptamer-protein interaction[37,38] antigen-antibody interactions[39-41] etc. Generally a flexible linker such as polyethylene glycol is attached to the tip to tether ligands during imaging and force measurements. The linker serves as a spacer between the tip and the ligand and prevents non-specific interactions between the tip and the substrate.

Thus, the AFM is a powerful tool not only for its ability to image samples with nanometer resolution, but also to measure single molecule interaction forces in the order of piconewtons. The force spectroscopy is performed in contact mode. A typical force-distance curve is shown in Figure 14.[42] During force spectroscopy a tip functionalized with a recognition molecule (such as aptamer, antibody etc.) is brought in contact with the surface coated with a monolayer of the corresponding cognate protein or biomolecule that can bind with the recognition moiety attached to the tip, following which the tip is retracted to its original position. During retraction the linker gets stretched due to interaction between the recognition moiety and the surface protein following which the cantilever bends and finally unbinding occurs and the retraction curve comes back to zero force. The unbinding force between the recognition moiety and the protein on the surface

can be measured from the resulting force curve by employing the Hooke's law: $F = - k_c d$, where F is the force acting on the cantilever, k_c is the spring constant of the cantilever, and d is its deflection. During force spectroscopy experiment the approach and retraction of the tip is performed a number of times to generate force curves following which a histogram is plotted with the unbinding force data obtained from the force curves. The mean unbinding force can then be calculated by fitting the histogram.

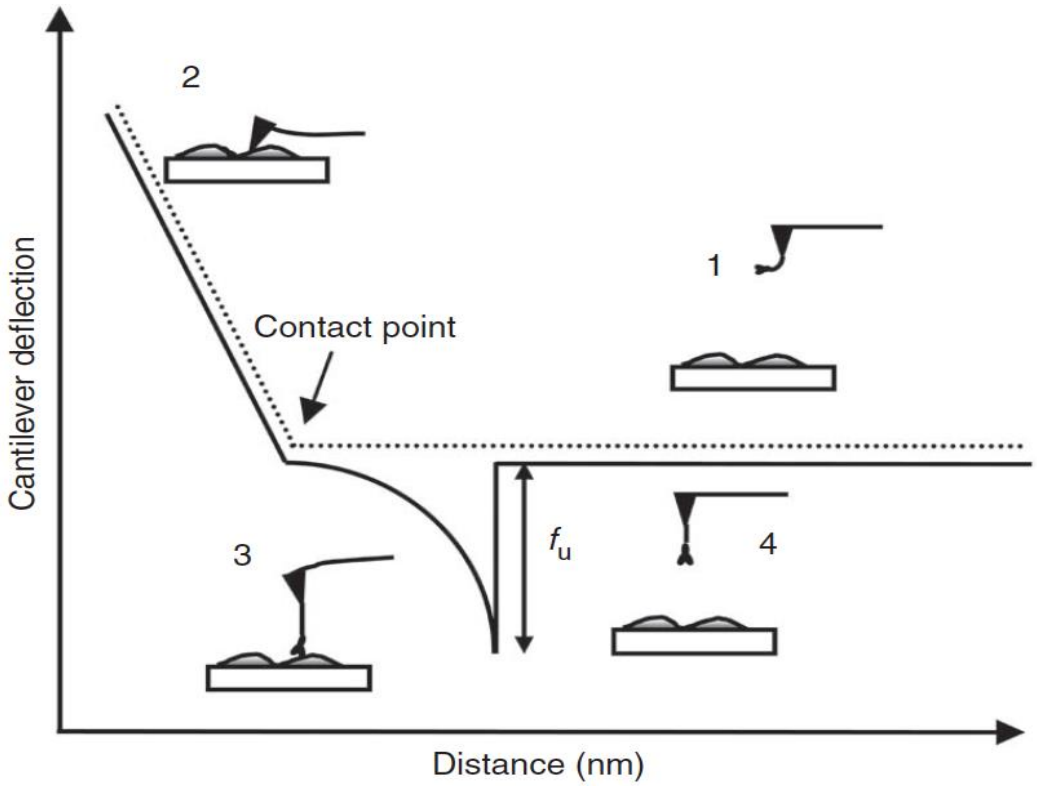

Figure 14. Typical force distance curve. Reproduced with permission from reference (39) copyright 2011 Nature Publishing Group.

The AFM is popularly known for imaging samples with nanometer resolution. During AFM imaging a harmonically oscillating tip is scanned over the surface in X-Y direction. During to interactions of the molecules on the surface the minima of the oscillations

changes giving rise to a corresponding topography image. However if a cantilever containing a tip functionalized with a recognition molecule is scanned over the surface, due to changes in the topography the minima of the oscillations changes while the maxima changes if there is an interaction between the functionalized tip and the substrate.[43,44]

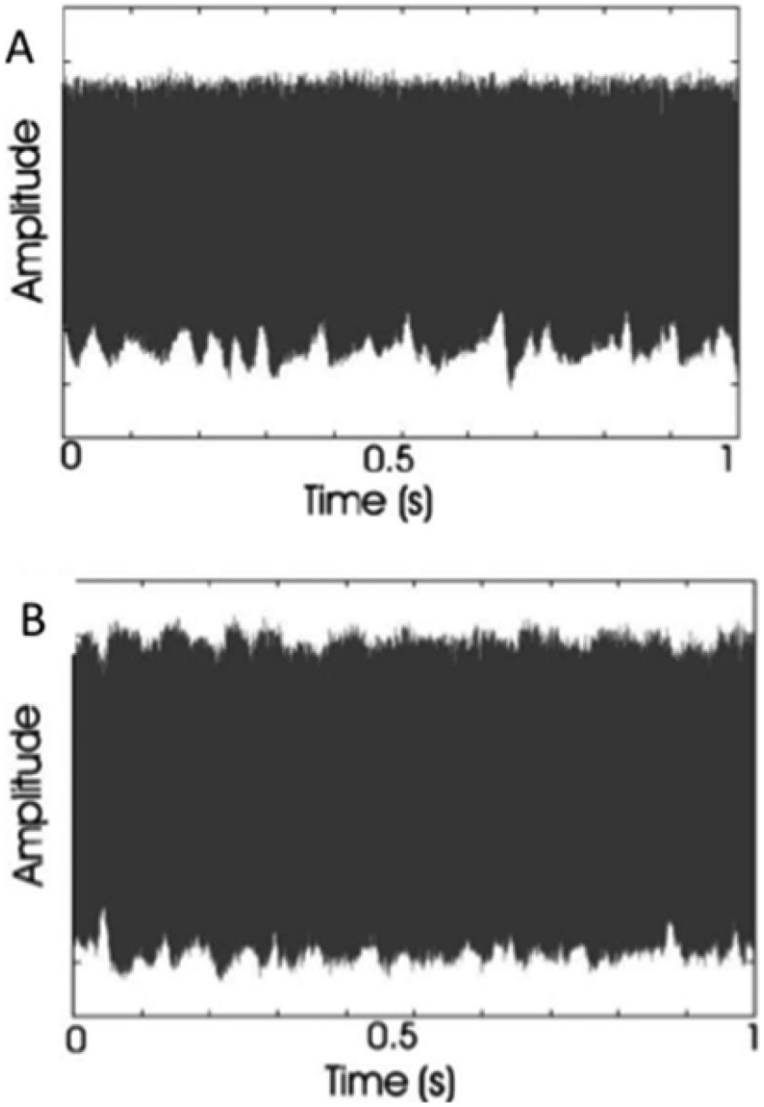

Figure 15. Oscillation amplitude with (A) Bare tip (B) Functionalized tip. Reproduced with permission from reference (40) and (41) copyright 2016 American Chemical Society and 2004 Biophysical Society.

The changes in the minima of the amplitude of oscillation amplitude gives rise to a topographic image which appears as white spots while changes in maxima of the amplitude gives rise to a recognition image which appears as black spots. During imaging, the TREC box separates the maxima and the minima of the oscillation amplitude and the topography and recognition image gets generated simultaneously.[45] The recognition imaging has an advantage that it does not require any tags or labels like most other techniques and has resolution in the range of about 20 nm. The specificity of the recognition experiment is checked by passing a blocking solution to block the ligand on the tip. Once this ligand gets blocked, the tip generates no more recognition.

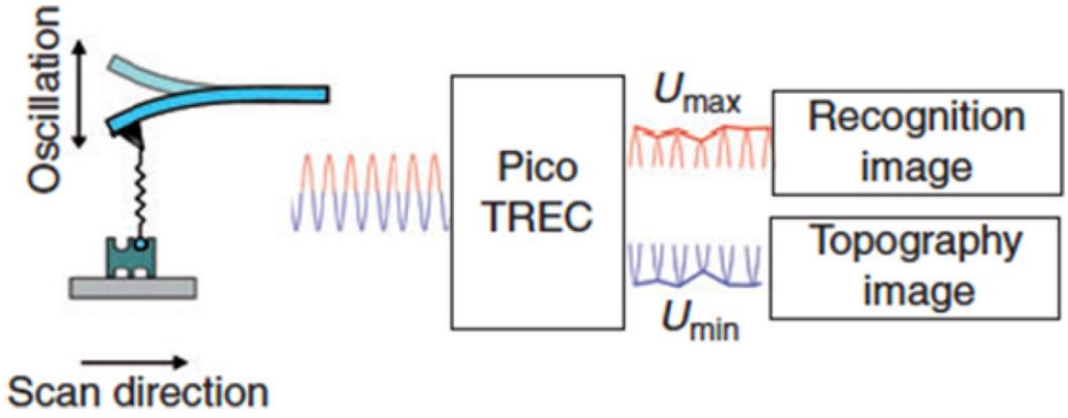

Figure 16. Simultaneous Topography and Recognition (TREC) Imaging. Reproduced with permission from reference (40), (41) and (42) copyright 2016 American Chemical Society and 2004 Biophysical Society and 2005 John Wiley & Sons, Inc.

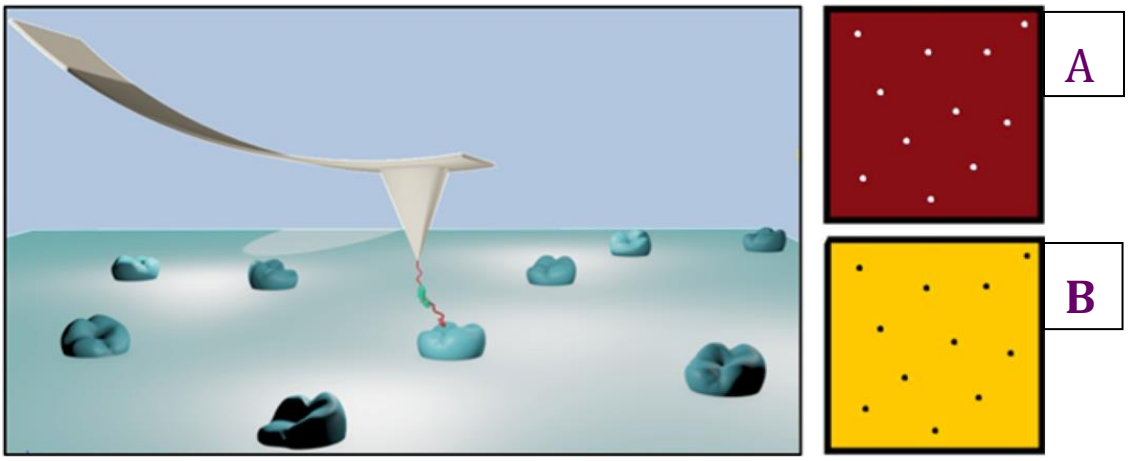

Figure 17. Simultaneous Topography and Recognition (TREC) Imaging. A. Topography B. Recognition. Reproduced with permission from reference (40) copyright 2016 American Chemical Society.

CHAPTER 2

APPLICATION OF AFM TO STUDY MULTIVALENT INTERACTIONS

2.1. Introduction

The human proteome consists of millions of proteins, many of which occur in minute concentrations below limits of detection (LOD) of current technologies such as ELISA, mass spectrometry, and protein microarrays. Therefore, there is a long felt need of a molecular tool capable of directly detecting those disease relevant protein biomarkers present in low abundance without any additional manipulation such as post assay signal amplification.

AFM has developed into a surface imaging tool with nanometer spatial resolution and an important nanobiotechnique. A ligand attached to an AFM tip with a flexible polyethylene glycol linker can be used to scan over a surface to measure the forces of interactions (force spectroscopy) or to generate a map of these interactions (recognition imaging). Thus AFM has been envisioned as a means of nanodiagnostics due to its single molecule sensitivity. However, compared to fluorescence microscopy, the AFM based recognition imaging lacks a multiplex capacity to detect multiple analytes in a single test. Hence, our idea was to synthesize recognition heads, develop a chemistry to attach them to AFM tips, and further implementation in detecting multiple proteins simultaneously.

2.2. Application of Catalyst-Free Click Reactions in Attaching Affinity Molecules to Tips of Atomic Force Microscopy for Detection of Protein Biomarkers

2.2.1. Introduction

During AFM imaging and force spectroscopy a molecular linker is often employed to attach affinity molecules to AFM tips, which provides an advantage in distinguishing between specific and nonspecific interactions.[46] The heterobifunctional poly[ethylene glycol] (PEG) has become a commonly used linker for this purpose. [47,48] The popular attachment is a three-step process that includes functionalizing an AFM tip with a chemically reactive group, tethering the PEG linker to the AFM tip, and reacting with an affinity reagent. (3-Aminopropyl)triethoxysilane (APTES) is a choice reagent for amination of silicon tips[49,50], but it is notoriously problematic for forming uniform monolayers, especially when the reaction is carried out in a liquid phase. [51,52] APTES should be freshly redistilled before use in order to achieve reproducible results. Chemical vapor deposition of APTES has been developed to improve the outcome,[50] but the process is tedious, requiring a thorough purge of the deposition chamber with argon to remove trace of moisture. Without developing an automated apparatus, it is difficult to be scaled up. The reaction of amine with N-hydroxysuccinimide (NHS) ester has been one of the most commonly used methods for tethering carboxylated PEG linkers to AFM tips.[53-57] The NHS ester is sensitive to moisture and is prone to rapid hydrolysis with increasing in pH (a half-life time of 4−5 h at pH 7 and 1 h at pH 8).[58,59] On the other hand, the amine exists in an ammonium form at the neutral pH, requiring basic conditions to be deprotonated for its nucleophilic activity. These caveats make it difficult to handle the NHS ester reaction in aqueous solutions, and one has to fine-tune pH and reaction time in order to achieve optimal outcomes.

Hence, we have developed a new scheme for attachment of affinity molecules to AFM tips based on Click Chemistry.[60]

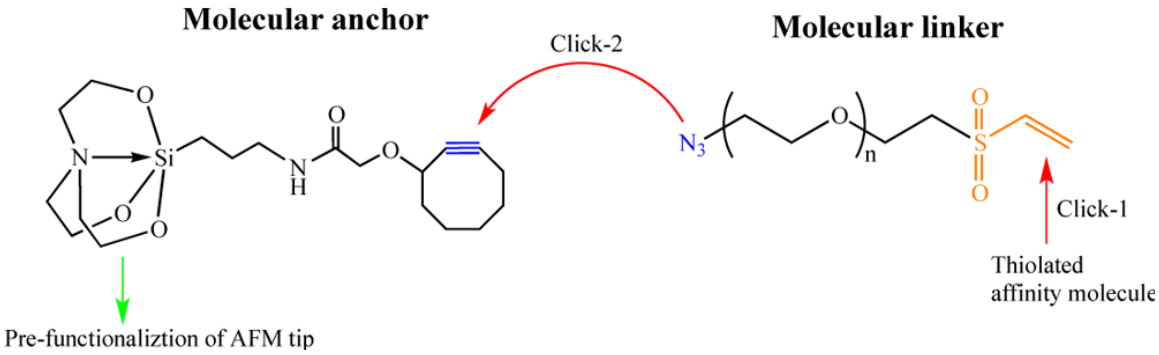

Figure 18. Copper-free Click Chemistry approach for attachment of affinity molecules to AFM tips. Adapted from reference (57).

Chen et al. have employed a copper-catalyzed alkyne−azide reaction to attach antibodies to a gold coated AFM tip through an azido-PEG-thiol linker.[61] To take it further, we implement two orthogonal catalyst-free click reactions for the attachment of affinity molecules to silicon tips. First, we have synthesized a molecular anchor composed of cyclooctyne and silatrane for the introduction of an alkyne function to the silicon tip. In aqueous solution, the silatrane moiety reacts with silanols on silicon surfaces to form a monolayer. It has been known that silatrane is less reactive than alkoxysilanes and extremely resistant to polymerization at a neutral pH.[62] Lyubchenko and co-workers have employed 1-(3-aminopropyl)silatrane (APS) as a substitute of APTES in functionalization of AFM tips and mica surfaces. [63-66] Thus, we expected that the new anchoring molecule would form a uniform cyclooctyne monolayer on the silicon tips. The ring strained cyclooctyne promotes the alkyne−azide reaction without the copper catalyst.[67] In addition, we have synthesized a new class of molecular linkers, azido-PEG-

vinyl sulfone with defined lengths, for connection of affinity molecules to AFM tips. In the present study, we have focused on attaching thiolated oligonucleotide aptamers and affinity peptides to AFM tips because they are rapidly growing areas in molecular diagnostics.[68] The reaction of vinyl sulfone with thiol in aqueous solution comprises another category of click chemistry in bioconjugation,[69] being used for the labeling of proteins[70] and proteomes.[71] We adapt it as a first click reaction to connect thiolated affinity molecules to the PEG linker as illustrated in Figure 17. The second click (azide to alkyne) finishes the process of the attachment. These two click reactions are orthogonal so that there is no cross talk between each other.

2.2.2. Results and Discussion

Synthesis. The molecular anchor (3) was synthesized simply by reacting APS (1)[66] with 2-(cyclooct-2-yn-1-yloxy)-acetic acid (2)[72] in the presence of 1-ethyl-3-(3-dimethylaminopropyl)carbodiimide (EDC, Scheme 2.2.1a). The desired product was separated as a white solid by silica gel chromatography with a yield of 60%. The molecular linker for Recognition Imaging (RI) (6a,Scheme 2.2.1b) was synthesized starting from hexaethylene glycol. First, azido-(CH2CH2O)6-Ts (4, Ts = Tosyl) was synthesized in a multigram scale following a method reported in literature.[73,74] Azido-$(CH2CH2O)_{12}$-H (5) was prepared in a 71% yield by reacting 4 with sodium hexaethylene glycoxide (3 times excess) that was generated in situ by treating hexaethylene glycol with sodium hydride. In presence of potassium t-butoxide, 5 reacted with divinyl sulfone to furnish the desired product 6a in a fairly good yield (64%). In the same manner, the linker azido-$(CH2CH2O)_{36}$-vinyl sulfone (6b) was synthesized by

reacting azido-dPEG$_{36}$-alcohol with divinyl sulfone in a yield close to that of 6a (Scheme 2.2.1c). These two products were characterized with FTIR, NMR, and mass spectroscopy.

Although it has been reported that vinyl sulfones react with azides in presence of $CuSO_4$ and sodium ascorbate,[75] we found by NMR monitoring that 6a and 6b were stable both in its pure form and in chloroform at room temperature at least for two days. Maleimide is another widely used reactive group that functions similarly to vinyl sulfone in bioconjugation,[76] but it may not be amenable to coexisting with azide because a [3 + 2] cycloaddition could spontaneously take place between these two functions in some circumstances.[77] In addition, maleimide can undergo the thiol exchanges and ring hydrolysis (above pH 8),[78,79] which would complicate outcomes of the conjugating reaction. It is also a reason why we chose vinyl sulfone as a Michael addition receptor of thiols in our attachment chemistry.

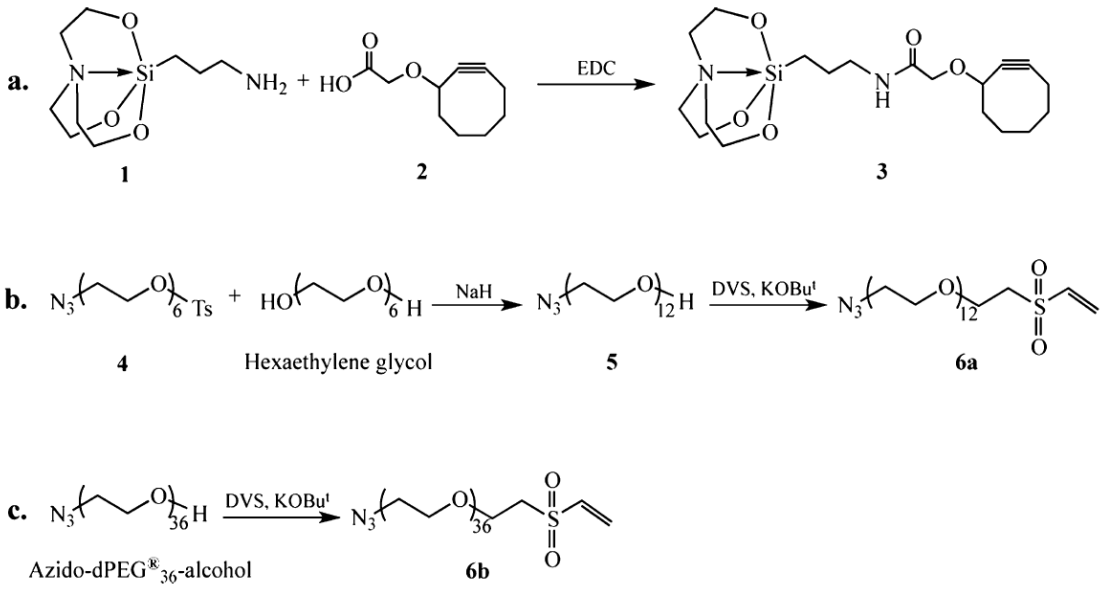

Scheme2.2.1. Schematic diagram of chemical synthesis.

Click 1: Tethering Molecular Linkers to Affinity Molecules.

Two affinity molecules, thrombin-binding DNA aptamer (TBA)[80] and cyclic RGDfC peptide containing a RGD motif that binds to integrin receptors such as α5β1,[81] were chosen to study the attachment chemistry. First, the disulfide at the 3′-end of the DNA aptamer from custom synthesis was reduced to thiol using tris(2-carboxyethyl)phosphine (TCEP), which then reacted with linker 6a and 6b at pH 8.0 in phosphate buffered aqueous solutions, respectively. Through the Michael addition of thiol to vinyl sulfone (Scheme 2.2.2a), the DNA aptamer was converted to azido-PEGylated products D-1a with a 95% yield and D-1b with a 89% yield, based on HPLC analysis. The disulfide DNA was used as a negative control, and it did not react with 6a and 6b, implying that the vinyl sulfone is specific to thiol under the current conditions. Also, we observed that the reaction between the vinyl sulfone and the thiolated DNA at pH 7−7.5 was very slow and did not complete even after 1 day. The thiol reaction is driven by the thiolate that is a much stronger nucleophile than its conjugate acid thiol. Since the alkylthiol is fairly acidic with pKa of about 10−11, the increase of pH surely increases existence of the thiolate anion, resulting in an increased reaction rate. This is consistent with what has been reported in literature.[82] Under similar conditions, the thiolated RGDfC was converted to products P-1a and P-1b quantitatively (Scheme 2.2.2b). We did not observe any side products by MALDI mass spectrometry and reverse phase HPLC analysis. In addition, no apparent time differences between reacting with 6a and 6b were observed. In sum, all these reactions were completed within 3 h when starting with DNA or peptides

in a range of millimolar concentrations. It should be noted that the vinyl sulfone also reacts with alkyl amines under basic conditions.[83] In our case, the amine functionalized aptamer and the cyclic RGDfK reacted with both 6a and 6b in phosphate buffered solutions at pH 8.8, but the reactions were very slow and not completed even after 10 h. This shows that the vinyl sulfone can specifically react with thiol in the presence of amino function with well-tuned pH.

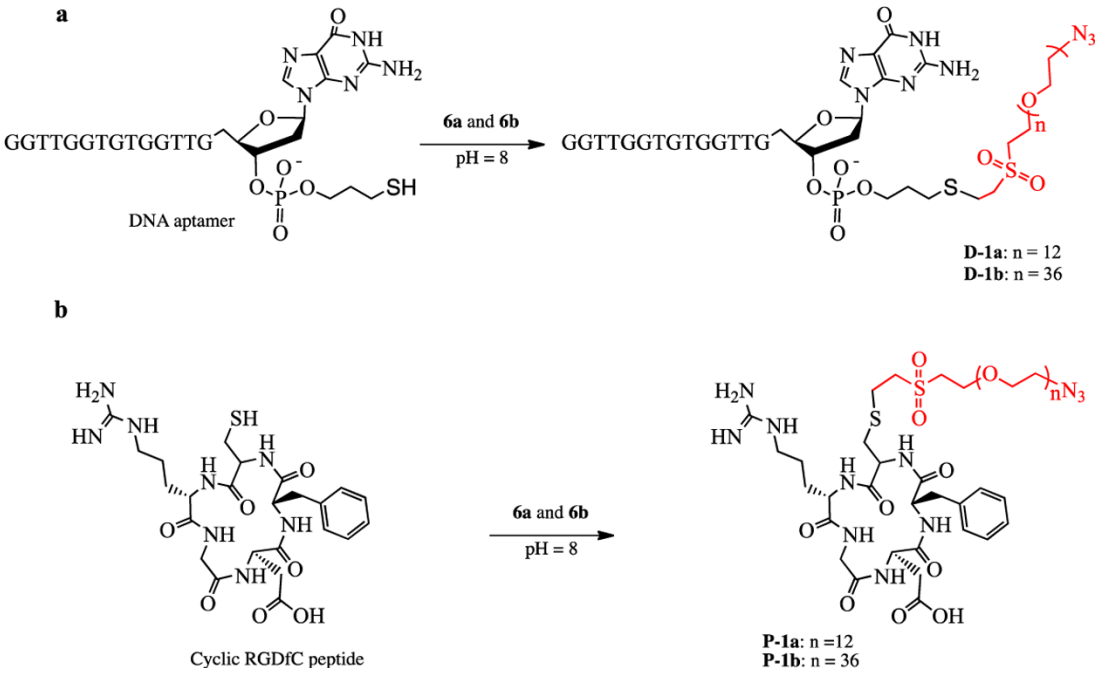

Scheme 2.2.2. Schematic Description of Tethering the Molecular Linkers to Affinity Molecules through the Michael Addition of Thiol to Vinyl Sulfone

Click 2: Attaching Affinity Molecules to AFM tips.

We have developed a two-step protocol for the attachment. As illustrated in Figure 18,

a bare AFM tip is first functionalized with the molecular anchor 3 in aqueous solution, followed by reacting with the azide functionalized affinity molecules under physiological conditions. It is worth noting that all the reactions were carried out in aqueous solutions without using any organic solvents. The attachment chemistry has worked well on two different AFM tip materials: SiN tipped probes (from Olympus and Bruker) and silicon probes (from NanoWorld). Before the chemical functionalization, these tips were cleaned sequentially with UV-ozone and oxygen plasma to increase the silanol density on the silicon surface for the silanization reaction.

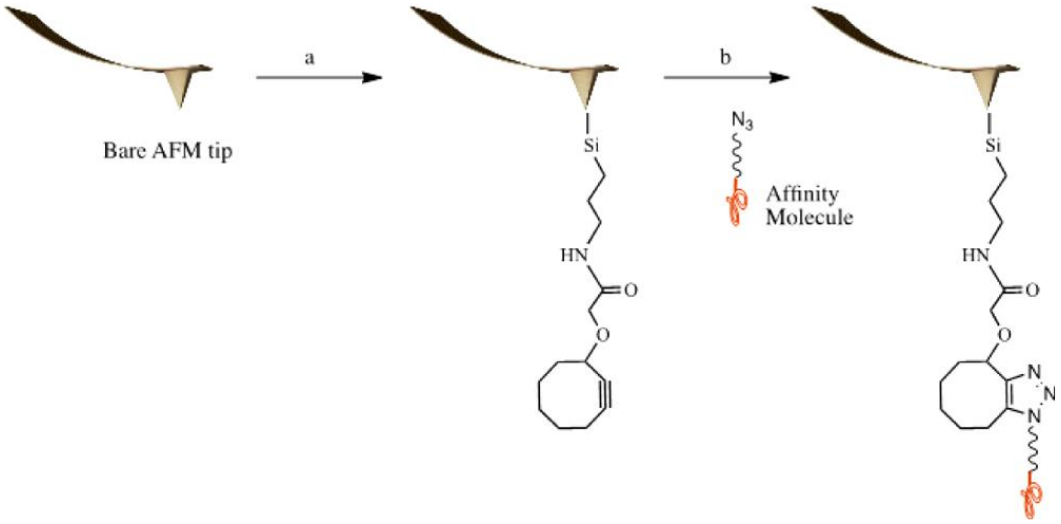

Figure 19. Process of functionalizing AFM tips with affinity molecules: (a) coupling cyclooctyne to an AFM tip through silanization; (b) attaching affinity molecules to an AFM tip through alkyne−azide click reaction.

Force Measurement. The attachment chemistry was validated by measuring forces of affinity molecules tethered to SiN tips unbinding from their protein cognates. The protein

samples were immobilized on APS-modified mica substrates using glutaraldehyde as a cross-linker according to a procedure reported in literature.[84] Initially, we collected about 1000 force−distance curves from each of measurement experiments with either D-1b against thrombin or P-1b against integrin α5β1. The blue solid lines in panels A and C of Figure 19 show typical retracting force−distance curves we used for data analysis, which accounts for more than one fourth of the collections. The selection was based on an assumption that a rupture directly related to unbinding of an affinity molecule from its protein cognate is likely to take place around the distance corresponding to the stretched length of a PEG linker (~13.5 nm in our case).

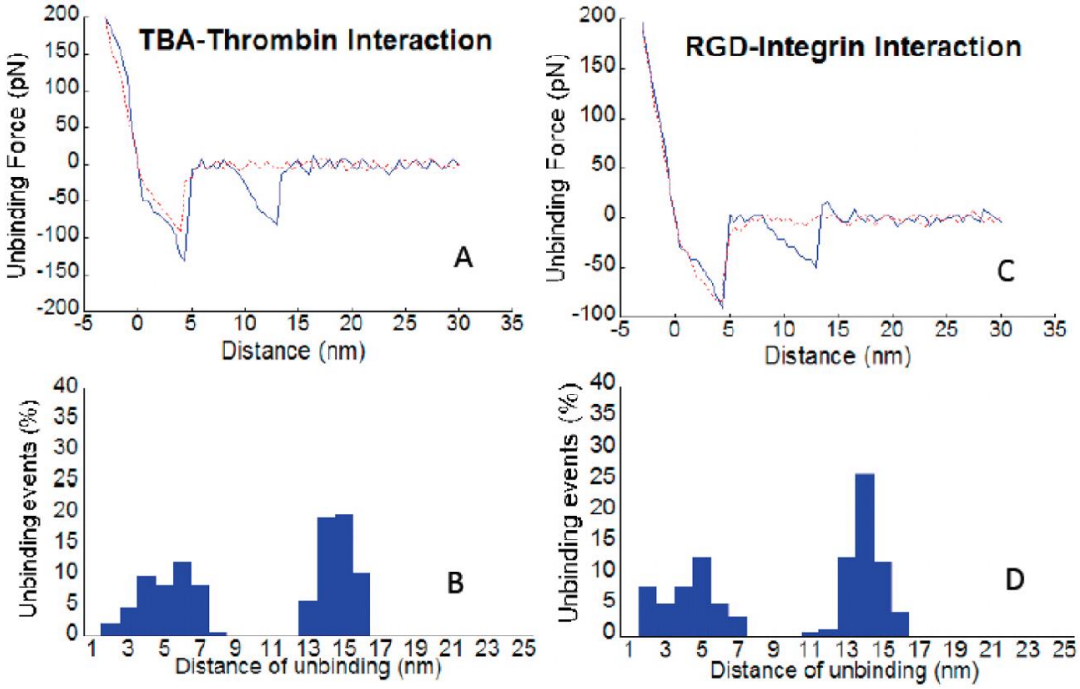

Figure 20. A. Force-distance curve for TBA-Thrombin unbinding, B. Distance histogram for TBA-Thrombin unbinding, C. Force-distance curve for RGD-Integrin unbinding, D. Distance histogram for RGD-Integrin unbinding.

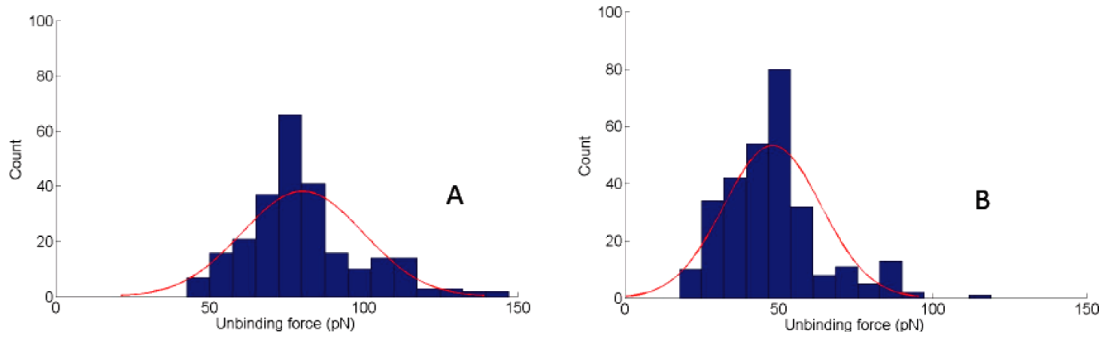

Figure 21. A. Force histogram of TBA-Thrombin unbinding, B. Force histogram of RGD-Integrin unbinding.

Recognition Imaging (RI). We did recognition imaging to confirm that our chemistry works with the RI technique. Unexpectedly, the recognition imaging of clinically relevant proteins thrombin and integrin has not been reported. It has been demonstrated that a PEG linker with 12 ethyleneoxy (CH2CH2O) units can effectively produce quality recognition images.[85] Linker 6a was tailored for RI. Its conjugate D-1a or P-1a was attached to Ni-coated MacMode tips (from Nanoworld) following the same protocol as mentioned above. The protein samples (thrombin or α5β1integrin) were deposited on mica using the same glutaraldehyde chemistry. However, the optimal protein concentration (50 pg/μL in 1× PBS buffer, pH 7.4) for the RI was 20 times lower than that for the force measurements, which was predetermined by imaging the surface with bare AFM tips in the air mode, ensuring that the protein molecules were well distributed in a predefined area. For one measurement, only 2−3 μL of protein sample is needed in the current setup. Thus, a few femtomoles of proteins can readily be detected by the AFM based recognition imaging. Figure 21 shows the images obtained from our RI experiments. In general, RI simultaneously produces both topographic and recognition

images. Each bright round spot in the topographic image presumably represents a protein molecule (thrombin in panel A and integrin in panel D of Figure 21). This can be verified by examining the recognition images (panels B and E of Figure 21) where the dark spots represent recognition of those bright ones within the corresponding locations in the topographic image as expected protein molecules. We obtained about 77% recognition of thrombin and 84% recognition of integrin by comparison between their topography and recognition images. The recognition was further confirmed by the same blocking experiments as in the force measurements. After injecting a protein (thrombin or integrin) solution to the flow cell, most of the dark spots disappeared from the recognition images (panels C and F of Figure 22). These experiments demonstrate that our attachment chemistry works effectively for RI as well.

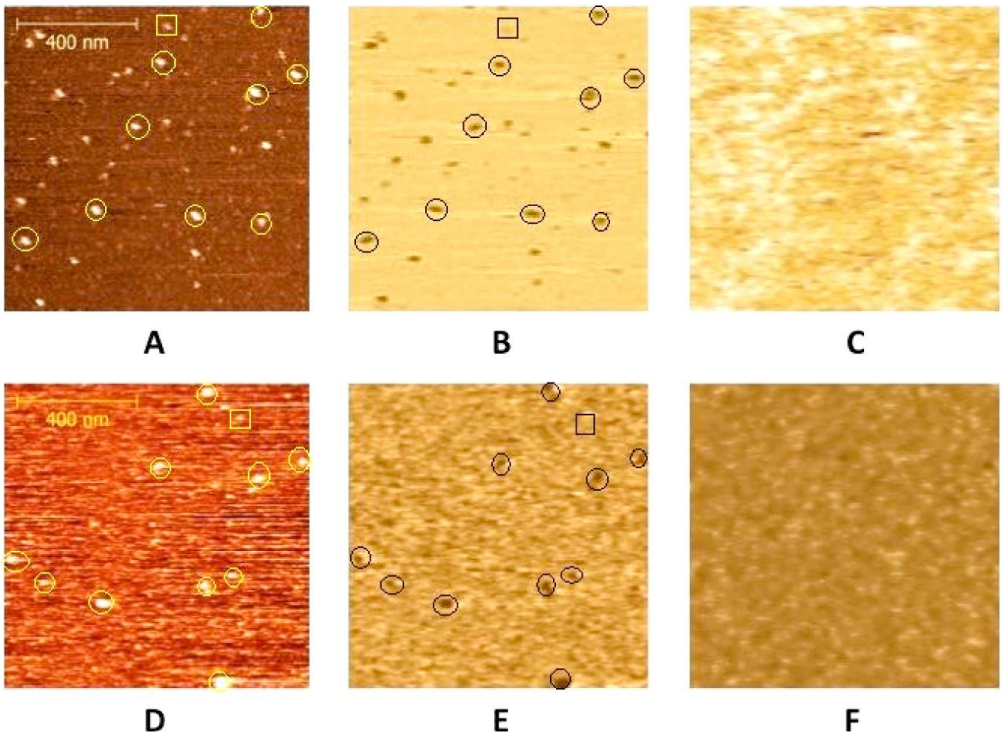

Figure 22. (A) Topographic image of thrombin proteins on mica. (B) Corresponding recognition image of (A). (C) Recognition image from using a thrombin solution to block the TBA tip. (D) Topographic of integrin proteins on mica. (E) Corresponding recognition imaging of (D). (F) Recognition image from using an integrin solution to block the RGD tip (the circles in the images indicate those protein molecules that were recognized, whereas the square indicates the protein that was not recognized).

2.2.3. Experimental details.

General information

All chemicals were purchased from commercial suppliers (Sigma-Aldrich, Fluka, Santa Cruz Biotechnology, Alfa Aesar). Anhydrous organic solvents were Sure/SealTM from Aldrich. Thrombin aptamers were custom synthesized by IDT (Integrated DNA Technologies) and human α thrombin was purchased from Abcam, Azido-dPEG® 36-alcohol was purchased from Quanta Biodesign, human α5β1 integrin from YO Proteins AB (Sweden), cylco(RGDfK) and cyclo(RGDfC) from Peptides international. All the synthetic reactions were carried out under nitrogen atmosphere. Thin layer chromatography (TLC) was used to monitor progress of organic reactions. An automated flash chromatography system (CombiFlash Rf, Teledyne Isco, Inc.) was used to separate the organic compounds with silica gel columns. FTIR data were collected using Thermo Scientific Nicolet™ 6700 FT-IR spectrometer. The HPLC purification was carried out in Agilent 1100 series equipped with a UV detector and a fraction collector. All the proton NMR (1H) spectra were recorded on a Varian 400 MHz instrument. 1H chemical shifts were referenced relative to the residual solvent peak (such as CDCl3: δH = 7.24 ppm).

MALDI-TOF analysis was performed on Voyager-DE STR instrument. Water was from Millipore's Milli-Q water purification system with a real time monitor of total of carbon (TOC) connected to a BioPak Polisher to remove biological contaminates. TOC level is strictly maintained below 5 ppb and resistivity at 18.2 MG x cm.

N-(3-(silatranyl)propyl)-2-(cyclooct-2-yn-1-yloxy)acetamide (3):

EDC (115 mg, 0.6 mmol) was added to a solution of 2-(cyclooct-2-yn-1-yloxy)acetic acid (100 mg, 0.5 mmol) in anhydrous dichloromethane (2 mL). The solution was stirred for 30 minutes, followed by the addition of APS (140 mg, 0.6 mmol). After 3 hours, the reaction was stopped by rotary evaporation to remove the solvent. The crude product was purified by flash chromatography in a silica gel column using a gradient of methanol (0-5% over 3 h) in dichloromethane to give a white solid (130 mg, 60%). 1H NMR (400 MHz, $CDCl_3$): δ = 0.4 -0.44 (m, 2 H), 1.15 - 2.25 (m, 10 H), 1.58 - 1.64 (m, 2 H), 2.79 (t, 6 H, J= 6 Hz), 3.24 (m, 2 H), 3.74 (t, 6 H, J = 6 Hz), 3.81 (d, 1 H, J = 15.2 Hz), 4.0 (d, 1 H, J = 15.2 Hz), 4.2 (t, 1 H), 6.65 (s, 1H, broad); ^{13}C NMR (50 MHz, $CDCl_3$): δ = 13.2, 20.6, 24.9, 26.2, 29.6, 34.2, 41.8, 42.1, 51.1, 57.7, 68.5, 73.0, 91.5, 101.3, 169.1. HRMS (FAB): *m*/*z* (M+H) calculated for $C_{19}H_{32+1}N_2O_0Si$: 397.2158; found: 397.2159.3

Special note on nomenclature: To avoid excessive use of a long series of numbers, the mathematical shorthand for expressing arithmetic progressions is used to denote the positions of oxygen atoms in the elongated PEG chains, as proposed by Hii and coworkers.[73]

35-azido-3n33^3-undecaoxapentatriacontan-1-ol (5):

Sodium hydride (0.71g, 29.5mmol) was added to a solution of hexaethylene glycol (6.42g, 22.7 mmol) in anhydrous tetrahydrofuran (THF) (40 mL) with stirring at 0 °C. After 1 hour, to the mixture a solution of compound **4** (3.5g, 7.5mmol) in anhydrous THF (20 mL) was added. The mixture was allowed to warm to room temperature, stirred for another 15 hours, to which methanol (5 mL) was added dropwise to stop the reaction. After removing the solvent, the crude product was purified in a silica gel column by flash chromatography using a gradient of methanol (0-5% over 4 h) in dichloromethane. Compound **5** was obtained as a colorless liquid (3.1g, 71%). 1H NMR (400 MHz, CDCl3): δ = 2.7 (s, 1 H, broad), 3.34 (t, 2 H, J = 4.8 Hz), 3.55-3.69 (m, 46 H); HRMS (APCI): *m/z* (M+H) calculated for $C_{24}H_{49+1}N_3O_{12}$: 572.3395; found: 572.3391.

1-Azido-35-(2-(vinylsulfonyl)ethoxy)-3n33^3-undecaoxapentatriacontane (6a):

To a solution of **5** (100 mg, 0.18 mmol) in anhydrous THF (2 mL), divinyl sulfone (180 μL, 1.8 mmol) was added with stirring, followed by the addition of potassium t-butoxide (23 mg, 0.2 mmol). The reaction was monitored by thin layer chromatography (TLC). Within one hour, the starting material **5** was consumed and a less polar spot observed on the TLC plate. The reaction mixture was filtered, concentrated, and purified in a silica gel column by flash chromatography using 0-4% gradient (over 4 hours) of methanol in dichloromethane to furnish compound **6a** as a colorless liquid (77 mg, 64%). FTIR (cm-1)**:** 1102 (S=O symmetric stretch), 1313 (S=O asymmetric stretch), 1605 (C=C stretch), 2101 (N=N=N stretch), 3056 and 3097 (sp^2 C-H stretch); 1H NMR (400 MHz, $CDCl_3$): δ = 3.24 (t, 2 H, J = 5.2 Hz), 3.36 (t, 2 H, J = 5.2 Hz), 3.6-3.87 (m, 46 H), 3.88 (t, 2 H, J = 5.2 Hz), 6.06 (d, 1 H, J = 9.6 Hz), 6.37 (d, 1 H, J = 16.8 Hz), 6.8 (dd, 1 H, J = 16.8 Hz

and 10 Hz); 13C NMR (50 MHz, $CDCl_3$): characteristic peaks for PEG were observed. Two characteristic peaks for carbon atoms of vinyl sulfone was observed at δ = 126.68, 137.99; HRMS **(**APCI**):** *m/z* (M+H) calculated for $C_{28}H_{55+1}N_3O_{12}S$: 690.3483; found: 690.3469.

1-Azido-35-(2-(vinylsulfonyl)ethoxy)-3n105^3-pentatricontaoxaheptahectane (6b): To a solution of Azido-dPEG®36-alcohol (50 mg, 0.03 mmol) in anhydrous THF (1 mL), divinyl sulfone (36 mg, 0.3 mmol) was added with stirring, followed by the addition of potassium t-butoxide (4 mg, 0.035 mmol). The reaction was monitored by thin layer chromatography (TLC). Within one hour, the starting material was consumed and a less polar spot observed on the TLC plate. The reaction mixture was filtered, concentrated, and purified in a silica gel column by flash chromatography using 0-4% gradient of methanol in dichloromethane. The product **6b** was separated as a white solid (33 mg, 61%). FTIR **(**cm^{-1}):1104 (S=O symmetric stretch), 1315 (S=O asymmetric stretch), 1600 (C=C stretch), 2100 (N=N=N stretch), 3060 and 3100 (sp^2 C-H stretch); ^{1}H NMR (400 MHz, $CDCl_3$): δ = 3.26 (t, 2 H, J = 5.6 Hz), 3.39 (t, 2 H, J = 5.6 Hz), 3.5 - 3.7 (m, 142 H), 3.9 (t, 2 H, J = 5.6 Hz), 6.09 (d, 1 H, J = 10 Hz), 6.39 (d, 1 H, J = 16.4 Hz), 6.82 (dd, 1 H, J = 10 Hz and 16.4 Hz); 13C NMR (50 MHz, $CDCl_3$): characteristic peaks for PEG were observed. Two characteristic peaks for carbon atoms of vinyl sulfone was observed at δ = 128.7, 137.9; MALDI-MS: m/z (M-H+Na) calculated for $C_{76}H_{151-1}N_3O_{38}SNa$: 1769.0651; found: 1769.2117.

Reactions of DNA Aptamers with molecular linkers (5)

A solution (20 μL, 10 mM) of Thrombin-binding DNA aptamer 5'-GGTTGGTGTGGTTGG with a disulfide linker at 3'-end (IDT code: 3ThioMC3-D) in 0.1 M phosphate buffer (pH 8.0) was treated with TCEP (5 μL, 170 mM in 0.1 M TEAA buffer, pH 7.0). After 3 h, the reaction mixture was passed through a size-exclusion G-25 column (GE Healthcare) to remove small thiol molecules. The G-25 column was prepared following the protocol described by the manufacturers. First, the storage buffer was removed by centrifugation (1 min, 735 x g). Then the column was rehydrated again with double distilled water, followed by centrifugation (1 min,735 x g). Finally, the reaction mixture was added to the column, followed by centrifugation (2 min, 735 x g). The eluted solution containing thiol-functionalized aptamers (~25 μL) was then added to a solution of PEG linker **6a** in 0.1 M phosphate buffer, pH 8.0 (20 μL, 50 mM). The reaction was finished in three hours, monitored by MALDI-TOF mass spectrometry. The product **D-1a** was purified using reverse phase HPLC with a Zorbax Eclipse Plus C18 column (4.6 x 150 mm, particle size 5 μm) with a gradient of 0% to 70% over a period of 25 mins (solvent A: a 0.1 M TEAA buffer, pH 7.0; solvent B: acetonitrile). The product has retention time of 17.4 min (with ~95% conversion). MALDI-TOF Mass: m/z (M+H) calculated for **D-1a**: 5570.51; found: 5571.63. After collecting the product using HPLC, the fraction was lyophilized to get the pure product.

D-1b was synthesized in the same way and purified by HPLC with retention time of 17.1 min (with conversion ~89%). MALDI-MS: m/z (M + H) calculated for **D-1b**: 6649.23; found: 6650.37. After HPLC purification, the collected fraction was lyophilized.

Reaction of cyclo-RGD with molecular linkers (P-1b)

A solution of cyclo(RGDfC) (4 mM , 10 μL) in a phosphate buffer (0.1 M, pH 8.0) is mixed with **6b** (4 mM, 10 μL) dissolved in phosphate buffer (0.1 M, pH 8.0). The reaction was stirred for three hours at room temperature, monitored by MALDI mass spectrometry for its completion. The conversion was 99.5%, determined by HPLC analysis. The product was purified by HPLC using a Zorbax Eclipse Plus C18 column (4.6 x 150 mm, particle size 5 μm) under a gradient of 20% to 70% over a period of 25 mins (Solvent A: 0.1% trifluoroacetic acid in de-ionized water; Solvent B: 0.09% trifluoroacetic acid in 80:20 acetonitrile: De-ionized Water; injection volume: 14 μL), monitored with a UV detector at a wavelength of 230 nm. The conjugate **P-1b** was eluted out at retention time of 17 min. MALDI-MS: *m/z* (M+H) calculated for **P-1b**: 2325.72; found: 2325.81. **P-1a** was prepared in the same way as did **P-1b**, purified by RP-HPLC, and characterized by MALDI-MS. MALDI-MS: *m/z* (M + H) calculated for **P-1a**: 1268.57; found: 1268.49. The conversion of peptide to its conjugate was quantitative. Both **P-1a** and **P-1b** fractions were lyophilized after HPLC purification.

General Procedure for Attaching Affinity Molecules to AFM Tips. AFM tips (a batch of four or five) were first immersed in ethanol for 5 min, dried with ultrapure argon, and then treated with ultraviolet ozone in a Boekel UV cleaner for 15 min and oxygen plasma (medium power) in a Harrick Plasma Cleaner for 2 min. These tips were immediately placed in a Petri dish, to which an aqueous solution of compound 3 (50 mM) was added. After 1 h, the tips were taken out, rinsed with water thrice, and dried gently with nitrogen. In a humid surrounding, the cyclooctyne functionalized tips were placed in a Petri dish, and a solution of D-1a (50 μM, 20 μL) in 1X PBS buffer (pH 7.4) was added to cover all

the tips. The tips were incubated at room temperature for 1 h and then were rinsed thrice with the same buffer and used immediately. Other conjugates including D-1b, P-1a, and P-1b were also attached to the AFM tips under the exactly same conditions.

Immobilization of Proteins on Mica Substrates. Freshly cleaved mica sheets (1.5 × 2.0 cm2) were immersed in an aqueous solution of APS (50 mM). After 1 h, the mica sheets were taken out and rinsed thoroughly with water thrice. In a humid surrounding, an aqueous solution of glutaraldehyde (1 mM, 200 μL) was added on the APS mica sheet. After 10 min, the mica substrates were rinsed with water thrice, and then a solution of protein in a 1X PBS buffer (3 μL) was placed on each sheet, incubated for 1 h, and rinsed with the 1X PBS buffer thrice. In general, protein concentrations were made around 10 ng/μL for force measurements and 0.05 ng/μL for recognition imaging. It should be noted that the integrin we used was a lyophilized product from a solution containing 0.26 mg/mL $\alpha_5\beta_1$, 20 mM Tris-HCl pH 7.5, 150 mM NaCl, 2 mM $MgCl_2$, 0.2% Triton X-100, which was reconstituted by dissolving it in 1× PBS buffer.

AFM Experimental Setup. An Agilent AFM 5500 (with inverted light microscope) system was used for the AFM experiments. Both force measurement and recognition imaging were carried out in 1X PBS buffer (pH 7.4). For force measurements, Veeco probes (Bruker, SiN tips) were used, having a force constant 0.05 N/m and a gold back coating, and the loading rate was 25 000 pN/s. For recognition imaging, magnetic cantilevers were used in AC (MAC) mode operation. Tips from NanoWorld were made of silicon and had a length of 125 μm, width 35 μm, and thickness 800 nm with force constant value of 0.14 N/m. The back sides of these tips were coated with 1 nm Ti/40 nm

Ni. They have a remarkably low spread in force constant (a few percentage) and give stable MacMode operation in even quite reactive solution. Also, Olympus tips (silicon nitride, a force constant 0.08 N/m) were functionalized and used for few recognition experiments. Each image was taken by scanning a $1 \times 1 \mu m^2$ area.

For a blocking experiment, a protein solution (50 μL, 0.01 ng/μL in 1X PBS buffer, pH 7.4) was added to the flow cell, and the surface was imaged again. In general, a 15−20 min waiting time is needed to effectively block the tip. The blocking for force measurements proceeded in the same way.

2.2.4. Conclusion.

We have developed a new scheme to attach affinity molecules to AFM tips for force spectroscopy and recognition imaging, based on two orthogonal click chemistries: catalyst free azide−alkyne cycloaddition and thiol-vinyl sulfone Michael addition. All the reactions can be carried out in aqueous solutions without the use of organic solvents. We synthesized two new reagents for this implementation. The first one is an APS derivative of cyclooctyne for introduction of a chemically reactive group to AFM tips. The silatrane chemistry allows for the formation of a uniform monolayer in aqueous solution, which is particularly useful when the chemical is not volatile and the vapor deposition would not work. The operation is more convenient compared to the vapor deposition technique and the resulting surface is highly reproducible. The second one is a class of heterobifunctional linkers with a form of "azido-PEG-vinyl sulfone". Our data show that it works for both AFM based force measurement and recognition imaging. The attachment process is easy to follow since there are no special requirements for the

chemical reactions. With an increasing number of affinity oligonucleotides and peptides, more and more proteins will be detected with these synthetic materials. Incorporating thiol to peptides and oligonucleotides has become a routine process in custom synthesis. Hence, our attachment method should be applicable to a broad range of affinity molecules.

2.3 Interactions of a Dipeptide with Universal Reader ICA on a Gold Substrate

2.3.1. Introduction

We used a scanning tunneling microscope (STM), operated in buffered aqueous solution, to create a tunnel gap set to a reproducible distance by controlling the gap conductance, collecting useful signals up to 25 kHz in frequency. Palladium probes, partially insulated with polyethylene, and Pd substrates[86], functionalized with the recognition molecule, 4(5)-(2-mercaptoethyl)-1H-imidazole-2-carboxamide (ICA), were used as electrodes[87]. We found that a tunnel current of 4 pA at a bias of 0.5 V produced Recognition Tunneling (RT) signals from all but two of the 20 naturally occurring amino acids, while phosphate-buffer controls were almost free of signals. This is surprising considering the fact that the reader molecule was designed to interact with DNA bases. [88] Hence, we studied the binding of a dipeptide with the universal reader ICA with AFM force spectroscopy.

2.3.2. Results and discussion

We have studied the interactions of a dipeptide Cys-Gly with ICA on a single molecule level by means of Force Spectroscopy. The ICA was bound to a gold-coated mica surface

through its thiolated linker. The dipeptide was attached to AFM tips through the azido-$(CH_2CH_2O)_{36}$-vinyl sulfone linker discussed earlier.[60]

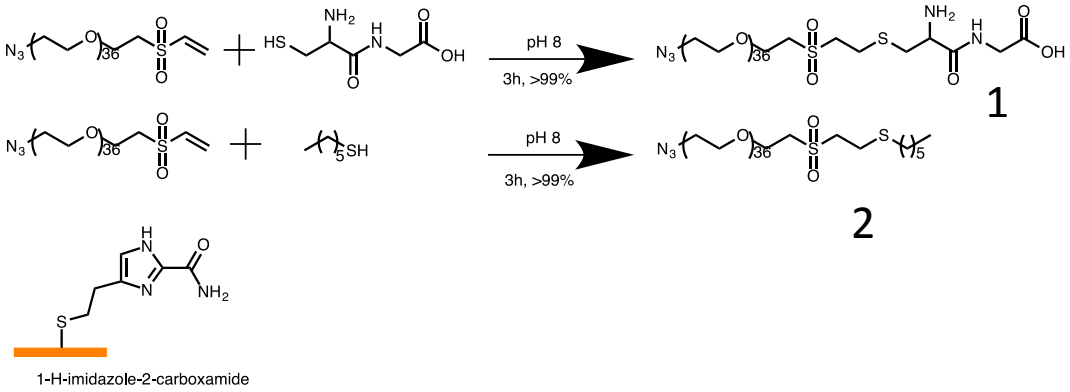

Scheme 2.3.1. Attachment of Cys-Gly and hexanethiol to vinylsulfone linker and attachment of ICA reader to Gold coated mica substrate.

As shown in Scheme 2.3.1, the peptide was first reacted with the linker, yielding a conjugate (**1**) containing an azide at its end, a functional group that was used for attaching the dipeptide to AFM tips through a alkyne-azide click reaction.[60] Inspection of the structure in scheme 2.3.1 suggests that the dipeptide could be capable of forming 3 or more hydrogen bonds (the primary amine will be protonated and the carboxylate deprotonated at neutral pH).

Meanwhile, a control molecule (**2**) containing an alkane chain at its end was synthesized by reacting the same linker with hexanethiol, which should have not have hydrogen bonding interactions with ICA.

An AFM tip functionalized with the dipeptide **1** was brought down to contact a surface coated with ICA and then retracted back, and force-distance curves were recorded. In each experiment, we collected one thousand five hundred curves. About 10% of these

showed evidence of an event involving stretching of the PEG linker. Of this subset, we retained only those curves that fitted a WLC extension curve14 with a contour length of 15±3 nm and for which the baseline force had returned close to 0 pN after the peak owing to non-specific interactions. An example of a force curve satisfying these criteria is shown in Figure S14a. We took over 500 force curves with the control molecule (2 is scheme 1) and none shown of these controls evidence of specific binding with all adhesion gone by 10 nm extension. We also measured the interactions of the dipeptide (**1**) with a bare gold surface finding no force curves in which the PEG tether was fully stretched.

Figure S14b shows a histogram of bond-breaking forces obtained from curves like those in Figure S14a using a probe of force constant 0.05 N/m (SiN probes from Veeco Probes) and a retraction speed of 700 nm/s.

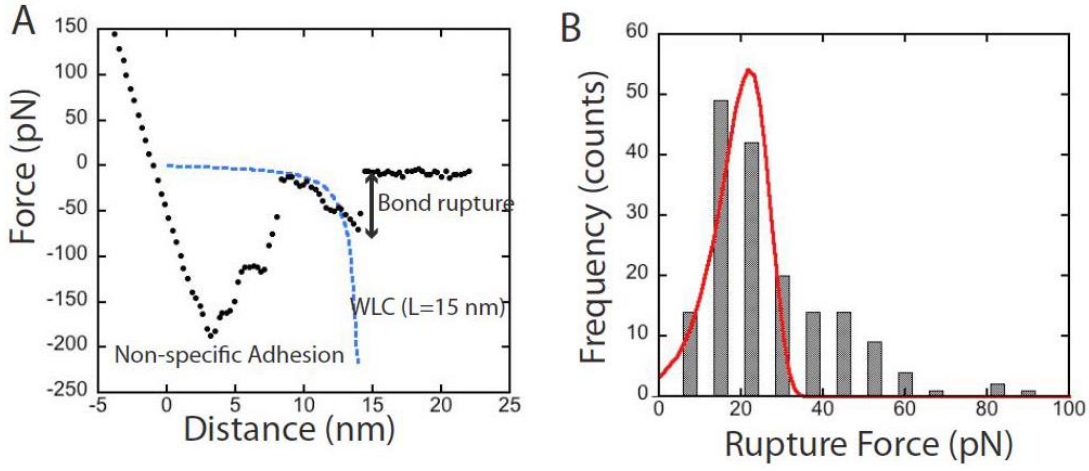

Figure23. Force spectroscopy of the glycine-ICA interaction. (a) Force curve showing a specific bond-rupture event consistent with stretching of the PEG linker of contour length 15 nm (blue dashed curve is a fit to the WLC model). (b) Histogram of the distribution of

bond-rupture forces for a retraction speed of 700 nm/s and a force constant of 0.05 N/m. The red solid line is a calculated distribution for two hydrogen bonds using parameter values from Fuhrmann et al.[89]

Using the data presented in Fuhrmann et al.[89], the modal breaking force for a complex involving 2 hydrogen bonds is about 22 pN, and this is consistent with the data shown in this histogram. More specifically, taking the force barrier, $fB = 1/\alpha$, to be 5.8 pN (using the value for γ=1 from Fuhrmann et al.[89]), the calculated distribution[90] is shown by the solid line. Clearly many of the events are consistent with two hydrogen bonds between the glycine and the ICA monolayer, though events at both lower and higher forces indicate that other bonding motifs are possible (and expected, given the structure of the peptide as discussed above).

2.3.3. Experimental details:

Synthesis of the dipeptide conjugate (1). To a solution of azido-$(CH2CH2O)_{36}$-vinyl sulfone (50 μL, 1.0 mM) in pH 8 phosphate buffer was added a solution of the dipeptide (50 μL, 20 mM) in pH 8 phosphate buffer. The reaction was stirred for 3hrs at room temperature, followed by RP-HPLC purification using a Zorbax C18 column on an Agilent 1100 HPLC equipped with an ELSD detector under a gradient of 10 to 80% Methanol in a 10 mM TEAA buffer (pH 7.0) over a period of 25 mins. The retention time of the desired product was 12.6 mins. The collected solution was lyophilized and characterized by MALDI-MS on a Voyager MALDI-TOF instrument. MS: m/z (M+H) calculated for $C_{29}H_{59+1}N_5O_{15}S$: 1948.28; found: 1948.01.

Synthesis of the control molecule (2). To a solution of azido-$(CH2CH2O)_{36}$-vinyl sulfone (50 μL, 1.0 mM) in DMSO was added a solution of hexanethiol (50 μL, 20 mM) in DMSO and triethylamine (1 μL). The reaction was stirred for 3 hrs at room temperature, followed by RP-HPLC purification using a Zorbax C18 column on an Agilent 1100 HPLC equipped with an ELSD detector under of gradient of 10 to 80% Methanol in a 10 mM TEAA buffer (pH7.0) over a period of 25 mins. The retention time of the desired product was 19.8mins. The collected solution was lyophilized and characterized by MALDI-MS on a Voyager MALDI-TOF instrument. MS: m/z (M+H) calculated for $C_{30}H_{63+1}N_3O_{12}S$: 1888.31; found: 1888.03

Attachment. Both dipeptide conjugate **1** and control **2** were attached to AFM tips (Veeco probes, Bruker, SiN tips, force constant 0.05 N/m) by an azide-alkyne click reaction using N-(3-(silatranyl)propyl)-2-(cyclooct-2-yn-1-yloxy)acetamide as an anchoring molecule in a two-step protocol as discussed earlier.

Functionalization of Gold substrates. Gold-coated mica substrates (Au(111), 2.4 x 1.6 cm2, Agilent Technologies) were immersed in a solution of ICA (0.1 mM) in absolute ethanol for 1day, followed by rinsing with ethanol and water, and used immediately for AFM measurement

AFM force measurement and data analysis. The force measurements were carried out at a loading rate of 35 nN/s on an Agilent 5500 AFM using functionalized tips against the ICA functionalized Gold substrates. Control experiments were performed using tips functionalized with the dipeptide conjugate **1** against the bare Gold substrate and tips functionalized with the control molecule **2** against the ICA coated Gold substrate. All the

experiments were carried out in 1X PBS buffer, pH 7.4. The force spectra were recorded using Agilent Picoview software.

2.3.4. Conclusion.

This experiment convincingly proves that a dipeptide attached to an AFM tip interacts with universal reader ICA. Hence it is highly expected that ICA would be able to interact with amino acids in an STM tunnel gap. The AFM experiment also demonstrates that very weak unbinding forces between a functionalized tip and the substrate can be measured using our chemistry to functionalize AFM tips.

2.4. A Three-Arm Scaffold Carrying Affinity Molecules for Multiplex Recognition Imaging by Atomic Force Microscopy

2.4.1. Introduction

One can conceive of using the recognition imaging for detection of low-abundance proteins in a biological sample. Compared to fluorescence microscopy, however, the AFM based recognition imaging lacks a multiplex capacity to detect multiple analytes in a single test. Wang et al. attempted to address the multiplexing issue by functionalizing AFM tips with an equimolar mixture of two types of antibodies.[91] This approach attaches the antibody molecules to the apex of an AFM tip completely by random chance. As a result, it only showed marginal success in the multiplex recognition imaging. The challenge has been how to tether two different affinity molecules to the AFM tip so that they can interact with their respective cognates with an equal probability. In the present study, we have developed a "recognition head" built on a three-arm linker that can carry affinity molecules and be connected to AFM tips for the multiplex recognition imaging

(mRI). As illustrated in Figure 1, when such a recognition head tethered to an AFM tip scans across a surface covered with proteins, the two affinity moieties are bought to contact with each of these individual molecules, which generates a recognition image to localize each of cognate proteins through the specific affinity interactions. To identify each of these proteins, one of the affinity moieties in the recognition head will be blocked, for example, with its cognate protein for a second scan over the same area. This would allow us to distinguish between two different proteins. Here, we report on synthesis of the recognition heads, their attachment to AFM tips, and implementation in detecting proteins.

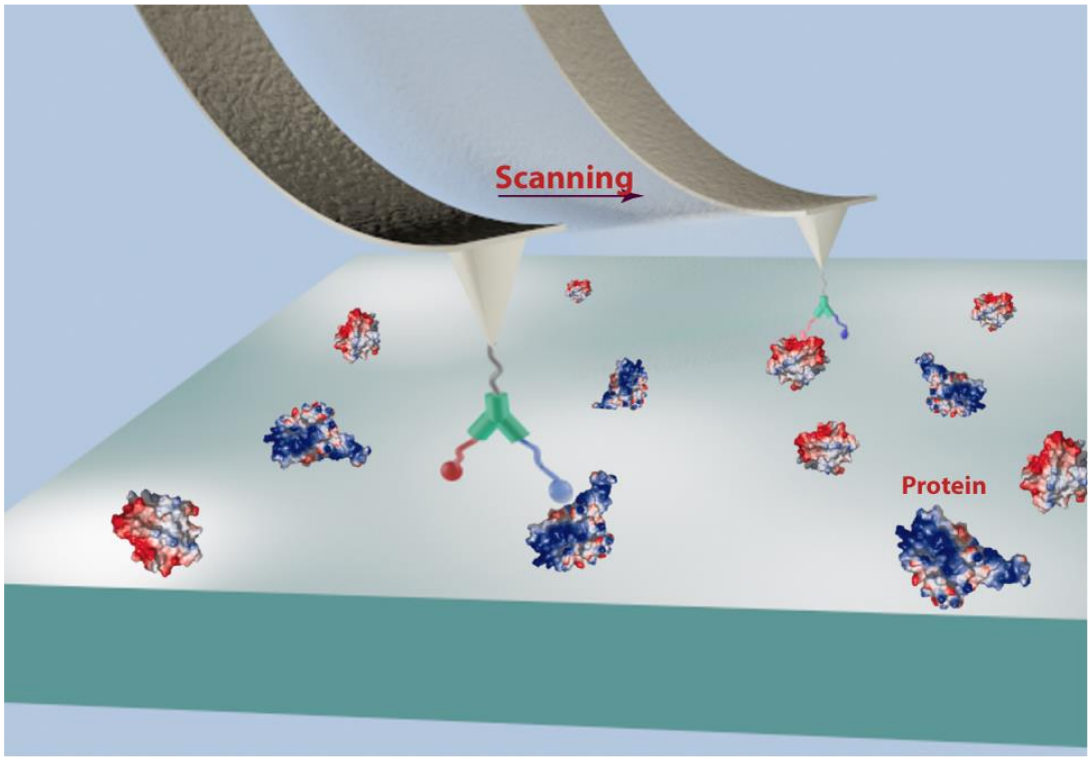

Figure 24. AFM tip functionalized with a recognition head containing two affinity molecules through a three arm linker.

2.4.2. Results and discussion

Three-Arm Linker. We devised a C3-symmetrical linking molecule with azide functional groups at its ends (Ar3, Scheme 2.4.1) as a scaffold for construction of the recognition heads. Although heterotrifunctional linkers are advantageous for orthogonal bioconjugation,[92,93] a homotrifunctional linker has the advantages of simpler synthesis and reduced structural variations at the linkage sites. We synthesized Ar3 by reacting 1,3,5-triethynylbenzene (1) with 1-azido-37-(4-iodophenyl)-3n_{36}[3]-dodecaoxaheptatriacontane under the Sonogashira coupling conditions (Reaction 1.1).[94] The product was obtained with a 35% yield, purified with column chromatography, and fully characterized with NMR, and mass spectrometry (see Experimental Section). The three-arm linker Ar3 features a rigid hard core flanked by three flexible poly(ethylene glycol) (PEG) chains with azido functions at their ends for the bioconjugation and attachment. In general, the recognition imaging requires a fairly long linker to tether the affinity molecule to an AFM tip so that it can keep the AFM tip away from a substrate for most of the measurement period. A PEG chain with 12−18 units of ethylene glycol meets this requirement and suffices to accurately locate the binding sites of analyte molecules immobilized on a surface.[85,95] This is why it is commonly used as a flexible linker for the recognition imaging. By contrast, we designed the three-arm linker differently by placing a sizable hard core in the center of the linker, attempting to reduce the flexible portion of the linker to a minimum without affecting the binding efficiency of the affinity moieties. Thus, the increased rigidity should reduce the loss in conformational and rotational entropy caused by binding to the target molecule(s) immobilized on the surface, which is

thermodynamically unfavorable.[96] We adapted tris(phenylethynyl)benzene due to its large π conjugating structure to increase the rigidity of the linker as well as to avoid the possible collision between two affinity moieties by pointing them in opposite directions. Meanwhile, we have to ensure that the linker has sufficient solubility for the following bioconjugating reactions. We found that three 12-unit PEG chains were needed to give the linker the solubility of ~0.1 mg/μL in aqueous solution when they were attached to the 4′ position of tris(phenylethynyl)benzene hard core (see Scheme 2.4.1).

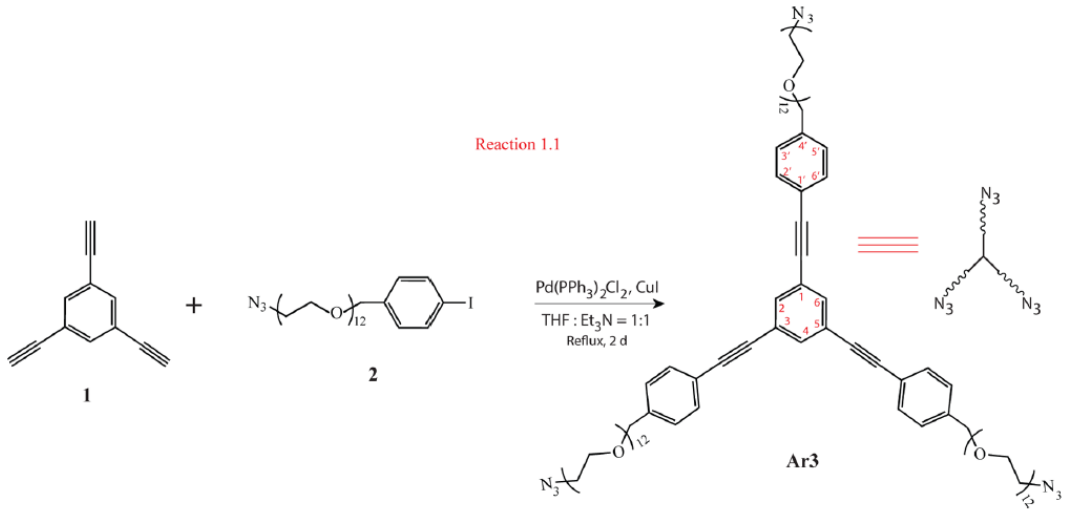

Scheme 2.4.1. Reaction for synthesis of Three-Arm Linker

Conjugating Affinity Molecules to the Three-Arm Linker. We have constructed two recognition heads: RH-1, which is composed of anti-VEGF[97] and anti-TNFα[98] DNA aptamers (Figure 23A), and RH-2, which is composed of antithrombin aptamer[80,99] and cyclo-RGDfK that binds to integrin receptors[100] (Figure 23B), for the mRI studies. These aptamers have nanomolar affinities to their respective cognate proteins (Kd: 403.6 nM for

anti-VEGF,[97] 7.0 nM for anti-TNFα,[98] 240 ± 16 for anti-thrombin[101]), and the cyclo-RGDfK binds to both intergrin $\alpha_5\beta_1$ and $\alpha_v\beta_3$ with IC50 of 133 and 2.6 nM.[102]

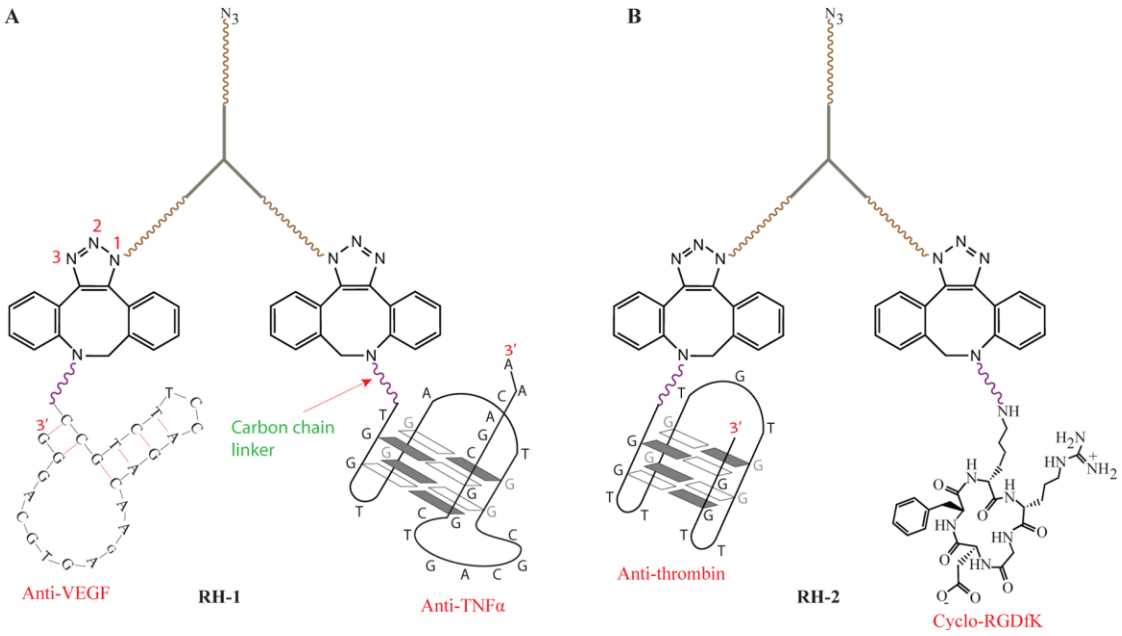

Figure 25. Chemical structures of Recognition heads

Previously, we demonstrated that both cyclo-RGDfK and antithrombin aptamer could effectively generate recognition images with their cognate proteins when they were attached to AFM tips through a linear linker.[60] Compared to antibodies, these affinity molecules are much smaller in size and chemically more robust, making them ideal candidates for construction of the recognition heads. To attach them to the three-arm linker, each of these custom-synthesized DNA aptamers was synthesized to bear a dodecylamino chain at their 5′-ends and the cyclopeptide contained a lysine residue. We converted them into aza-dibenzocyclooctyne (ADIBO) derivatives, named as ADIBO-anti-VEGF, ADIBO-anti-TNFα, ADIBO-anti-Thrombin, and ADIBO-cyclo-RGD, by reacting with ADIBO-Nhydroxysuccinimidyl ester (see experimental section). The

ADIBO group spontaneously reacts with azide in aqueous solution, known as catalyst-free click addition, which has allowed us to readily construct the recognition heads, as discussed below. We synthesized RH-1 with a route described in Figure 25.

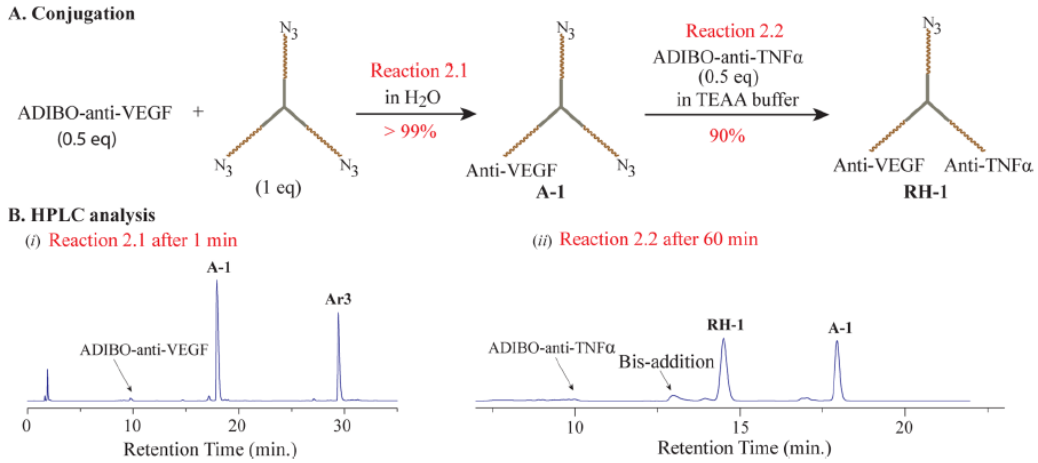

Figure 26. Synthesis of RH-1

First, ADIBO-anti-VEGF reacted with Ar3 with a ratio of 1:2 in water (Reaction 2.1 in Figure 25). Reverse Phase (RP) HPLC analysis indicated that the reaction was finished in less than 1min, forming a monoaddition product A-1 with a high yield (>99%, Figure 25B,i). We attribute the high selectivity to the solvent condition. In water, the negatively charges of an aptamer is much less shielded than in the buffered solution. Once one aptamer was attached to Ar3, the second addition of an aptamer stalled because of the electrostatic repulsion. A-1 was separated by HPLC and characterized as a pure product (see details in RH-1 of Experimental Section). It reacted with ADIBO-anti-TNFα (0.5 equiv) in a triethylammonium acetate (TEAA) buffer (Reaction 2.2), resulting in the desired product RH-1 with a yield of ~90% plus ~10% of a bis(anti-TNFα) byproduct (Figure 25B, ii). Beforehand, we had attempted to carry out the reaction in water, and

found out that it went so slowly that no significant amount of product was observed even after 1 h. We hypothesized that the charge repulsion prevented A-1 from reacting with the same negatively charged reactant ADIBO-anti-TNFα. A TEAA buffer was used for the reaction to shield the negative charges, giving us a fairly good selectivity (~90%) as mentioned above. RH-1 were separated by HPLC and characterized by MALDI mass spectrometer (see RH-1 in Experimental Section). RH-2 was synthesized by first reacting with peptide (ADIBO-cyclo-RGD) and then with aptamer ADIBO-antithrombin (Figure 26A). This route offered advantages over the other way around with better control over the addition of the affinity molecules to Ar3 and more easily separating the final products. As shown in Figure 26, the reaction 3.1 was well controlled at a monoaddition stage by applying an excess amount of Ar3 to it (Ar3 to ADIBO-cyclo-RGD = 5:1). RP HPLC analysis indicated that ADIBO-cyclo-RGD was consumed soon after these two starting materials were mixed in water, yielding two products with a ratio of 86% to 14% (Figure 26B, i). These two products could readily be separated by HPLC. MALDI mass spectrometry identified that the major product resulted from monoaddition of ADIBO-cyclo-RGD to Ar3 (A-2) and the minor product from the bis-addition. The following reaction was carried in water as well with a 25% excess of A-2 (Reaction 3.2). As shown in Figure 4B, ii, most of ADIBO-anti-thrombin was consumed in a minute. Extending the reaction to 30 min resulted in RH-2 with a 93% yield and a small amount of bis-addition byproduct (~7%), which was separated by HPLC and characterized with MALDI mass spectrometry (see RH-2 in Experimetnal Section for details).

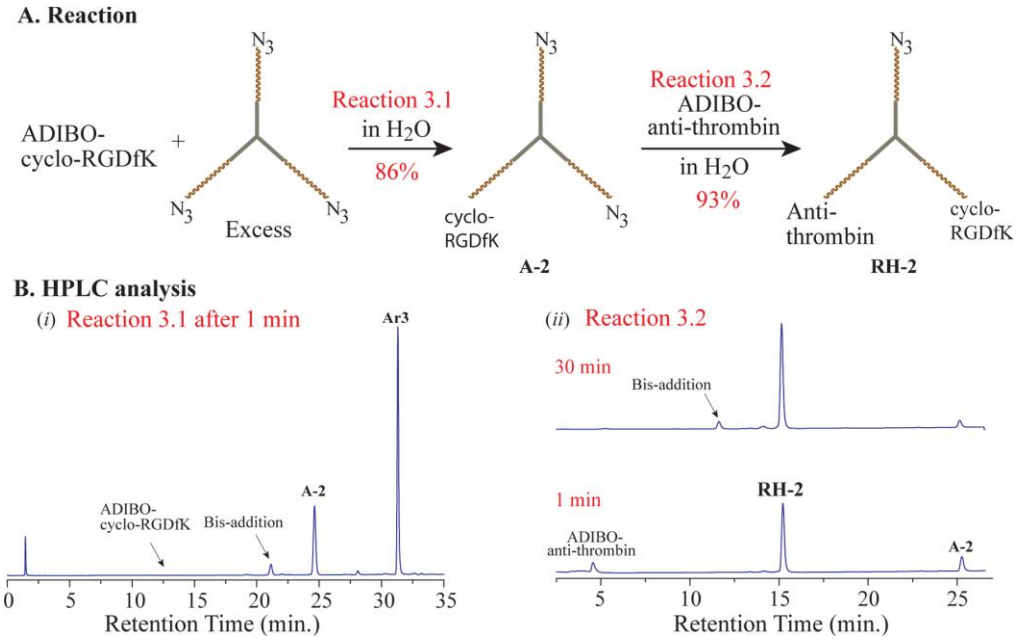

Figure 27. Synthesis of RH-2

In this section, we describe facile methods to synthesize a DNA−organic molecule−DNA (or peptide) conjugate with a high yield and high reaction rate by means of click chemistry. Lee et al. reported a three day reaction of amino functionalized DNA with N-hydroxysuccinimide (NHS) ester of 1,3,5-benzenetricarboxylic acid in DMSO/water, which only produced the desired product with a 10% yield.[103] They attribute such a low yield to a consequence of steric hindrance and electrostatic repulsion between DNA molecules. Interestingly, Seela and co-workers reported that a DNA containing a tripropargylamino side chain readily reacted with azido functionalized oligonucleotides in the presence of a copper catalyst.[104] Since the reaction was accelerated significantly in the presence of benzoic acid, we believe that reduction of the electrostatic repulsion may be a key factor for production of DNA−organic molecule−DNA hybrids with high yields. We have found utilization of Mg2+ to shield the negative charges of the DNA backbone

could produce the same effects as benzoic acid did (data not shown). Here, we demonstrate that the addition of charged molecules to the three-arm linker can be well controlled simply by changing the solvent. It should be noted that the ADIBO-azide reaction normally results in a regioisomeric mixture of the triazole connection. In our case, the affinity molecules were connected to Ar3 through either N-1 or N-3 of the triazole ring (see Figure 24). However, we have not observed that the subtle difference in structure exerts any significant effects on the recognition imaging (vide infra).

Attaching Recognition Heads to AFM Tips. We have previously developed a method to attach affinity molecules through a linear linker to AFM tips using a catalyst-free click reaction.[60] We adopted this method for attachment of these recognition heads. As illustrated in Figure 27, Ni-coated silicon tips (from Nanoworld particularly for recognition imaging) were first functionalized with a cyclooctyne function by reacting with a cyclooctyne derivative of 1-(3′-amino)propylsilatrane (3)[60] in aqueous solution, and then reacted with a recognition head in buffered solution (see Experimental Section for details).

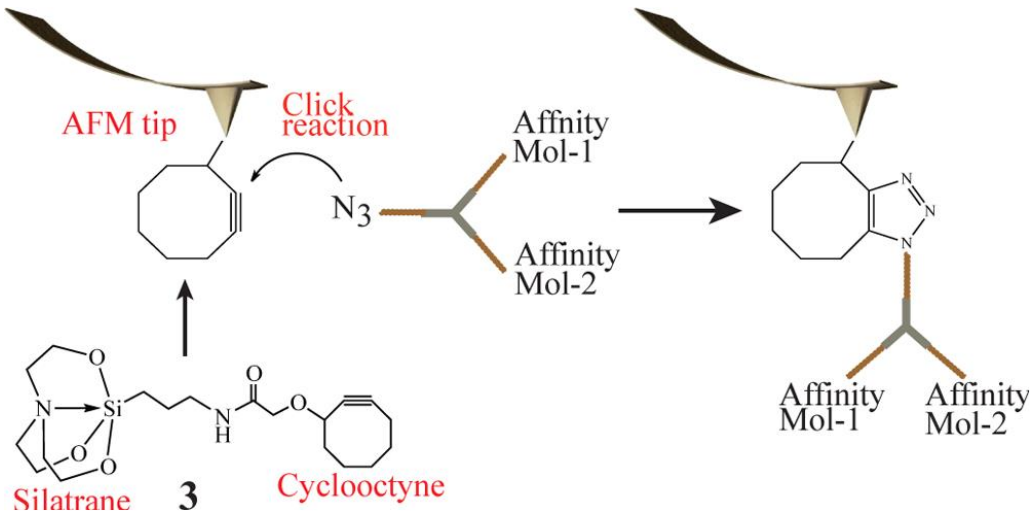

Figure 28. Attaching Recognition heads to AFM tips.

Since there is presently no effective way to characterize the covalent bonding on AFM tips, we attempted to provide evidence that there was a chemical attachment by means of force measurement. We measured the interacting forces of RH-1 attached to a silicon nitride tip with one of its cognate proteins VEGF. From the force−distance curves, we observe that the binding rupture occurred at a distance around 14 nm, which corresponds to the length of the recognition head plus other carbon chains, and the unbinding force was around 65 pN with a loading rate of 60 nN/s (Figure 29). This shows the existence of a recognition head on the AFM tip.

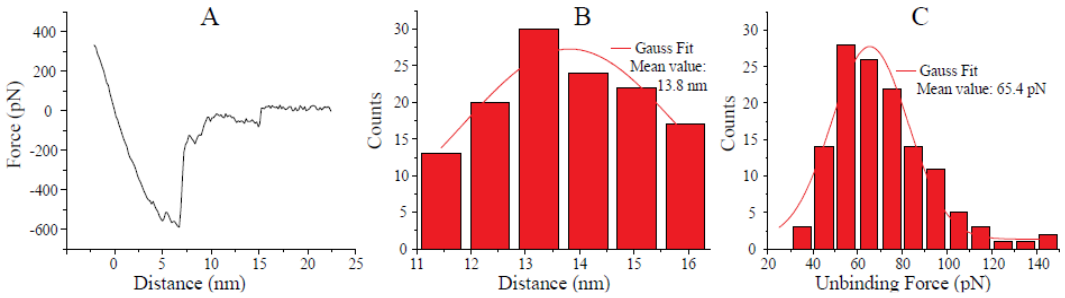

Figure 29. (A) Force−distance curve of a **RH-1** functionalized tip retracting from a VEGF immobilized mica surface; (B) Distance histogram of the unbinding events; (C) Force histogram of **RH-1** unbinding from VEGF immobilized on the mica surface.

Multiplex Recognition Imaging (mRI) of Proteins. We adapted a procedure reported by Wang et al.[91] to perform mRI experiments, which involves three sequential steps: (1) imaging a protein surface by driving an AFM tip carrying an recognition head across a 2 × 2 μm^2 area and recording the simultaneous topographic and recognition images; (2) injecting a first blocking solution to the liquid flow cell, and repeating the step 1 in the

same area; (3) injecting a second blocking solution to the cell and repeating the step 1 again. We first tested RH-1 on imaging its cognate proteins VEGF and TNFα. A 1:1 mixture of these two proteins in a phosphate buffer (pH 7.4) was deposited on a mica surface functionalized with glutaraldehyde. We have routinely used glutaraldehyde as a cross-linker to immobilize proteins for recognition imaging.[84] Using RH-1, we were able to generate recognition images from the VEGF-TNFα surface (Figure 30).

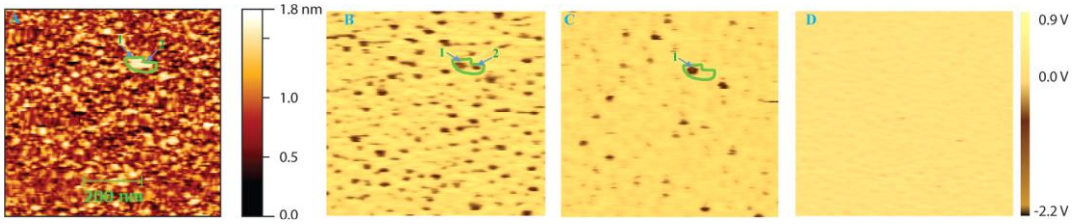

Figure 30. Topographic (A) and recognition (B) image of a VEGF and TNF-α mixture; (C) anti-VEGF aptamer-blocked recognition image; (D) both aptamers-blocked recognition image. Imaging size: 0.75 × 0.75 μm and all of recognition images have the same amplitude scale.

In general, the AFM based recognition imaging produces not only a recognition image, in which the recognition sites appear as dark spots, but also a topographic image simultaneously, in which each feature appears as white. From the topographic image (Figure 29 A), we can immediately notice a complex surface morphology, features of which vary in sizes and shapes. This may reflect differences in structures between VEGF and TNFα as well as effects of the surface chemistry, assuming that each feature represents either an individual protein or a protein aggregate. First, the crystal structures show that VEGF (PDB ID: 2VPF) has approximate dimensions of 6.5 × 3.5 × 2.0 nm,

flatter than TNFα (~5.9 ×5.5 × 4.8 nm, PDB ID: 1TNF). Also, both VEGF and TNFα have pI values very close to 7.0 (7.5 for VEGF and 7.4 for TNFα, calculated from http://protcalc.sourceforge.net), so they may easily form aggregates around neutral pH. Second, since glutaraldehyde mainly reacts with lysine residues (11 for VEGF and 5 for TNFα) and the N-terminal amines, the immobilization chemistry may result in each protein molecule displaying on the surface with different orientations. All of these factors may contribute to the complicated surface morphology of the VEGF and TNFα mixture, making it impossible to distinguish between these two proteins from the topography. However, the recognition image (Figure 29 B) seems more resolvable. This is because the recognition imaging only "sees" the binding site, a small portion of protein. As an example, the feature in the green circle in Figure 29 A could be an aggregate of multiple proteins according to its size (W × L × H = ~38 × 80× 1.6 nm). By examining the recognition image (the green circle in Figure 29 B), we can tell that the feature possibly consists of two protein molecules. The following blocking experiments allowed us to unambiguously assign the spot 1 as TNFα and spot 2 as VEGF (to be discussed in the next paragraph). Furthermore, we counted those spots both in Figure 29 A,B, and found that there were about 80% features in Figure 29 A recognized as protein by RH-1. This recognition rate is consistent with our previous results from using AFM tips functionalized with one type of affinity reagent.[60] Since the purity of the protein materials in this study was greater than 95%, we believe that the immobilization chemistry placed a statistical limit on the recognition efficiency because glutaraldehyde randomly reacted with amines of proteins, rendering some of the binding sites blocked by the mica surface

and not reachable by the affinity moieties. Following the first scan, a VEGF solution was injected into the flow cell to block the anti-VEGF aptamer attached to the AFM tip, and the same surface area was scanned again to acquire a second recognition image (Figure 29 C). By comparing with Figure 29 B, we can clearly see that the spot 1 remained and spot 2 disappeared in Figure 29 C. As a result, we could assign these two spots to the corresponding proteins. Presumably, all of the spots in Figure 29 C resulted from the anti-TNFα aptamer interacting with the TNFα protein. To confirm this, a TNFα solution was injected into the flow cell, which resulted in an image with no recognition (Figure 29 D). The above results demonstrate that the two aptamers of RH-1 can specifically interact with their respective cognate proteins, subject to no interference from each other. To further confirm the specificity of RH-1, we scanned a 1:1 mixture of thrombin and streptavidin deposited on the mica surface, which resulted in no recognition image. Therefore, we assign those spots in Figure 29 C as the protein TNFα with high confidence. By superimposing the image C on B we created a superimposed recognition image from which we identified all of protein spots in the first recognition image (Figure 30 A). In figure 30 A black topped-by-green spots correspond to the TNFα protein and the rest of black spots to the VEGF protein. By counting the green and black spots we determined that the ratio of VEGF to TNFα on the surface is about 0.9:1, close to that in the parent solution (1:1). To further test RH-1, we deposited a solution of VEGF and TNF-α mixed in a 5:1 ratio on the mica surface, and found that the recognition efficiency of RH-1 was still about 80%. In the same fashion as described above, a superimposed image was created for identification of individual proteins (Figure 31 B). Figure 31 B

shows the superimposed image, from which we can clearly see there are less green spots, compared to Figure 30 A. The ratio of VEGF to TNFα on the surface was determined as ~5:1 by counting those black and green spots in Figure 31 B.

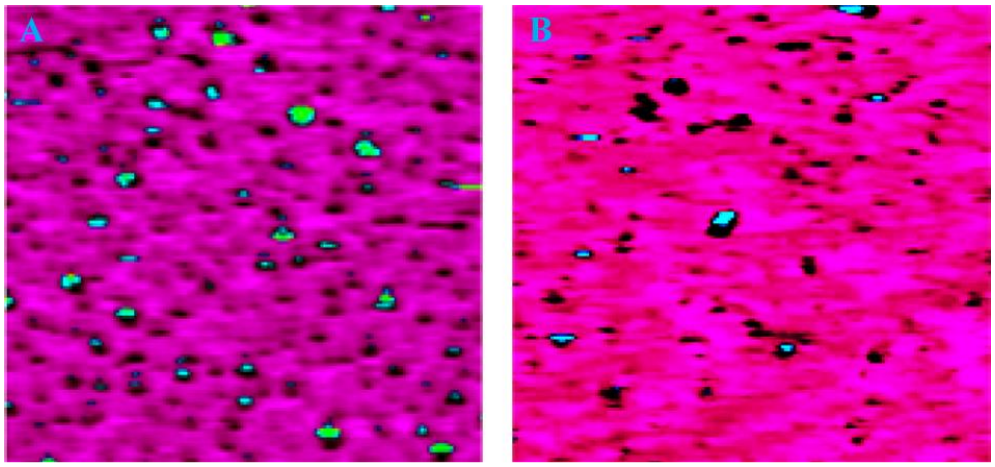

Figure 31. Superimposed recognition images in (A) VEGF and TNF-α (1:1 in solution) deposited on the mica surface, and (B) from a mixture of VEGF and TNF-α (5:1 in solution) deposited on the mica surface. Black topped-by-green spot, TNF-α protein; black, VEGF protein. Imaging size: 0.75 × 0.75 μm.

We further tested RH-1 on a more complex mixture consisting of four proteins VEGF, TNF-α, thrombin, and streptavidin. First, we examined the specificity of mRI by performing a series of control experiments: using a RH-1 tip to scan a mica surface modified with a 1:1 mixture of thrombin and streptavidin, which only yielded a topographic image (Figure 32 A), but no recognition image (Figure 32 A′); using a bare AFM tip and a tip functionalized with the cyclooctyne 3 to scan a surface modified with a VEGF and TNFα mixture, which again only yielded topographic images (Figure 32 B and 32 C), and no recognition images (Figure 32 B′ and 32 C′). When scanning a mica

surface on which a mixed solution of four proteins (VEGF/TNFα/thrombin/streptavidin = 1:1:2:1.5) was deposited, we were able to obtain both topographic and recognition images (Figure 32 D, D′) using a tip functionalized with RH-1.

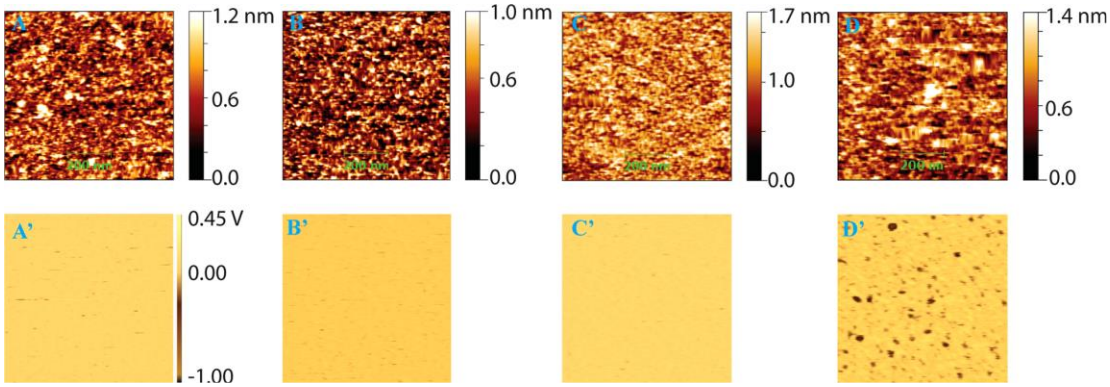

Figure 32. AFM images with different tips and substrates. Top panel: topographic image of (A) a tip functionalized with RH-1 against a 1:1 mixture of thrombin and streptavidin deposited on mica; (B) a bare tip against a 1:1 mixture of VEGF and TNF-α deposited on mica, (C) a tip functionalized with cyclooctyne against a 1:1 mixture of VEGF and TNF-α deposited on mica, (D) a tip functionalized with RH-1 against a mixture of VEGF, TNF-α, thrombin and streptavidin deposited on mica. Bottom panel: recognition image of A′ relating to topographic image A, B′ to B, C′ to C, and D′ to D. All of recognition images have the same amplitude scale. Imaging size: 0.75 × 0.75 μm.

There were 26% of proteins in Figure 831 D recognized, a 72% recognition rate which is slightly smaller than what we have had from the mixture of two proteins. The recognition specificity was confirmed by blocking experiments. In the same manner as described above, the ratio of VEGF/TNFα on the surface was determined as 1.5:1, higher than that

in their parent solution. Nonetheless, this is the first demonstration that the recognition imaging is able to detect multiple proteins in such a complex mixture.

Next, we tested RH-2 for mRI with a 1:1 mixed solution of thrombin and integrin α5β1 deposited on the mica surface. Similarly, RH-2 yielded a recognition image with 80% of protein in the topographic image recognized (Figure 33 A, B). From the superimposed recogntion image (Figure 33 E) generated by overlapping the image C over B in Figure 33, we determined the ratio of thrombin to integrin α5β1 on the surface as 1:0.9. Note that those pale yellow spots in the recognition image C and D in Figure 33 may be caused by the spillover of amplitude from topographic image to recognition image.[57]

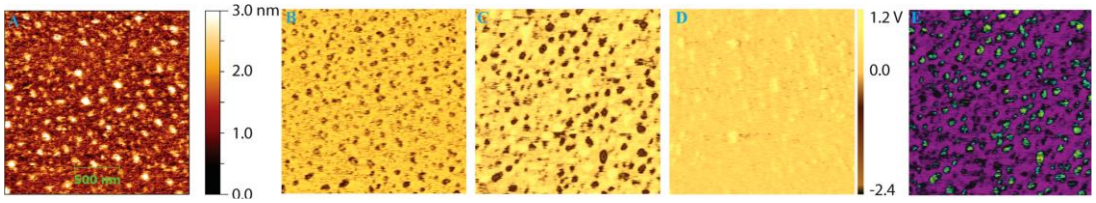

Figure 33. Topographic (A) and recognition (B) image of a thrombin and integrin α5β1 mixture; (C) recognition image from blocking anti-thrombin aptamer; (D) recognition image from blocking both aptamer and RGD; (E) superimposed recognition image of C over B. Black topped-by-green spot, integrin; black, thrombin. Imaging size: 2 × 2 μm and all of recognition images have the same amplitude scale.

Further, we also notice that the measured ratios in all the cases varied from those in the sample solutions more or less. To fully understand the discrepancies, thus, further studies are needed on molecular immobilization and on thermodynamic and kinetic effects on interactions of the affinity molecule tethered to an AFM tip with its cognate protein immobilized on the surface.

2.4.3. Experimental details

General Information. All reagents and solvents were purchased from commercial suppliers (Sigma-Aldrich, Alfa Aesar, Fluka, TCI America) and used as received unless otherwise noted. ADIBO-*N*-hydroxysuccinimidyl ester was purchased from Click Chemistry Tools. All experiments requiring anhydrous conditions were performed in flame-dried glassware under nitrogen atmosphere. Reactions were monitored by thin layer chromatography (TLC) using silica gel precoated on glass plates (EMD Millipore). ^{1}H NMR and ^{13}C NMR spectra were recorded on Varian INOVA 400 (400 MHz) spectrometer at 25 °C. Chemical shifts (δ) are given in parts per million (ppm) and referenced to the residual solvent peak ($CDCl_3$, δH = 7.26 ppm; CD_3OD, δH = 3.31 ppm; DMSO-d6, δH = 2.50 ppm). Coupling constants (J) are expressed in hertz (Hz) and the values are rounded to the nearest 0.1 Hz. Splitting patterns are reported as follows: br, broad; s, singlet; d, doublet; dd, doublet of doublets; t, triplet; dt, doublet of triplets; q, quartet and m, multiplet. High-resolution mass spectra (HRMS) were acquired at the Arizona State University CLAS High Resolution Mass Spectrometry Facility. Flash chromatography was performed in an automated flash chromatography system (CombiFlash Rf, Teledyne Isco, Inc.) with silica gel columns (60−120 mesh). RP-HPLC analysis and separation were performed with either a Zorbax C-18 column or with Zorbax 300 SB-C18 column (4.6 × 150 mm, particle size 5 μm) in an Agilent 1100 HPLC equipped with UV monitor and fraction collector. VEGF (Vascular Endothelial Growth Factor, Human Recombinant,95%), a lyophilized product from a concentrated (1 mg/mL) solution with no additives, TNFα (Tumor Necrosis Factor-Alpha, Human

Recombinant, 95%), a lyophilized product from 1 mg of TNF-α Human contain 20 mM PB, pH-7.2, and 100 mM NaCl were purchased from ProSpec; Integrin from Yo proteins AB (Sweden), a lyophilized product from a solution containing 0.26 mg/mL α5β1, 20 mM Tris-HCl pH 7.5, 150 mM NaCl, 2 mM MgCl2, 0.2% Triton X-100. They were reconstituted by dissolving in water before use according to manufacture recommendation. Human α-thrombin and streptavidin were purchased from AbCam and Alfa Aesar, respectively. Recognition imaging was performed on Agilent's MacMode AFM equipped with a PicoTREC system, and silicon tips purchased from NanoWorld. The cantilever was made having length of 125 μm, width of 35 μm, and thickness of 800 nm with a force constant of 0.14 N/m. Its backside was coated with 1 nm Ti/40 nm Ni.

Synthesis of 1-Azido-35-((4-iodobenzyl)oxy)-3n33^3-undecaoxapentatriacontane (2). The compound 1 A was synthesized following a route described in Scheme 2.4.2. The starting material was synthesized following protocol outlined in section 2.4.1.

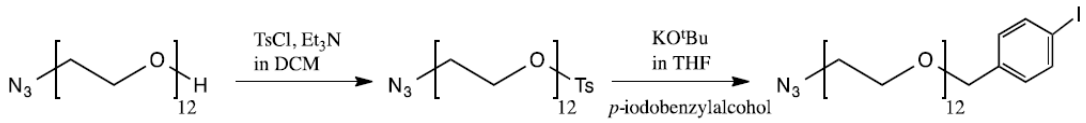

1 A **1 B** **2**

Scheme 2.4.2. Synthesis of compound 2.

Special note on nomenclature: To avoid excessive use of a long series of numbers, the mathematical shorthand for expressing arithmetic progressions is used to denote the positions of oxygen atoms in the elongated PEG chains, as proposed by Hii and coworkers.[73]

1-Azido-35-tosyloxy-3n33^3-undecaoxapentatriacontane (1 B). Tosyl Chloride (TsCl,

1.67g, 8.76 mmol) was added to a solution of 35-azido-3n33^{3}-undecaoxapentatriacontan-1-ol (**1 A**, 2.5g, 4.38 mmol) and triethylamine (Et3N, 3 mL, 21.53 mmol) in anhydrous dichloromethane (DCM, 15 mL) under nitrogen. The reaction mixture was stirred at room temperature for 12 h, and then the solvent was removed by rotary evaporation. The residue was purified by silica gel column chromatography using a gradient of 3.5% methanol in dichloromethane over 4 h, giving compound **1 B** as a colorless liquid (2.86 g, 90% yield). ^{1}H NMR (400 MHz, $CDCl_3$): δ 2.97 (s, 3 H); 3.37 (t, 2 H, J = 5.2 Hz); 3.58-3.3.69 (m, 44 H); 4.51 (t, 2 H, J = 4.8 Hz); 7.35 (d, 2H, J = 8 Hz); 7.79 (d, 2 H, J = 8 Hz); **^{13}C NMR** (100MHz, $CDCl_3$): δ 144.71, 132.92, 129.76, 127.85, 70.61-70.40, 69.92, 69.21, 68.54, 50.57, 21.54, HRMS m/z (M+H): found 726.3472; calcd. for $C_{31}H_{55+1}N_3O_{14}S$ 726.3483.

1-Azido-35-((4-iodobenzyl)oxy)-3n33^{3}-undecaoxapentatriacontane (2). Potassium-*tert*butoxide ($KO^{t}Bu$, 482.5 mg, 4.30 mmol) was added to a solution of **1 B** (2 g, 2.76 mmol) and *p*-iodobenzylalcohol (0.84 g, 3.59 mmol) in anhydrous tetrahydrofuran (THF, 4 mL) under nitrogen. The mixture was stirred at room temperature for 2 h, cooled down in an ice bath, and quenched by the addition of methanol (2 mL). The solvent was removed by rotary evaporation, and the residue was separated by silica gel column chromatography using a gradient of 3.5% methanol in dichloromethane over 4 h. Compound **2** was obtained as yellowish oil (1.85 g, 85%). ^{1}H NMR (400 MHz, $CDCl_3$): δ 3.30 (t, 2H, J = 5.2 Hz); 3.57-3.58 (m, 46H); 4.42 (s, 2H); 7.02 (d, 2H, J = 8Hz); 7.57 (d, 2H, J = 8.4 Hz); ^{13}C NMR (100MHz, $CDCl_3$): δ 138.00, 137.26, 129.45, 92.84, 72.32, 70.54-70.40, 69.91, 69.50, 50.54; HRMS m/z (M+Na): found 810.2642,

calcd. for $C_{31}H_{54}N_3O_{12}I$+Na 810.2650.

Synthesis of 1,3,5-Tris{[4-(1-azido-3n36^3-dodecoxaheptatriacontyl)phenyl]ethynyl}benzene (Ar3). 1,3,5-Triethynylbenzene (1, 62 mg, 0.41 mmol) and compound 2 (1.0 g, 1.27 mmol) were mixed in anhydrous tetrahydrofuran (7.5 mL) and triethylamine (7.5 mL) under nitrogen. The solution was degassed by slowly bubbling nitrogen for 10 min, to which bis(triphenylphosphine)palladium(II)dichloride (14.4 mg, 0.02 mmol) and copper(I) iodide (3.9 mg, 0.02 mmol) were added. The mixture was refluxed for 48 h, cooled to room temperature, and filtered. The solvent was removed by rotary evaporation. The residue was separated by silica gel column chromatography with a gradient of 4% methanol in dichloromethane over 4 h. The product Ar3 was obtained as a yellowish oil (307 mg, 35%). ^{1}H NMR (400 MHz, $CDCl_3$): δ 3.36 (t, J = 5.2 Hz, 6H, N_3CH_2); 3.62−3.68 (m, 138H, OCH_2CH_2O); 4.58 (s, 6H, $ArCH_2$); 7.33 (d, J = 8.4 Hz, 6H, ArH); 7.49 (d, J = 8.4 Hz, 6H, ArH); 7.62 (s, 3H, ArH). ^{13}C NMR (100 MHz, $CDCl_3$): δ = 139.03, 133.97, 131.68, 127.58, 124.02, 121.90, 90.43, 87.75, 72.79, 70.68−70.56, 70.01, 69.66, 50.67. MALDI-MS (M + Na): found m/z 2152.51; calcd for $C_{105}H_{165}N_9O_{36}Na$ 2152.46.

General procedure for functionalization of DNA aptamers with ADIBO.

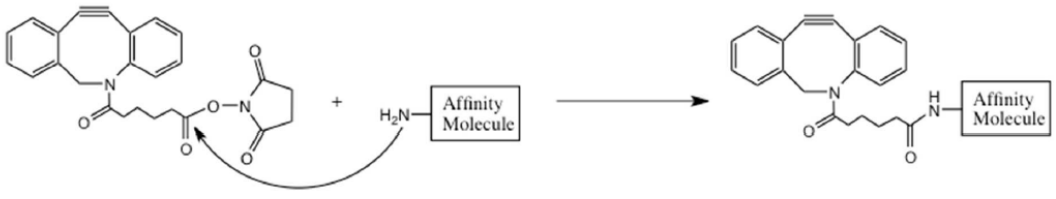

Scheme 2.4.3. ADIBO functionalization of DNA aptamers

ADIBO derivatives of aptamers were synthesized by a reaction described in Scheme 2.4.3. In detail, a stock solution of 5'-dodecylamine-modified DNA aptamer in water (1.0 mM, 10 μL) was diluted with a 100 mM phosphate buffer (30 μL), pH 8.5. The final pH measured 8.4. To the DNA aptamer solution, a DMSO solution of ADIBO-NHS ester (10 mM, 80 μL) was added. The mixed solution was vortexed for 15 min at room temperature, and then lyophilized. The solid residue was re-dissolved in water (120 μL) and centrifuged. The supernatant that contained the product was separated from the ADIBO precipitate. RP-HPLC analysis indicated that the aptamer was quantitatively converted to its ADIBO derivative. The product was purified using RP HPLC with an eluting system composed of (A) TEAA buffer (10 mM, pH 7) and (B) acetonitrile. The mobile phase started at 90% A and 10% B, linearly increasing to 60% B in 25 min, followed by increasing B to 100% in 5 min. The retention times for the ADIBO derivative of anti-Thrombin aptamer (ADIBO-anti-Thrombin) was 11.6 min, for the ADIBO derivative of anti-VEGF aptamer (ADIBO-anti-VEGF) was 11.0 min, for the ADIBO derivative of anti- TNFα aptamer (ADIBO-anti-TNFα) was 10.1 min. The collected fractions of the product were lyophilized, reanalyzed with HPLC and characterized by MALDI-mass spectrometry:

ADIBO-anti-Thrombin MALDI m/z: found 5307.3; calcd. for $C_{183}H_{230+1}N_{59}O_{99}P_{15}$: 5305.7

ADIBO-anti-VEGF MALDI m/z: found 8272.8; calcd. for $C_{276}H_{348+1}N_{101}O_{151}P_{25}$: 8271.7

ADIBO-anti-TNFα MALDI m/z: found: 8364.4; calculated for $C_{278}H_{348+1}N_{105}O_{152}P_{25}$: 8367.7

3. ADIBO derivative of cyclo-RGD. A solution of cyclo-RGDfK peptide in water (1.0 mM, 10 μL) was diluted with a 100 mM phosphate buffer (30 μL), pH 8.5. To the solution, a DMSO solution of ADIBO-NHS ester (80 μL, 10 mM) was added. The mixed solution was vortexed for 15 min at room temperature, and then lyophilized. The residue was re-dissolved in water (50 μL) and centrifuged. The supernatant was separated from the ADIBO precipitate. RP-HPLC analysis indicated that the peptide was quantitatively converted to its ADIBO derivative. The product was purified using RP HPLC with an eluting system composed of (A) 0.1% TFA in DI water and (B) 0.09% TFA in 80:20 acetonitrile:water. The retention time of the product in RP HPLC was 14.6 min with a mobile phase started at 80% eluent A and 20% eluent B, linearly increasing to 70% B in 25 min, followed by increasing B to 100% in 5 min.The ADIBO-RGD derivative was characterized by MALDI-mass m/z: found 919.8; calcd. for $C_{48}H_{58+1}N_{10}O_9$: 920.0

RH-1. A solution of Ar3 in water (400 μM, 30 μL) was added to a solution of ADIBO-anti-VEGF in water (200 μM, 30 μL). After 1 min, the reaction was checked by injecting 1 μL of the reaction solution into RP-HPLC. The HPLC analysis indicated that the aptamer was fully consumed and a new peak appeared at a retention time of 18.0 min in the chromatogram (eluent A, 10 mM TEAA buffer, pH 7; eluent B, acetonitrile; under a linear gradient of increasing B from 10 to 70% in 25 min). The monoaddition product A-1 was separated using HPLC with the same eluting system. MALDI-MS (M + H): found m/z 10401.8; calcd for $C_{381}H_{513+1}N_{110}O_{187}P_{25}$ 10402.2. Next, A-1 (150 μM, 15 μL) was mixed with ADIBO-anti-TNFα (75 μM, 15 μL) in a TEAA buffer (50 mM, pH 7).

The reaction was kept at room temperature for 1 h and separated using the same HPLC conditions for the monoaddition product. RH-1 has retention time of 14.5 min. MALDI-MS (M + H): found m/z 18768.6; calcd for $C_{659}H_{861+1}N_{215}O_{339}P_{50}$ 18766.7.

RH-2. A solution of Ar3 in water (1.0 mM, 30 μL) was added to a solution of ADIBO-cycloRGD in water (0.2 mM, 30 μL). The solution was checked by HPLC after 1 min. RP-HPLC analysis indicated that the peptide was completely consumed and a new peak appeared at retention time of 25.1 min in the chromatogram under the same elution conditions as the one for RH-1. The monoaddition product A-2 was separated by HPLC. MALDI-MS (M + H): found m/z 3050.2; calcd for $C_{153}H_{223+1}N_{19}O_{45}$ 3049.5. A-2 (100 μM, 15 μL) was mixed with ADIBO-anti-thrombin (80 μM, 15 μL) in water. The reaction was stirred at room temperature for 30 min. RH-2 was separated by RP HPLC under the same conditions mentioned above. The product has retention time of 15.1 min. MALDI-MS (M + H): found m/z 8349.2; calcd for $C_{336}H_{453+1}N_{78}O_{144}P_{15}$ 8354.2.

Attaching Recognition Heads to AFM Tips. AFM tips (a batch of four) were first soaked in ethanol in a Petri dish for 5 min, dried with nitrogen, and then treated with oxygen plasma (medium power) for 2 min in a Harrick Plasma Cleaner and then with ultraviolet-ozone in a Boekel UV cleaner for 5 min. These tips were immersed in an aqueous solution of N-(3-(silatranyl)propyl)-2-(cyclooct-2-yn-1-yloxy)acetamide (3, 50 mM) in a Petri dish. After 1 h, the tips were taken out, rinsed with water thrice, and dried gently with a nitrogen flow. In a humid surrounding, the cyclooctyne-functionalized tips were placed in a Petri dish and a recognition head solution (10 μM, 20 μL) in 1× PBS buffer (pH 7.4) was added to cover all the tips. After 1 h, the tips were rinsed thrice with

the same buffer and used immediately for AFM measurements. However, the probes can be stored in 1× PBS buffer (pH 7.4) at 4 °C at least for 2 days. Normally, there were about 50% of them that worked effectively for recognition experiments in every batch of 4 to 5 functionalized tips

Protein Immobilization. First, a mica surface was functionalized following an APTES/glutaraldehyde procedure developed in our laboratory.[84] Then, a protein solution (3 μL) was added to the glutaraldehyde-coated mica in a humid chamber, incubated for 30 min, rinsed with a 1× PBS buffer (pH 7.4) three times, and immediately placed on the AFM stage for use. The following solutions were used for the study:

A mixed solution of VEGF and TNF-α (0.35 nM each)

A mixed solution of VEGF (0.48 nM) and TNF-α (0.1 nM)

A mixed solution of VEGF (0.1 nM), TNF-α (0.1 nM), thrombin (0.2 nM) and streptavidin (0.15 nM)

A mixed solution of thrombin (0.28 nM) and streptavidin (0.28 nM)

A mixed solution of integrin α5β1 and thrombin (0.3 nM each).

Multiplex Recognition Imaging. AFM images were acquired by PicoTrec using magnetically (Ni) coated cantilevers in AC (MAC) mode operation with AC frequency at 8 kHz, set point of 4 V, and a scan speed of 2.2 μm/s. For imaging with RH-1 functionalized tips, the protein deposited on the mica surface was covered with 1× PBS buffer (pH 7.4, 600 μL). After initial scanning, a first blocking solution (0.3 nM VEGF in 1× PBS buffer, pH 7.4, 50 μL) was injected to the flow cell, incubated for 10 min, and followed by scanning in the same area. A second blocking solution (0.6 nM TNF-α in 1×

PBS buffer, pH 7.4, 50 μL) was injected into the flow cell, incubated for 10 min, followed by scanning in the same area. Four samples were examined with RH-1: two mixed solutions of VEGF and TNFα, respectively, with 1:1 and 5:1 molar ratios, a mixed solution consisting of VEGF, TNF, thrombin, and streptavidin with a ratio of 1:1:2:1.5, and a mixed solution of thrombin and streptavidin with a 1:1 molar ratio. For imaging with RH-2 functionalized tips, a mixed solution of thrombin and integrin α5β1 with a 1:1 molar ratio was deposited on the mica surface and covered with 1× PBS buffer containing 1 mM $MnCl_2$ (pH 7.4, 600 μL). The experiment was carried out in the same way as described above, and two blocking solutions, integrin (0.2 nM in 1× PBS buffer, pH 7.4, 50 μL) and thrombin (0.15 nM in 1× PBS buffer, pH 7.4, 50 μL), were used sequentially. Note: in some cases, injection of additional blocking solution (50 μL) was needed in order to achieve the effective blocking.

Force measurement. Force spectroscopy experiments were carried out in PBS 1x buffer (pH 7.4). For force measurements, Veeco probes (Bruker, SiN) tips were used having a force constant of 0.15 N/m and a gold black coating, and the loading rate was 60 nN/s. Vegf protein (270 nM) was immobilized on glutaraldehyde functionalized mica. Initially 800 force-distance curves were collected with RH-1 functionalized tips against Vegf following which tips were blocked with VEGF protein (2.7 nM, 50 μL in 1X PBS buffer, pH 7.4) and 500 more force-distance curves were collected. The force curves were analyzed in PicoView, and the specific unbinding forces (between 10-16 nm) were plotted in a histogram form and fitted into the Gaussian function using software

OriginPro 2015, in which the Levenberg–Marquardt algorithm was used for the curve fitting.

Data Analysis. All of the topographic and recognition images, and force spectra were recorded using Agilent PicoView software. Topography images presented in the manuscript were processed in Gwyddion software. Those spots were counted as proteins with a threshold around 1 nm. The recognition images were analyzed using Picoview. Background noises of the recognition images were scaled about −50 mV. Typical recognition events were observed to have intensity between −100 mV and −1.2 V. To determine the recognition rates, topography and recognition images were saved as image files and superimposed in Adobe Photoshop. The numbers of unrecognized and recognized proteins were manually counted from the superimposed image. In the same fashion, individual proteins were identified by image superimposing and manually counting.

2.4.4. Summary

In the present study, we have developed a new approach to using AFM for multiplex recognition imaging. With a recognition head attached to an AFM tip, we were able to scan multiple proteins immobilized on a surface. The recognition head was designed based on a hypothesis that two affinity molecules connected by a well-spaced linker should interact with their respective cognate molecules effectively. Our studies have shown that the affinity molecules tethered to the three-arm linker worked independently and equally, which allowed us not only to identify two different proteins but also to relatively quantitate them by counting.

CHAPTER 3

MOLECULAR TROJAN HORSE TO TARGET ADVANCED WEST NILE VIRUS INFECTION

3.1. Introduction

The West Nile virus (WNV), a mosquito born flavivirus, is a neurotropic, enveloped virus with a single-stranded, positive polarity, 11-kilobase RNA genome and has circulated in Africa, Asia, the Middle East, and Europe before entering USA in 1999 and had spread over all of continental USA by 2000.[105-107] Numerous cases have been diagnosed over the past decade and many infected people remain undiagnosed. Currently more than 2000 cases get reported to the CDC each year in the USA. However, in spite of considerable efforts an effective therapeutic is yet to be discovered.

The WNV viral lifecycle starts by attachment of the virus to an yet to be identified cellular receptor[108] following which the virus undergoes endosomal fusion and structural rearrangement of E glycoproteins and insertion of the hydrophobic fusion loop into the vesicular membrane.[108,109] In absence of data for human pathogenesis, animal models have aided our understanding about West Nile virus infection and disease.[108] Upon transmission from infected mosquitoes the virus is believed to replicate within keratinocytes and dendritic cells following which dendritic cell migration to lymph nodes leads to viral replication and transmission into peripheral organs following which the final deadly stage involves neuroinvasion and infection of the CNS [108,110] where it leads to severe malaise and death. Humoral response is extremely crucial against West Nile infection and disease.[111,112] Most neutralizing antibodies bind to viral surface E proteins

thus preventing receptor attachment and virus internalization.[112-116] Most potent neutralizing antibodies so far studied has been found to bind with the DIII domain of the E-glycoprotein.[108,112] Of these the E16 is the most potent and well characterized neutralizing antibody.[109,117] Humanized murine E16 and humanized plant E16 (hE16) has shown high efficacy and is shown to protect mice even four days after infection.[107,117] However once the infection gets transmitted to the CNS, the effectivity of E16 gets limited as the antibody is unable to cross the Blood Brain Barrier (BBB).[107]

Hence, we devised a new structure based on a molecular Trojan horse approach[21-23] for delivery of hE16 or monoclonal antibodies in general into the CNS.

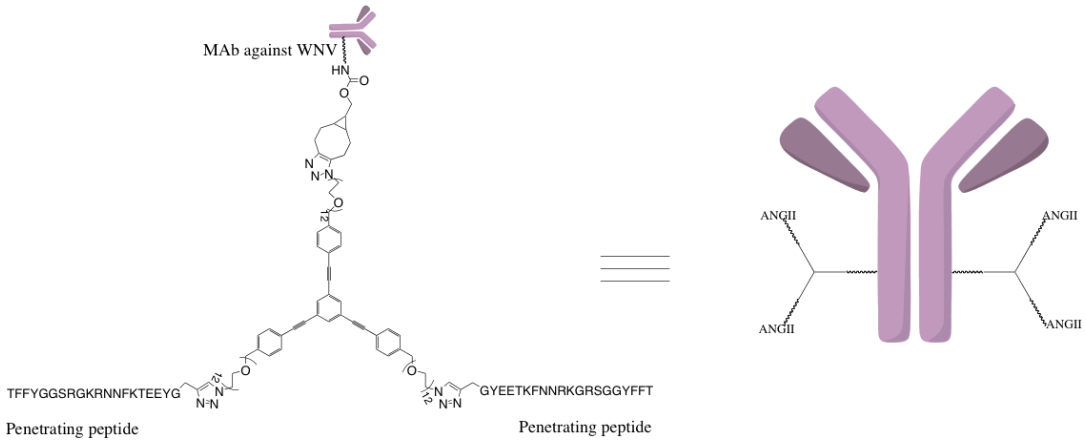

Figure 34. Structure of Molecular Trojan Horse

The central structure of the scaffold consists of a rigid hydrophobic core surrounded with multiple hydrophilic chains to promote the scaffold's solubility in water and tether multiple functional groups at the ends. Chemically the design balances hydrophobicity against hydrophilicity and flexibility against rigidity. In the present study, we have used

Angiopep-2, which targets the low-density lipoprotein receptor-related protein (LRP) and is reported to mediate transport of ligands across the BBB. [118-123]

Our conjugate shows superior efficacy in cell binding and neutralization assays and we are currently testing conjugates for survival studies in vivo.

3.2. Results and Discussion

Three Arm Linker. We devised a C3-symmetrical linking molecule with azide functional groups at its ends (Ar3, Scheme 2.4.1) by reaction between 1,3,5-triethynylbenzene (1) with 1-azido-37-(4-iodophenyl)-3n_{36}^{3}-dodecaoxaheptatriacontane as reported earlier[124] as a scaffold for construction of a bis-angiopep-2 linker. The scaffold consists of the rigid hydrophobic core and is attached multiple hydrophilic chains resulting in a solubility of 0.1 mg per mL of water.

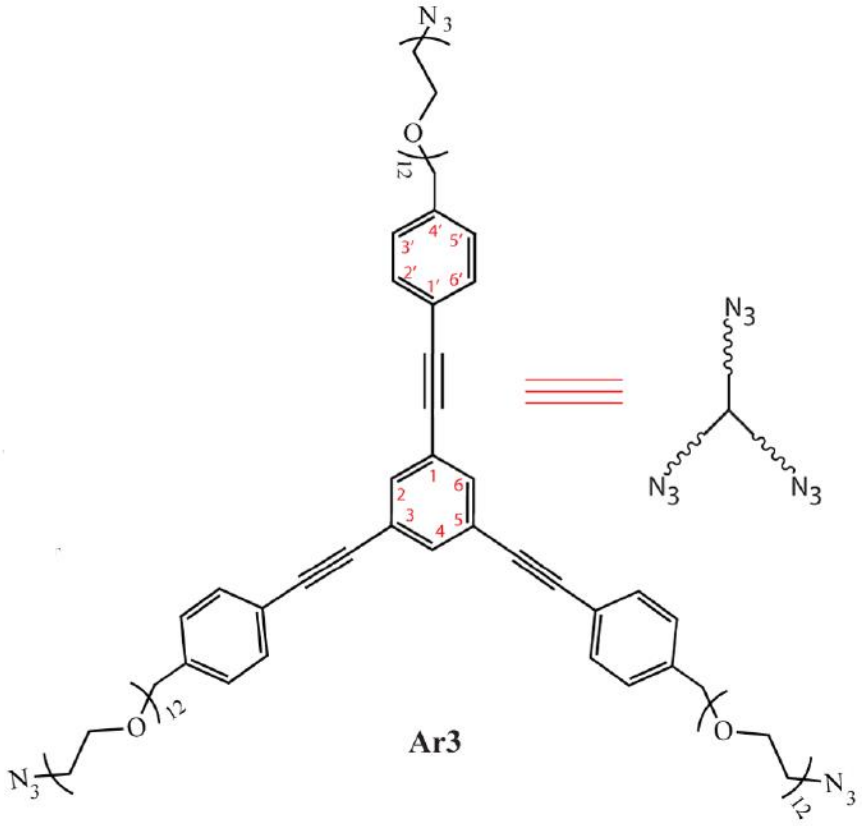

Figure 35. Structure of Three Arm Linker Ar3

Conjugating Angiopep-2 to Ar3. The Angiopep-2 is a 19 amino acid peptide. It was custom synthesized with propargylglycine amino acid at the C-terminus. The propargyl glycine is capable of reacting with an azide by copper catalyzed click chemistry.[125] Hence, we synthesized the bis-Angiopep-2 conjugate of Ar3 (compound CJ1) by mixing three molar equivalents of Angiopep-2 with Ar3 in presence of copper catalyst (see experimental section for details). A water soluble ligand tris(3-hydroxypropyltriazolylmethyl)amine (THPTA) [125] was employed for the reaction. HPLC

analysis showed that the Angiopep-2 was totally consumed after 1 hour and bis-Angiopep-2 conjugate was obtained in about 42% selectivity.

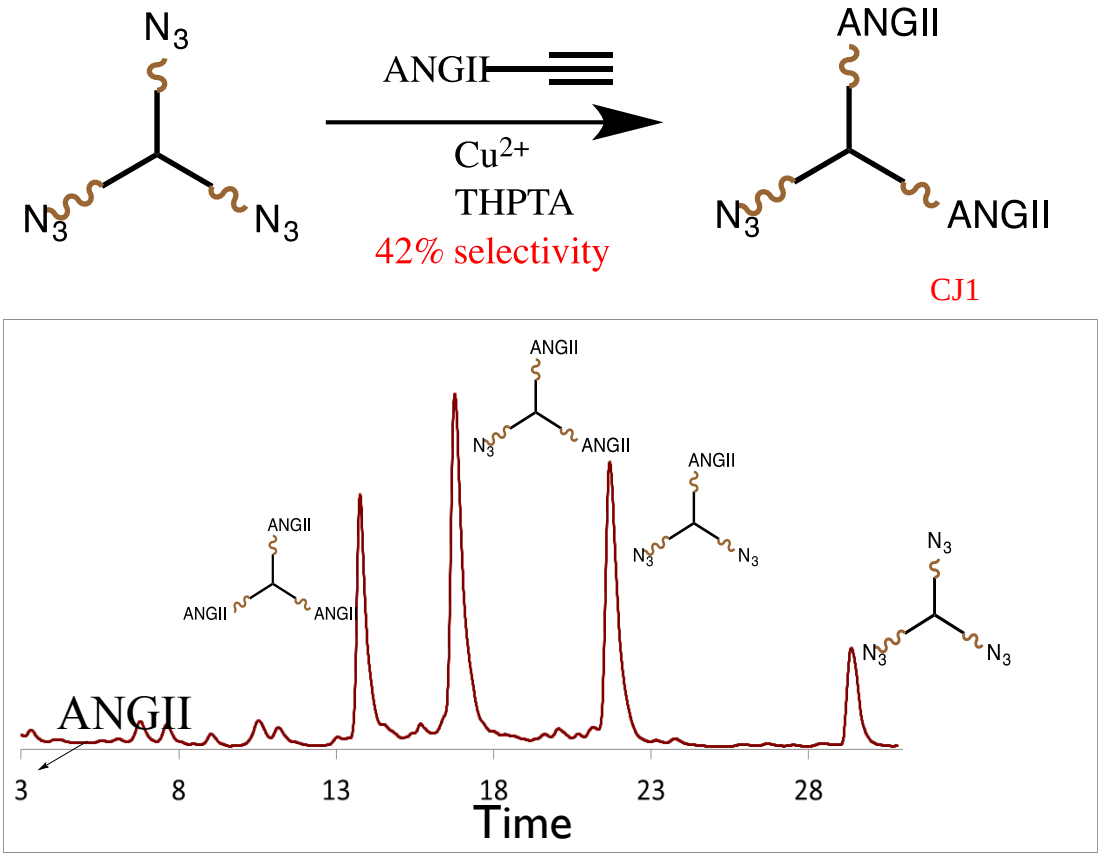

Figure 36. HPLC chromatogram of reaction between Ar3 and Angiopep-2 to prepare bis-Angiopep-2 (ANGII) conjugate.

Oxidation of hE16. Plant based hE16 was expressed and assembled in plants as per literature protocol.[107] Each heavy chain of the antibodies had N-linked glycans containing a fucose unit that can be oxidized with Sodium periodate. The E16 antibodies were buffer exchanged in 100 mM Sodium Actetate buffer (pH 5.5) following which the antibodies were oxidized using Sodium periodate in pH 5.5 Sodium Acetate buffer (see

experimental section for details) as per literature protocol.[126] The efficiency of the oxidation was checked by reacting the oxidized antibody with excess of hydrazine functionalized Lucifer yellow dye. A mixture of unoxidized antibody with Lucifer yellow and acetate buffer mixed with Lucifer yellow were used as controls for the experiment. Fluorescence spectroscopy after purification (figure 37) confirmed the conjugation of Lucifer yellow to oxidized antibody.

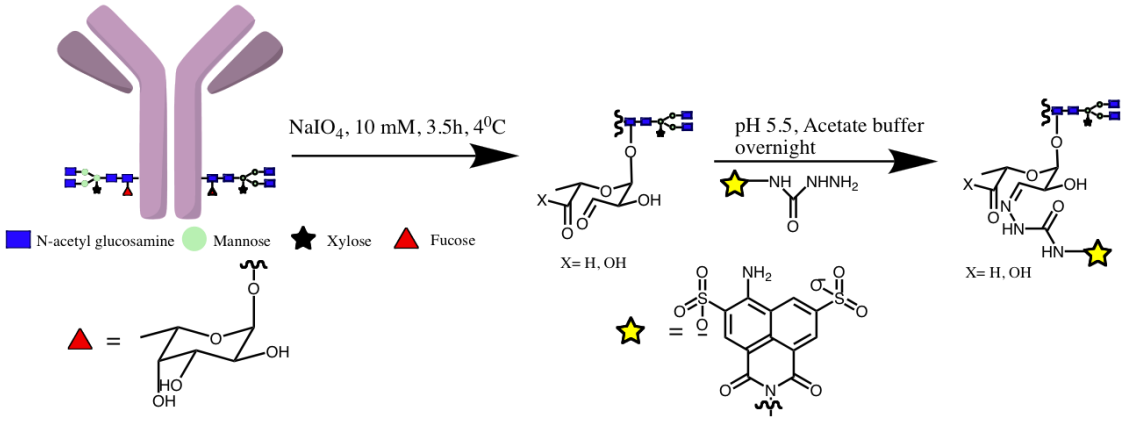

Scheme 3.1. Oxidation of hE16 with Sodium Periodate.

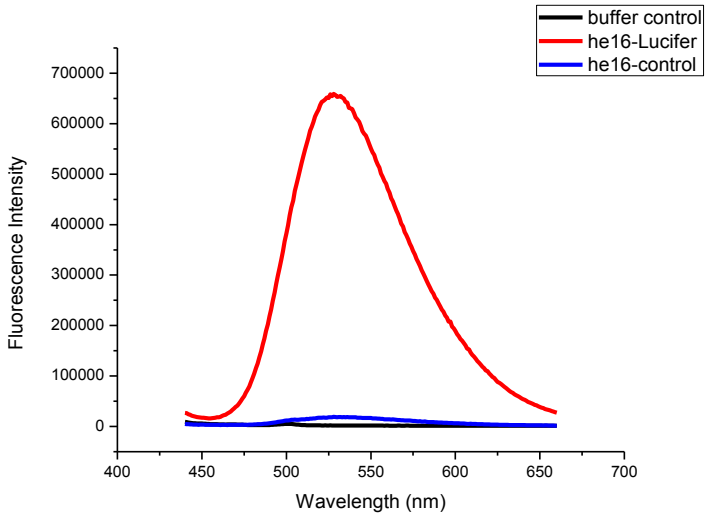

Figure 37. Fluorescence spectroscopy of Lucifer yellow conjugates.

BCN functionalization of E16.

(1R,8S,9R)- bicyclo[6.1.0]non-4-yn-9-ylmethyl(4-nitrophenyl)carbonate (BCN-NHS) was reacted with O,O'-[oxybis(2,1-ethanediyloxy-2,1 ethanediyl)]bis(hydroxylamine) to obtain compound 2 (scheme 3.2) (see experimental section for synthetic details).

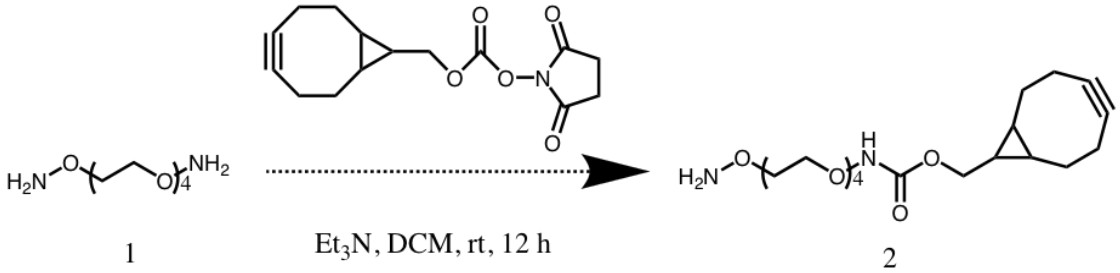

Scheme 3.2. Synthesis of compound 2

The oxidized antibody is reacted with compound 2 in pH 5.5 Sodium Acetate buffer following which it is purified to obtain BCN functionalized antibody (BCN-E16) (scheme 3.3)

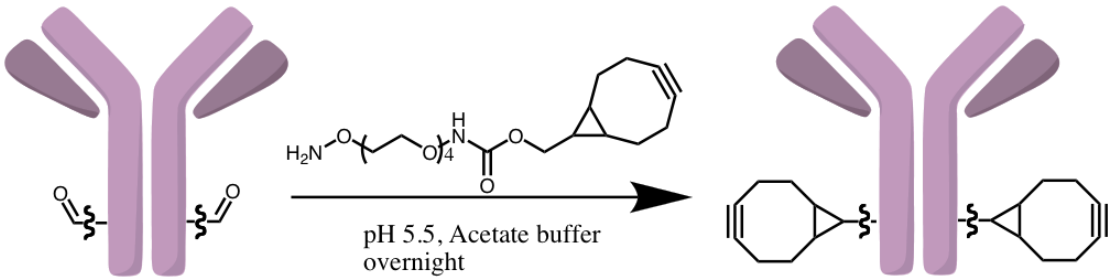

Scheme 3.3. BCN modification of hE16.

The BCN functionalization was confirmed by reacting BCN-E16 with two different Alexa Fluor 488 functionalized azides (3 and 4) (see experimental section for synthesis). Size exclusion chromatography showed absorbance at 495 nm indicating the attachment

of Alexa Fluor 488 on the antibody. On the contrary even when the unmodified antibody is mixed with 30 fold molar excess of Alexa Fluor there is no increase in absorbance at 495 nm indicating that the Alexa Fluor is only getting attached to the BCN-E16 by reaction of the azide with the BCN. UV-vis analysis of the purified Alexa Fluor 488 conjugates from a set of similar experiments demonstrated 1.3-1.6 dyes per antibody for conjugate with 3 and 1-1.4 dyes per antibody for conjugate with 4.

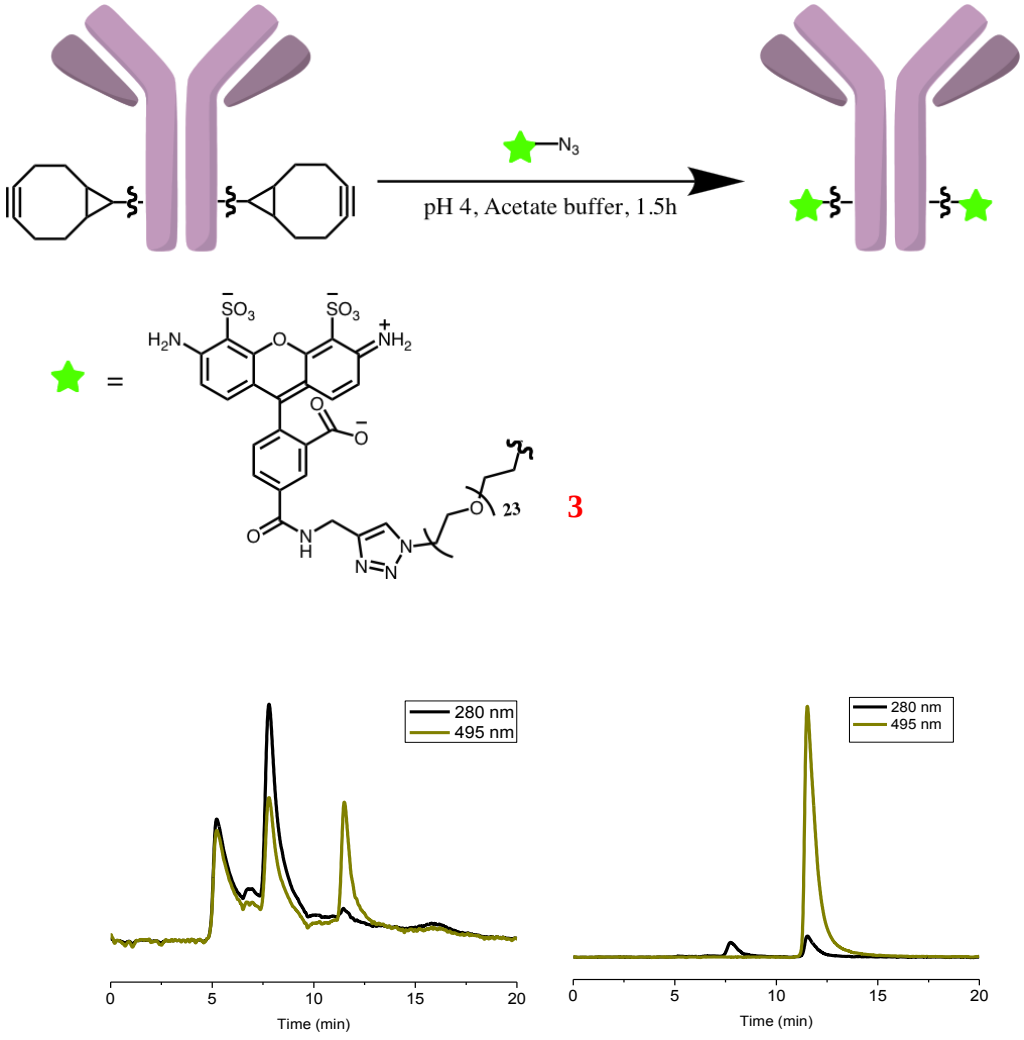

Figure 38. Reaction of BCN functionalized hE16 with Alexa Fluor azide 3.

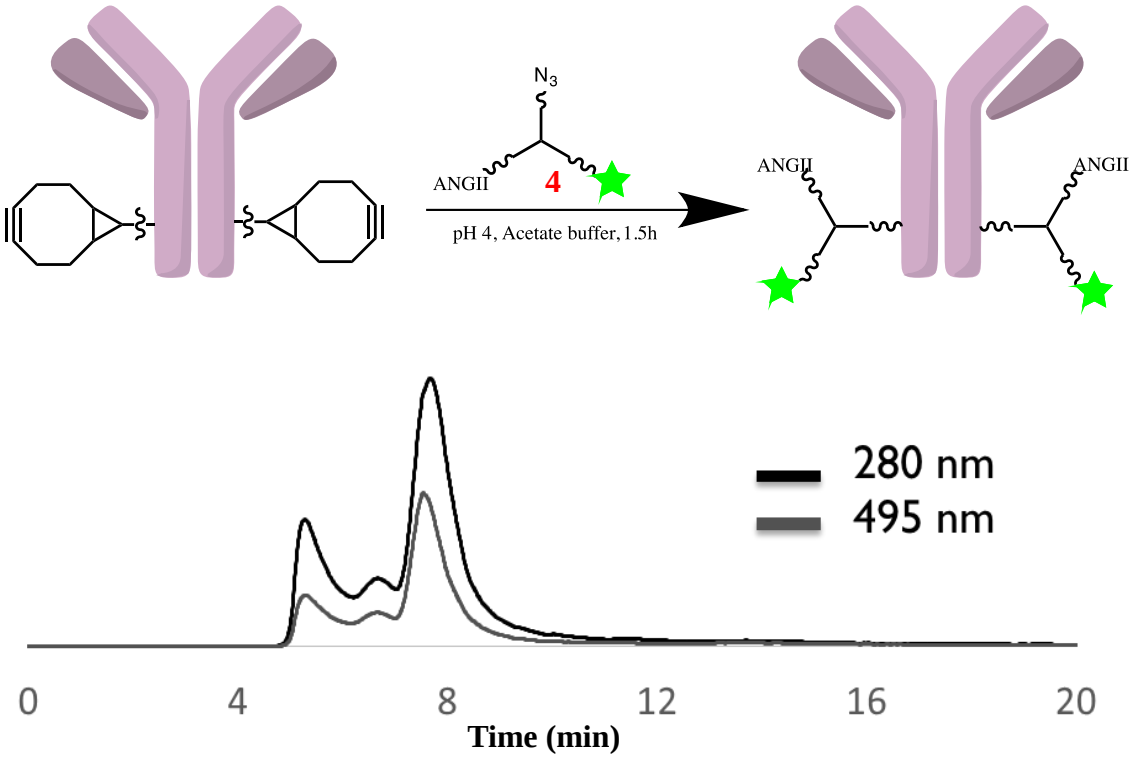

Figure 39. Reaction of BCN functionalized hE16 with Alexa Fluor azide 4.

Conjugation of CJ1 to BCN-E16. Following this we proceeded to conjugate the BCN-E16 with CJ1. 6 molar equivalents of CJI was mixed with mixed 1 molar equivalent of BCN-E16 in pH 4 acetate buffer and allowed to stir at room temperature for 1.5 hours following which they were purified by Size Exclusion Chromatography. For the conjugation reactions with BCN-E16 we observed that the best yields were obtained at pH 4. Reaction at pH 7.4 produced loss of yield due to precipitation probably due to aggregation of the conjugates in the concentrated mixture due to higher extent of labelling at neutral pH. We observed that CJ1 has a local maxima at 310 nm and hence, the BCN functionalized antibody after reaction with CJ1 showed an increased absorbance at 310 nm. We see two major peaks in the HPLC chromatogram of the E16-CJ1

conjugates. From GEL electrophoresis we concluded that the peak 1 with a retention time around 5.7 min is probably a mixture of antibody aggregates and highly labelled antibody conjugates while the peak 2 is a mixture of labelled and unlabeled antibody. The molecular weight of CJ1 appeared to be too small to cause a change in retention time in the HPLC chromatogram. A mixture of unmodified antibody and CJ1 was used as a control for this experiment. There was no increase in absorbance at 310 nm for the unmodified antibody indicating no reaction between CJ1 and the unmodified E16. After purification with size exclusion chromatography the UV-vis spectra for the E16-CJ1 conjugate shows a local maxima at 310 nm indicating the conjugation of E16 to CJ1. The UV-vis spectra for the unmodified antibody after purification with size exclusion chromatography does not show a local maxima at 310 nm indicating that CJ1 has not got conjugated to the unmodified antibody.

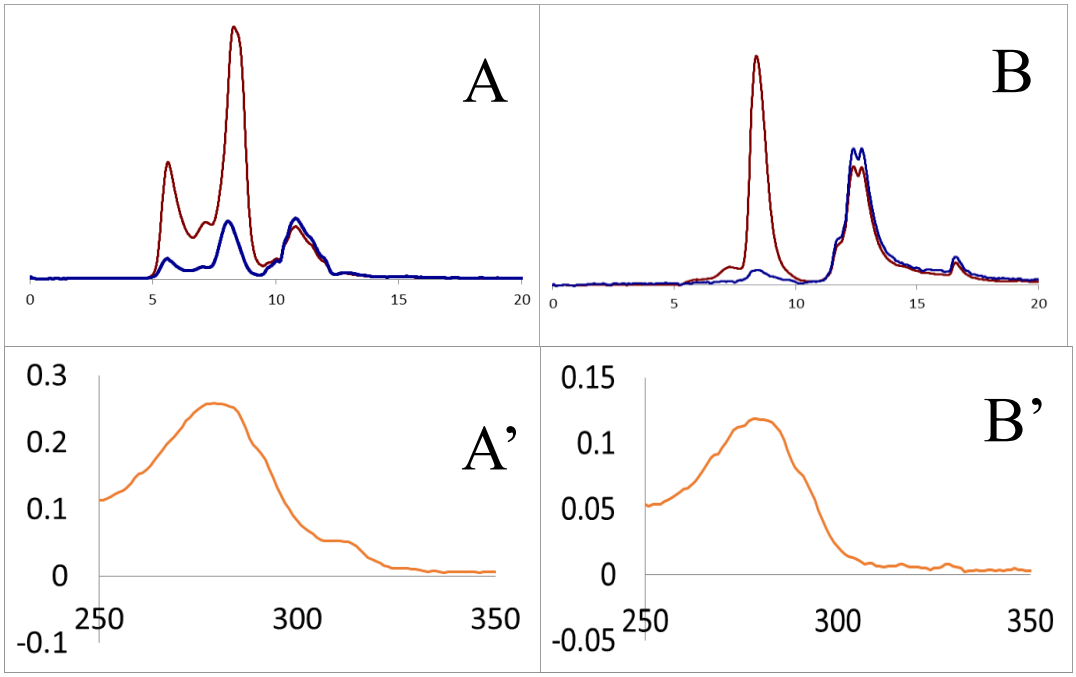

Figure 40. Conjugation of BCN-E16 with CJ1. A. HPLC chromatogram, A'. UV spectra of purified conjugate, B. HPLC chromatogram of unmodified E16 mixed with CJ1, B' UV spectra after purification.

Following purification MALDI-MS of the samples were obtained. The M/2 peak for the hE16 came around 74 kD while the M/2 peak for the E16-CJ1 comes around 77.5 kD.

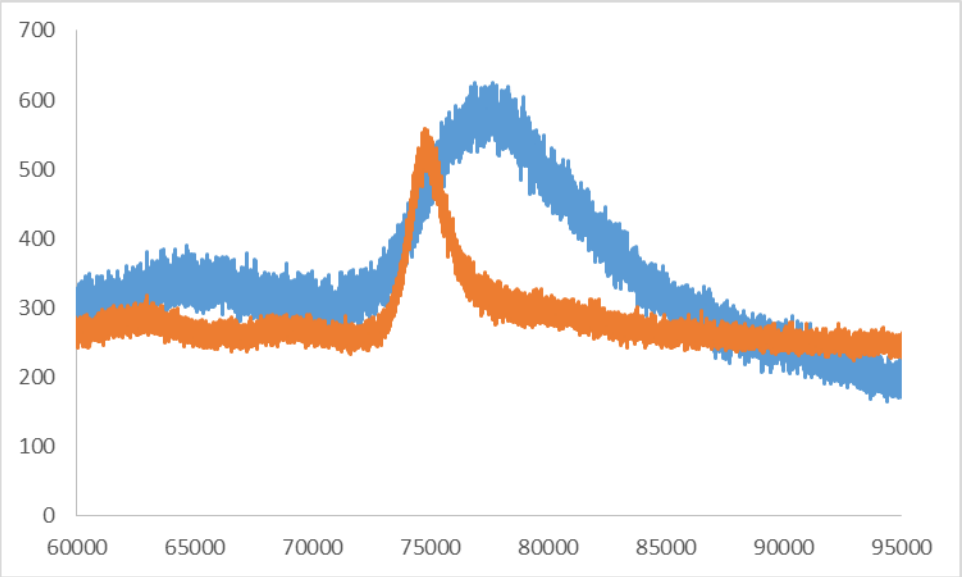

Figure 41. Maldi-MS of E16 (orange) and E16-CJ1 (blue).

Synthesis of linear linker-Angiopep-2 conjugate. An Angiopep-2 functionalized peg-24 linear linker, CJ2 was prepared by copper catalyzed click reaction between propargylglycine functionalized Angiopep-2 with peg-24-diazide (ccompound 5). CJ2 was then conjugated to the BCN-E16 in a similar manner as the three arm linker to synthesize E16-CJ2.

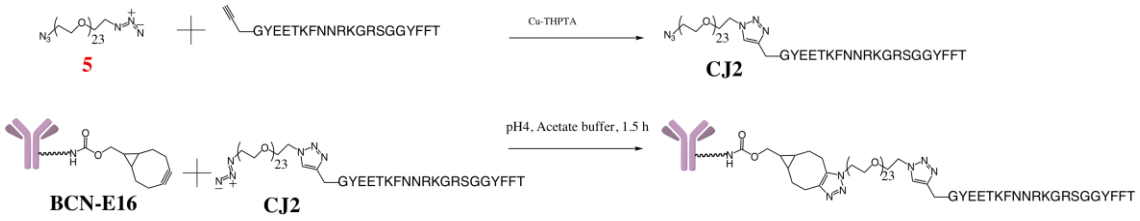

Scheme 3.4. Syntheis of E16-CJ2

SPRi studies. Analysis of antibody-antigen binding was carried out using Plexera Bioscience Surface Plasmon Resonance Imaging (SPRi) setup. In brief, the SPRi setup allows to build multiple sensitive spots using the same setup and a CCD camera is employed to ecord the intensity of the reflected light at a fixed angle and wavelength.[127] Rational signal sampling can be made from reproducible selection of sensing areas on the Gold biochip.[128] These sensing areas are known as Region of Interest (ROI). The SPRi technology allows to analyze multiple sensing areas (ROI) for a particular analyte and hence allows to analyze multiple analytes in the same experiment and also allows to look at the reproducibilty of the results.

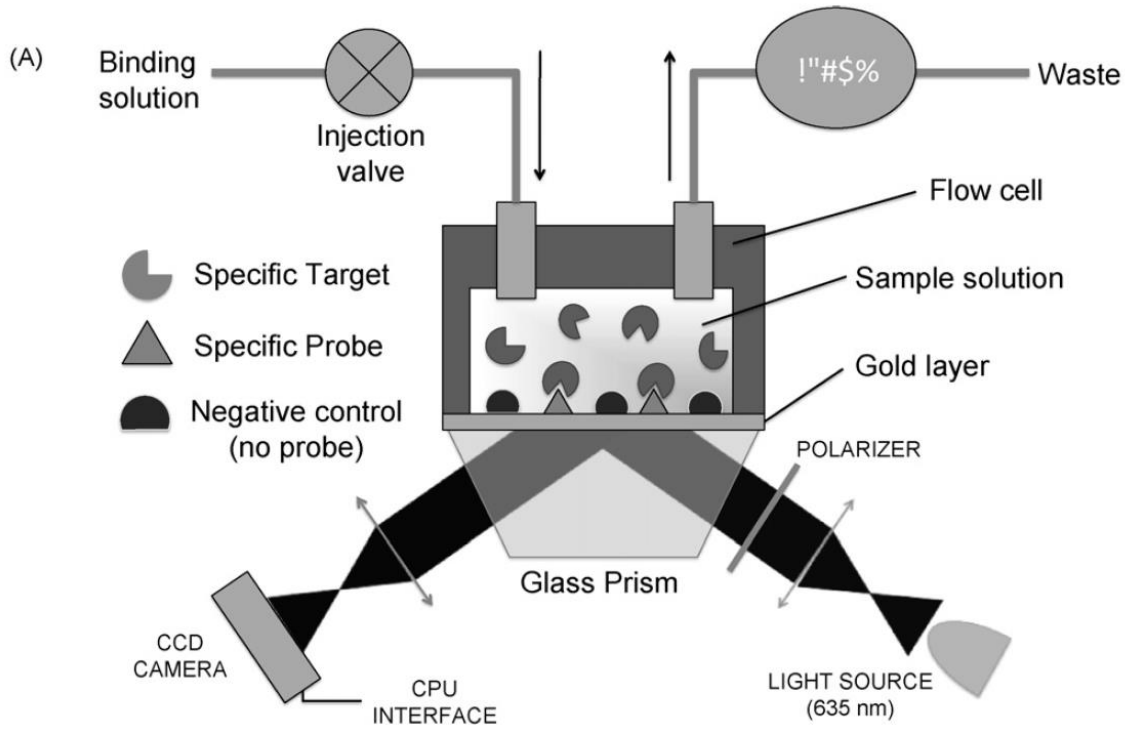

Figure 42. Scheme of SPRi apparatus. Reproduced with permission from reference (125) copyright 2011 Elsevier.

To perform the SPRi experiment thiolated protein A was immobilized on a Gold biosensor chip. The antibodies (E16 and E16-CJ1) were immobilized offline on the protein A functionalized chip. Multiple spots for each analyte are made by handspotting the samples on the biosensor chip with the assistance of a perforated PDMS membrane. Following this the biosensor chip is mounted on the SPRi instrument and two glycerol injections are made to optimize the signals and convert them to response unit (RU). Following this the antigen (DIII, 200 nM) is flown over the antibody functionalized biosensensor. The DIII is injected for 2 min at a flow rate of 5 µL/s following which

buffer is passed at a flow rate of 2 µL/s. Figure 43 gives the schematic diagram of the SPRi experiment.

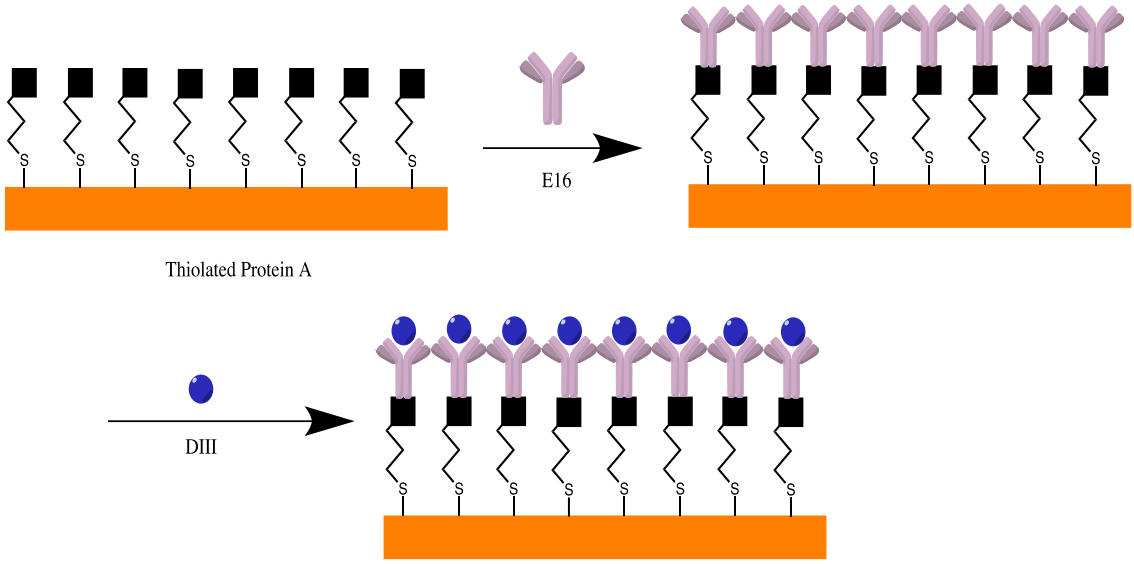

Figure 43. Scheme of SPRi experiment.

Figure 44 gives typical SPR curve for the experiment. Several ROIs for interaction between protein A and DIII is taken as control for this experiment. Figure 44 shows a typical SPRi signal for interaction of DIII with E16 and E16-CJ1.

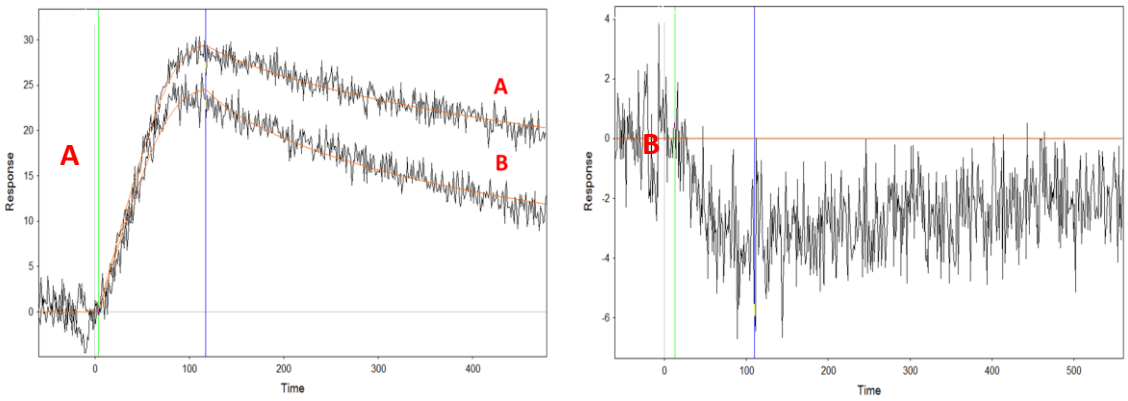

Figure 44. Typical SPRi curve for A. DIII binding to E16 (curve A) and DIII binding to E16-CJ1 (curve B) and B. DIII binding to protein A.

The results obtained from analyzing data from multiple ROIs is as follows:

Sample	k_a ($M^{-1}s^{-1}$)	k_d (s^{-1})	K_D (M^{-1})
E16	3.8 +/- 0.7 x 10^5	2.0 +/- 0.3 x 10^{-3}	4.95 +/- 1.6 x 10^{-9}
E16-CJ1	3.5 +/- 0.4 x 10^5	4.0 +/- 1.0 x 10^{-3}	10.01 +/- 3.4 x 10^{-9}

Table 3.1. Kinetic analysis of data obtained from multiple ROI during SPRi measurement

Antigen binding activity. Antigen binding activity was tested by studying binding activity between E16-CJ1 with yeast displaying DIII on their surface. Flow cytometric analysis showed higher fluorescence intensity for E16-CJ1 compared to basal fluorescence.

Cell binding assay. U87 cells were utilized to study cell-binding using both E16-CJ1 and E16-CJ2. Flow cytometric analysis indicated higher binding of E16-CJ1 to the U87 cells compared to E16-CJ2.

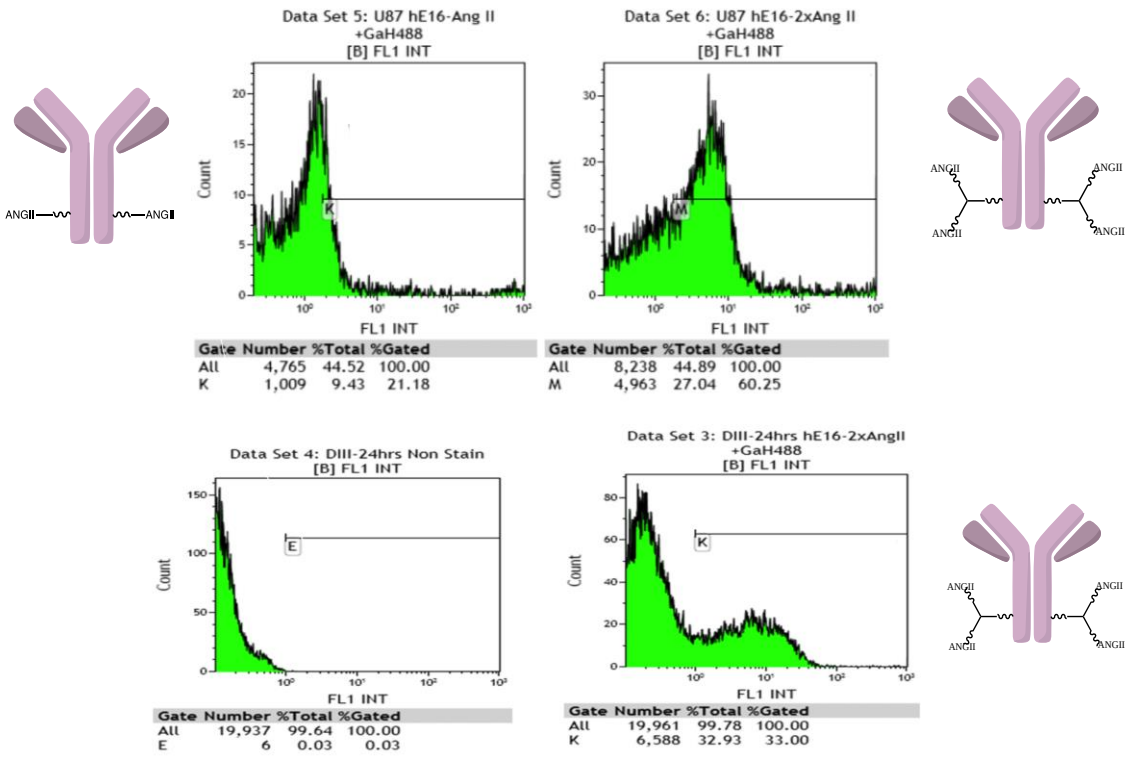

Figure 45. Antigen binding activity and cell binding activity of conjugates

Neutralizing activity. Neutralization potential of E16-CJ2 using WNV-reporter virus particles using literature based protocol. The E16-CJ2 showed similar efficacy as unmodified E16.

3.3. Experimental details.

General Information

All reagents and solvents were purchased from commercial suppliers (Sigma-Aldrich, Alfa Assar, Fluka, and TCI America) and used as received unless otherwise noted. Alexa Fluor 488 alkyne was purchased from ThermoFisher Scientific. Angiopep-2 was custom synthesized from CPC Scientific. Slide-A-Lyzer dialysis cassettes were purchased

ThermoFisher Scientific. Centrifugal filter units were purchased from EMD Millipore. All experiments requiring anhydrous conditions were performed in flame-dried glassware under nitrogen atmosphere. Reactions were monitored by thin layer chromatography (TLC) using silica gel precoated on glass plates (EMD Millipore). ^{1}H NMR and ^{13}C NMR spectra were recorded on Varian INOVA 400 (400 MHz) spectrometer at 25 °C. Chemical shifts (δ) are given in parts per million (ppm) and referenced to the residual solvent peak ($CDCl_3$, δH = 7.26 ppm; CD_3OD, δH = 3.31 ppm; DMSO-d6, δH = 2.50 ppm). Coupling constants (J) are expressed in hertz (Hz) and the values are rounded to the nearest 0.1 Hz. Splitting patterns are reported as follows: br, broad; s, singlet; d, doublet; dd, doublet of doublets; t, triplet; dt, doublet of triplets; q, quartet and m, multiplet. High-resolution mass spectra (HRMS) were acquired at the Arizona State University CLAS High Resolution Mass Spectrometry Facility. MALDI-MS was performed using a Bruker MALDI-MS instrument at ASU. SPRi analysis was performed by a PlexaArray HT instrument from Plexera Biosciences. Flash chromatography was performed in an automated flash chromatography system (CombiFlash Rf, Teledyne Isco, Inc.) with silica gel columns (60−120 mesh). RP-HPLC analysis and separation were performed with either a Zorbax C-18 column or with Zorbax 300 SB-C18 column (4.6 × 150 mm, particle size 5 μm) in an Agilent 1100 HPLC equipped with UV monitor and fraction collector. Size Exclusion Chromatography was performed on the same instrument using a Biosep-SEC-s3000 column.

Synthesis of CJ1. CJ1 was synthesized using a modified protocol reported by Finn and coworkers. In brief Ar3 (1.5 mM, 30 μL) was mixed with propargylglycine

functionalized Angiopep-2 (4.5 mM, 30 μL) followed by the addition of Phosphate buffer, pH 7 (30 μL), a 1:5 mixture copper sulfate (40 mM) and THPTA (100 mM) (3 μL), Aminoguanidine Hydrochloride (200 mM, 10 μL) and Sodium Ascorbate (200 mM, 10 μL) following which the reaction mixture is stirred at room temperature for 1 hour. HPLC monitoring showed the Angiopep-2 gets fully consumed after 1 hour. The bis-Angiopep-2 conjugate was purified by reverse phase HPLC using a 300 SB-C18 column. The retention time of the product in RP HPLC was 16.7 min with a mobile phase started at 70% eluent A and 30% eluent B, linearly increasing to 90% B in 25 min, followed by increasing B to 100% in 5 min. CJ1 was obatined in 42% selectivity. The sample was collected, lyophilized, redissolved in DI water and characterized by MALDI-MS: *m/z* (M+H) found. 6918.0 calcd. 6921.66

Synthesis of compound 1 and 2. Compound 1 and 2 was synthesized as described in literature.[129]

Synthesis of compound 5.

Compound 5 was synthesized by reaction between compound 5A and compound 5B (see chapter 2 for synthesis of compound 5A and 5B). To a solution of compound 5A (1 g, 1.75 mmol) in 2 mL anhyrous THF at 0°C is added sodium hydride (51 mg, 2.13 mmol) and allowed to stir for 30 min following which compound 5B (1.4 mg, 1.93 mmol) dissolved in 2 mL anhydrous THF is slowly added to the reaction mixture at 0°C. Following this, the reaction mixture is brought to room temperature and allowed to stir for 15 h. The completion of the reaction is monitored by TLC and the solvent is evaporated under vacuo and the reaction mixture is purified by silica gel column

chromatography under a gradient of 3.5% Methanol in DCM to obtain compound 5 as a colorless liquid. (1.38 g, 70% yield). ^{1}H NMR (400 MHz, CDCl3): δ 3.37 (t, 4 H, J = 4.8 Hz); 3.62-3.69 (m, 92 H); ^{13}C NMR (100MHz, CDCl3): δ 70.67-70.54, 70.02, 50.65. MALDI-MS. m/z (M+H): found 1147.45; calcd. for C48H96N6O23Na 1148.28

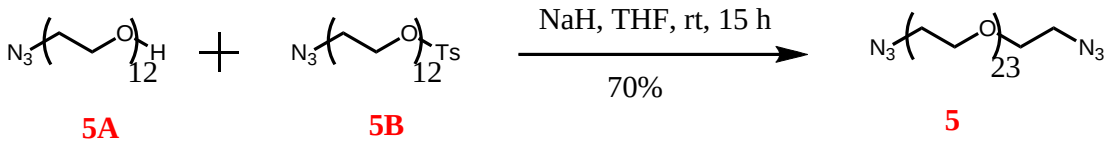

5A **5B** **5**

Scheme 3.5. Synthesis of compound 5.

Synthesis of compound 3. Alexa Fluor 488 alkyne (2 mM, 20 μL) was mixed with compound 5 (10 mM, 20 μL) followed by the addition of Phosphate buffer, pH 7, 100 mM (50 μL), a 1:5 mixture copper sulfate (20 mM) and THPTA (50 mM) (1.5 μL), Aminoguanidine Hydrochloride (100 mM, 5 μL) and Sodium Ascorbate (100 mM, 5 μL) following which the reaction mixture is stirred at room temperature for 1 hour. HPLC monitoring showed the Alexa Fluor 488 gets conjugated after 1 hour. The product was purified using RP HPLC with an eluting system composed of (A) 0.1% TFA in DI water and (B) 0.09% TFA in 80:20 acetonitrile: water. The retention time of the product in RP HPLC was 6.6 min with a mobile phase started at 80% eluent A and 20% eluent B, linearly increasing to 85% B in 25 min. The purified product was lyophilized and redissolved in DI water. MALDI-MS. m/z (M+H): found 1694.71; calcd. for C72H113+1N9O33S2 1697.82.

Synthesis of compound 4. Compound 4 is synthesized by following scheme 3.6 as illustrated below.

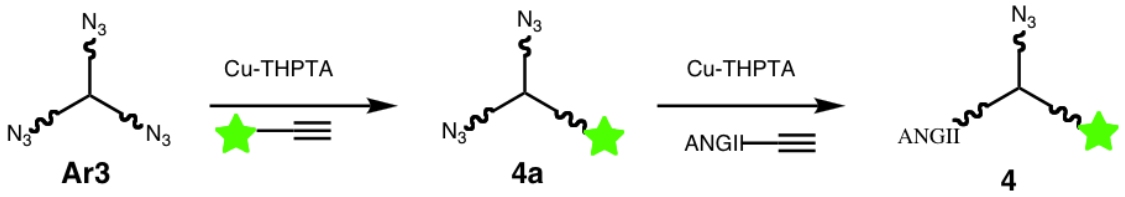

Scheme 3.6. Synthesis of compound 4.

Synthesis of 4a. Alexa Fluor 488 alkyne (2 mM, 20 μL) was mixed with Ar3 (10 mM, 20 μL) followed by the addition of Phosphate buffer, pH 7, 100 mM (50 μL), a 1:5 mixture copper sulfate (20 mM) and THPTA (50 mM) (1.5 μL), Aminoguanidine Hydrochloride (100 mM, 5 μL) and Sodium Ascorbate (100 mM, 5 μL) following which the reaction mixture is stirred at room temperature for 1 hour. HPLC monitoring showed the Alexa Fluor 488 gets conjugated after 1 hour. The product was purified using RP HPLC with an eluting system composed of (A) 0.1% TFA in DI water and (B) 0.09% TFA in 80:20 acetonitrile: water. The retention time of the product in RP HPLC was 16.9 min with a mobile phase started at 80% eluent A and 20% eluent B, linearly increasing to 85% B in 25 min followed by increase to 100% B in 30 mins.. The purified product was lyophilized and redissolved in DI water to obtain compound 4a. MALDI-MS. m/z (M+H): found 2698.38; calcd. for C129H182+1N12O46S2 2701.03.

Synthesis of 4. Angiopep-2 alkyne (0.5 mM, 20 μL) was mixed with 4a (0.75 mM, 20 μL) followed by the addition of Phosphate buffer, pH 7, 100 mM (50 μL), a 1:5 mixture copper sulfate (20 mM) and THPTA (50 mM) (1.5 μL), Aminoguanidine Hydrochloride

(100 mM, 5 μL) and Sodium Ascorbate (100 mM, 5 μL) following which the reaction mixture is stirred at room temperature for 1 hour. HPLC monitoring showed the Angiopep-2 gets conjugated after 30 min. The product was purified using RP HPLC with an eluting system composed of (A) 0.1% TFA in DI water and (B) 0.09% TFA in 80:20 acetonitrile: water. The retention time of the product in RP HPLC was 16.9 min with a mobile phase started at 85% eluent A and 15% eluent B, linearly increasing to 70% B in 25 min. The purified product was lyophilized and redissolved in DI water to obtain compound 4a. MALDI-MS. m/z (M+H): found 5093.6; calcd. 5096.6

Oxidation of hE16. hE16 antibodies were buffer exchanged to pH 5.5 NaOAc buffer (100 mM) using 10kD Amicon ultracentrifeugal filters. The antibodies are concentrated to about 15 mg/mL (100 μM). 100 μL Sodium periodate (20 mM) is mixed with 100 μL of the hE16 in an amber colored effendorf tube at 4°C and the reaction mixture is stirred for four hours at 4°C. The reaction is quenched by addition of 10 μL ethylene glycol at 0°C following which the mixture is purified by using 10kD Amicon ultracentrifeugal filters. The antibodies are kept in pH 5.5 NaOAc buffer (100 mM) for the next reaction. The efficiency of the reaction is tested by Lucifer yellow assay. To 100 μL of the antibody solution (10 μM) in pH 5.5 NaOAc buffer is added 10 μL of 6-Amino-2,3-dihydro-1,3-dioxo-2-hydrazinocarbonylamino-1H-benz[d,e]isoquinoline-5,8-disulfonic acid dilithium salt (Lucifer yellow hydradine) solution (22 mM). The reaction mixture is stirred overnight. As controls, 100 μL unmodified antibody solution (10 μM) in pH 5.5 NaOAc buffer and 100 μL of pH 5.5 NaOAc buffer are mixed with 10 μL of Lucifer

yellow hydrazine solution (22 mM) and stirred overnight at room temperature. Following this, the reaction mixtures are purified by10 kD Amicon ultracentrifeugal filters and the fluorescence intensity of the solutions are measured with a spectrofluoremeter.

BCN functionalization of E16.

100 µL of the oxidized hE16 antibody (100 µM) is mixed with 25 µL of 20 mM oxamine-BCN linker (compound 2) in pH 5.5 NaOAc buffer (100 mM) following which the reaction mixture is stirred overnight in an amber colored micro centrifuge tube. The reaction mixture is purified using Amicon ultracentrifugal 10 kD filters and the functionalized antibodies were buffer exchanged to pH 4 NaOAc buffer (100 mM). The attachment of the oxamine-BCN linker to the antibody was tested using the reaction between 15 µL of the BCN-conjugated antibody (40 µM) with 15 µL of Alexa Fluor-azide (compound 3) (200 µM) in pH 4 NaOAc buffer (100 mM). The reaction mixture was stirred for 1.5 h at room temperature following which it was purified by Size Exclusion Chromatography using a Biosep-SEC-s3000 column. The purified conjugates are collected and concentrated using Amicon ultracentrifugal 100 kD filters following which the compounds are buffer exchanged to PBS pH 7.4 by dialyzing for 6 hours using slide-a-lyzer dialysis cassettes with 3.5 kD molecular weight cut-off (Thermo scientific). UV analysis indicated two Alexa Fluor molecules attached to each antibody.

To test the attachment further, 15 µL of the BCN-E16 (40 µM) was mixed with 15 µL of compound 4 (80 µM) in pH 4 NaOAc buffer (100 mM) and the reaction mixture was stirred for 1.5 h at room temperature following which it was injected to HPLC and

purified by Biosep-SEC-s3000 column. The purified conjugates are collected and concentrated using Amicon ultracentrifugal 100 kD filters following which the compounds are buffer exchanged to PBS pH 7.4 by dialyzing for 6 hours using slide-a-lyzer dialysis cassettes with 3.5 kD molecular weight cut-off (Thermo scientific). UV analysis indicated two Alexa Fluor dyes per antibody.

Synthesis of E16-CJ1. 100 μL of the BCN-E16 (40 μM) was mixed with 100 μL of CJ1 (200 μM) in pH 4 NaOAc buffer (100 mM) and the reaction mixture was stirred for 1.5 h following which it was injected to HPLC and purified by Biosep-SEC-s3000 column using pH 3 Sodium Phosphate buffer (100 mM). The fractions from the HPLC are collected and concentrated using Amicon ultracentrifugal 100 kD filters following which the compounds are buffer exchanged to PBS pH 7.4 by dialyzing for 6 hours using slide-a-lyzer dialysis cassettes with 3.5 kD molecular weight cut-off (Thermo scientific).

Synthesis of CJ2. Propargylglycine functionalized Angipeptide-2 (2 mM, 20 μL) was mixed with compound 5 (10 mM, 20 μL) followed by the addition of Phosphate buffer, pH 7, 100 mM (50 μL), a 1:5 mixture copper sulfate (20 mM) and THPTA (50 mM) (1.5 μL), Aminoguanidine Hydrochloride (100 mM, 5 μL) and Sodium Ascorbate (100 mM, 5 μL) following which the reaction mixture is stirred at room temperature for 1 hour. HPLC monitoring showed the Angiopep-2 gets conjugated after 1 hour. The product was purified using RP HPLC with an eluting system composed of (A) 0.1% TFA in DI water and (B) 0.09% TFA in 80:20 acetonitrile: water. The retention time of the product in RP HPLC was 14.3 min with a mobile phase started at 85% eluent A and 15% eluent B,

linearly increasing to 75% B in 25 min. The purified product was lyophilized and redissolved in DI water. MALDI-MS. m/z (M+H): found 3518.6; calcd. 3521.9.

Synthesis of E16-CJ2. 100 µL of the BCN-E16 (40 µM) was mixed with 100 µL of CJ2 (200 µM) in pH 4 NaOAc buffer (100 mM) and the reaction mixture was stirred for 1.5 h following which it was injected to HPLC and purified by Biosep-SEC-s3000 column using pH 3 Sodium Phosphate buffer (100 mM). The fractions from the HPLC are collected and concentrated using Amicon ultracentrifugal 100 kD filters following which the compounds are buffer exchanged to PBS pH 7.4 by dialyzing for 6 hours using slide-a-lyzer dialysis cassettes with 3.5 kD molecular weight cut-off (Thermo scientific).

3.4. Summary. We have synthesized a bis-Angiopep-2 conjugate of hE16 antibody. The conjugate shows good efficacy in cell binding assays to U87 brain cells and binds to antigen displayed on yeast cell more strongly compared to the conjugate with mono-Angiopep-2 linker. The conjugate also shows good efficacy in neutralizing WNV-reporter virus particles. We are currently studying the efficacy of the conjugate is treating mice infected with WNV.

Chapter 4

SYNTHESIS OF MULTIVALENT CONSTRUCTS TO MIMIC ANTIBODIES

4.1 Introduction

While antibodies can specifically target pathogens, for example being used as "magic bullets" to treat cancers,[130] they exhibit poor extravasation and limited tissue penetration due to their large size and complexity.[131,132] In contrast, small molecule drugs can easily access intracellular disease targets, but they have notorious off-target toxicities and lack effectiveness to block protein-protein interactions.[133] Can we create a new molecular entity that bears merits of both large and small drugs to overcome their shortcomings? Recently, McEnaney *et al* have demonstrated that an antibody analogy containing targeting and effector moieties, which only has approximately 5% of the molecular weight of an antibody, can selectively elicit immune response for cellular phagocytosis through bivalent interactions.[134] This may open a new avenue of developing effective therapeutics by creating structural mimics of the antibody with small drug molecules. Hence, inspired by the structure of immunoglobulin G (IgG), we designed and synthesized small sized antibody mimics to enhance the ligand to receptor interaction. The two systems that we designed were:

1. A Y shaped bis-biotin as a small sized structural mimic
2. A tripod antibody to target glycoproteins of ebola virus.

4.2. Synthesis of a Y-shaped Scaffold for building small-sized Antibody Mimics

4.2.1. Introduction

In the present study, we have designed a Y-shaped scaffold composed of three arms, assuming that such a structure has a more favorable geometry for bivalent ligand binding to two separated binding sites of a receptor than a linear linker does. An antibody mimic can be constructed by attaching two ligands to the scaffold, leaving one of its arms for immobilization or attachment to monitor the ligand-to-receptor bivalent interactions by means of ensemble and single molecule methods.

4.2.2. Results and discussion

We have designed the Y-shaped ligand taking the following in consideration: (a) make the structure have sufficient flexibility so that its pendent ligands can bind to the receptor in much the same way as they are in the free state, (b) maximize the rigidity of the structure to reduce the possible loss in conformational entropy upon binding, and (c) avoid non-specific interactions of the scaffold with the receptor and other non-targeting molecules. For example, when DNA is used as a linker, it can interact with proteins through electrostatic attraction, which may become an entropically favorable process due to release of the counterions[135-137] resulting in strong nonspecific binding.

To demonstrate the principle of design, we chose the biotin-streptavidin interaction as a model system because it has been well studied so high-resolution crystal structures of biotin-streptavidin complexes are available, allowing us to design details at an atomic level. We designed a Y-shaped bis-biotin (hereinafter referred to as y-Bisbiotin) ligand, based on a biotin-streptavidin crystal structure with a 0.95Å resolution.[138] Streptavidin is a tetrameric molecule with 222 point group symmetry, each subunit bearing a biotin binding site.[139] From the projection shown in Figure 46, three bound biotin molecules are

observable, indicating that a bi- or tri-valent ligand can readily access these binding sites simultaneously. This has been demonstrated by Taylor *et al* using trisbiotinylated oligonucleotides with the length of > 20 nucleotides to occupy three of streptavidin's four biotin-binding sites.[140] In the complex, the distances between the biotin molecules are measured ranging from 19 to 35 Å (Figure 46-B). Based on these data, we designed the y-Bisbiotin molecule with a rigid core of 3,5-bis(phenylethynyl)aniline with a width of ~17 Å, which is connected to three flexible oligo[ethylene glycol] (OEG) linkers (Figure 46-C). In the structure, two biotin molecules are respectively attached to those OEG linkers situated at the para positions of the phenyl ring 1 and 3, and an azido function to

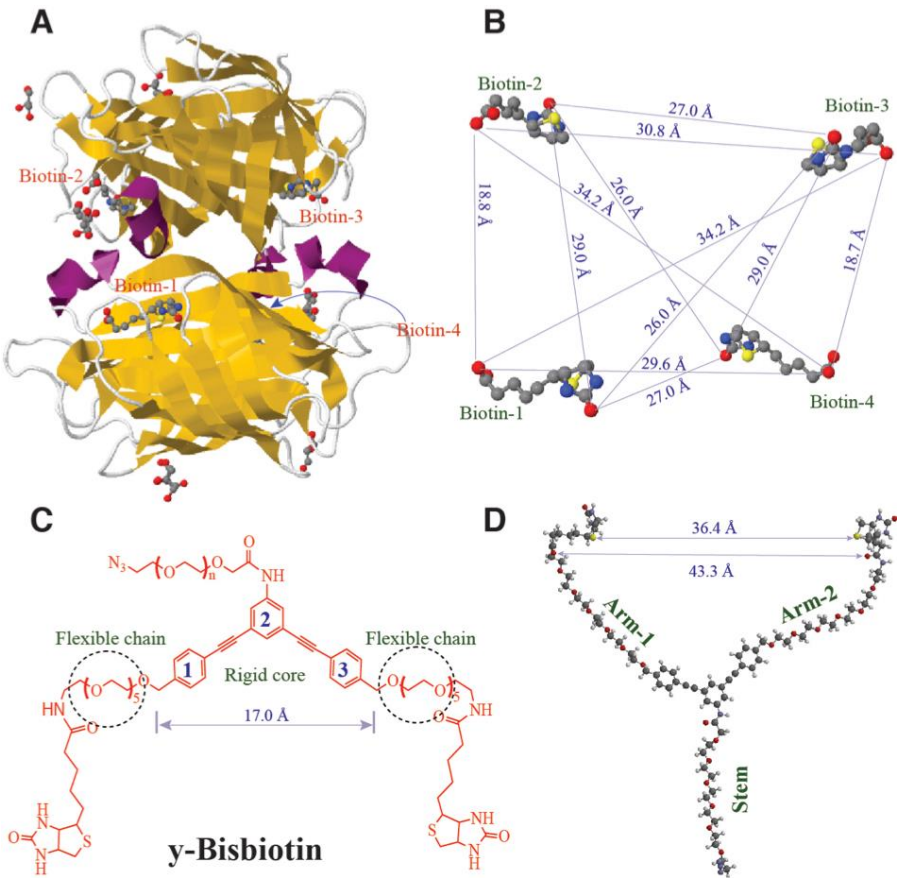

Figure 46. A) A view of the crystal structure of a biotin-streptavidin complex, adopted from Protein Data Bank (PDB ID: 3RY2); (B) Distances between biotins in the complex, determined by measuring the distance between the ureido oxygen atoms, and between oxygen atoms of the carboxylates in the crystal structure; (C) Chemical structure of a y-Bisbiotin ligand; (D) A DFT model of y-Bisbiotin, calculated by B3LYP in combination with a 6-31G* basis set in a vacuum using software Spartan'14.

the OEG linker of the aniline fragment. The DFT (Density Functional Theory) calculation shows that the structure can display as a Y shape with its two biotins separated by a distance of about 34 Å (Figure 41-D), which matches the distance between biotin 1 and biotin 2 in the crystal structure (see Figure 41-B). In addition, the bivalent ligand shows a dyad axis of symmetry the same as those in the streptavidin-biotin complex. We designate the two branches connecting to biotins as Arm 1 and Arm 2, and the third one as the Stem (see Figure 41-D). The OEG linker with 6 ethylene glycol units should provide sufficient flexibility for the biotin ligands binding to streptavidin and solubility for y-Bisbiotin dissolving in water. In aqueous solution (a good solvent), the OEG chain likely adapts a helical structure with its –O-C-C-O- backbone folded into a trans-gauche-trans conformation[141 142] so the Flory radius (R_f)[143] of a OEG chain with 6 units of ethylene glycol can be estimated as

$$R_f = N^{3/5}\,(\text{monomer length}) = 6^{3/5} \times 2.78 = 8.1\ \text{Å}$$

Thus, the span (~17+8.1Å) between the two biotins in y-Bisbiotin should be wide enough for them to simultaneously bind to the streptavidin in aqueous solution without be strained. In the present study, we used the stem (Figure 41-D) to immobilize the y-

Bisbiotin on an SPR chip for studying kinetics of the bivalent interaction and to attach the y-Bisbiotin molecule to an atomic force microscopy (AFM) tip for studying the bivalent interactions at a single molecule level (vide infra).

Synthesis. We first synthesized the scaffold, to which two biotin molecules were then attached to form the y-Bisbiotin. As shown in Scheme 4.2.1, under the Sonogashira cross-coupling conditions,[144,145] 3,5-diethynylaniline (**1**)[146] reacted with *p*-iodobenzyloxy-$(OEG)_6$-NHBoc (**2,** see its synthesis in experimental section), to produce compound **3** in a 75% yield. In the presence of pyridine, the arylamine of compound **3** reacted with α-OEGylated acetyl chloride **S7a** and **S7b** (see experimental section for their synthesis) respectively, generating **4a** (59%) and **4b** (69%), which were subsequently treated with trifluoroacetic acid to remove the Boc protecting groups, resulting in the scaffold molecules **5a** (69%) and **5b** (70%). The desired y-Bisbiotin ligands **6a** and **6b** were produced via **5a** and **5b** reacting with biotin N-hydroxysuccinimide ester in a yield of ~ 62% and 67%, respectively. The molecules **6a** and **6b** differ in the length of their stems, used to study the bivalent interactions with streptavidin by gel electrophoresis and AFM, respectively.

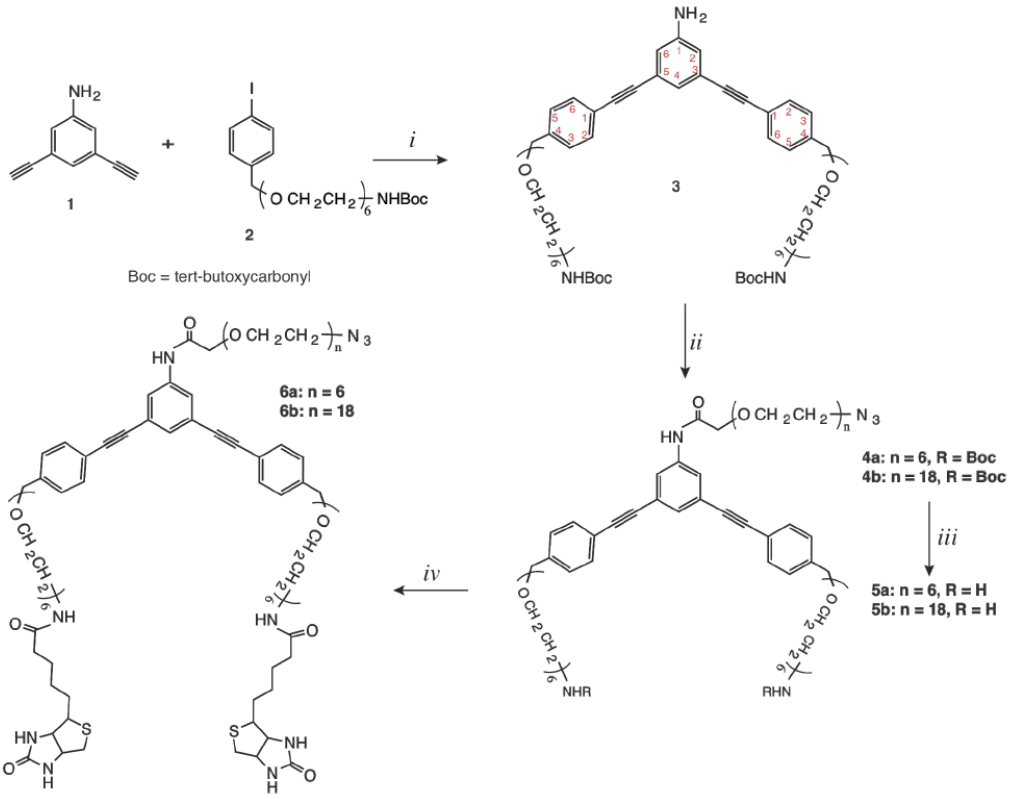

Scheme 4.2.1. Synthesis of y-bisbiotin ligands.

Reagents and conditions: (*i*) $Pd(PPh_3)_2Cl_2$, CuI, THF : Et_3N = 1:1, rt, 5 h; (*ii*) **S7a** or **S7b**, pyridine in dichloromethane, rt, 12 h; (*iii*) trifluoroacetic acid, rt, 10 min; (*iv*) biotin N-hydroxysuccinimide ester, triethylamine, DMF, rt, 3 h.

4.2.3. Experimental Section

General information. All chemicals were purchased as reagent grade and used without further purification unless otherwise noted. The Sure/Seal^{TM} anhydrous solvents were purchased from Sigma-Aldrich. All reactions were performed under an atmosphere of argon using the standard Schlenk technique. ^{1}H and ^{13}C NMR spectra were recorded at 400 MHz (^{1}H) and 100 MHz (^{13}C), respectively. Chemical shifts are given in parts per

million (ppm) on the delta scale (δ) and referred either to tetramethylsilane (^{1}H and ^{13}C NMR δ = 0 ppm) or the residual solvent peak. High-resolution mass spectra (HRMS) were acquired at the Arizona State University CLAS High Resolution Mass Spectrometry Facility. MALDI-TOF analysis was performed on Voyager-DE STR instrument at Biodesign Institute of Arizona State University. Streptavidin and Dulbecco's phosphate buffered saline solution (PBS, pH 7.4) were purchased form Sigma-Aldrich.

Special note on nomenclature. To avoid excessive use of a long series of numbers, the mathematical shorthand for expressing arithmetic progressions is used to denote the positions of oxygen atoms in the elongated PEG chains, as proposed by Hill and co-workers.[73]

Synthesis of 1-(tert-butoxycarbonylamino)-17-p-iodobenzyloxy-3n$_{15}^{3}$-pentaoxaheptadecane (2).

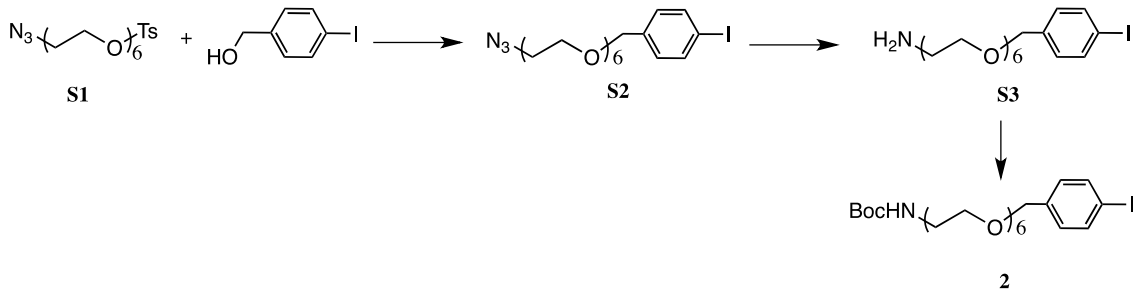

Scheme 4.2.2. Synthesis of 1-(tert-butoxycarbonylamino)-17-p-iodobenzyloxy-3n$_{15}^{3}$-pentaoxaheptadecane **(2).**

1-Azido-17-*p*-iodobenzyloxy-3n$_{15}^{3}$-pentaoxaheptadecane (S2). Potassium *tert*-butoxide (1.26 g, 11.27 mmol) was added to a solution of 4-iodobenzyl alcohol (2.23 g, 9.5 mmol) in anhydrous THF (25 mL) followed by addition of **S1** [147] (4.0 g, 8.6 mmol) and the mixture was stirred at room temperature for 5 h, concentrated by rotary evaporation. The

residue was purified by flash chromatography using a gradient of methanol (0-2.5% over 4 h) in dichloromethane to give **S2** as colorless oil (3.17 g, 70%). ^{1}H NMR (400 MHz, $CDCl_3$): δ 3.37 (t, 2H, J = 5.2 Hz), 3.58-3.68 (m, 22H), 4.50 (s, 2H), 7.10 (d, 2H, J = 8 Hz), 7.66 (d, 2 H, J = 8 Hz). ^{13}C NMR (100 MHz, $CDCl_3$): δ 40.3, 69.5, 70.0, 70.5-70.6, 72.4, 129.5, 129.8, 137.4, 138.0. HRMS (APCI) (M+H): found m/z 524.1253, calcd for $C_{19}H_{30+1}IN_3O_6$ 524.1254.

1-Amino-17-*p*-iodobenzyloxy-3n$_{15}^{3}$-pentaoxaheptadecane (S3). To a solution of **S2** (3 g, 5.7 mmol) in anhydrous THF (20 mL), triphenylphosphine (2.25 g, 8.6 mmol) was added and stirred at room temperature for 12 h. Water (1 mL) was added to the mixture, which was stirring for another 4 h, concentrated by rotary evaporation. The crude product was purified by flash chromatography using a gradient of methanol (0-20% over 4 h) in dichloromethane to give **S3** as colorless oil (2 g, 70%). ^{1}H NMR (400 MHz, $CDCl_3$): δ 2.12 (s, 2H), 2.87 (t, 2H, J = 5 Hz), 3.37 (t, 2H, J = 5.2 Hz), 3.58-3.68 (m, 20H), 4.50 (s, 2H), 7.10 (d, 2H, J = 8 Hz), 7.66 (d, 2H , J = 8 Hz); ^{13}C NMR (100MHz, $CDCl_3$): δ 40.4, 69.5, 70.1, 70.5-70.6, 72.4, 129.5, 129.8, 137.4, 138.0. HRMS (APCI) (M+H): found m/z 498.1334, calcd for $C_{19}H_{32+1}INO_6$ 498.1335.

1-(*tert*-butoxycarbonylamino)-17-*p*-iodobenzyloxy-3n$_{15}^{3}$-pentaoxaheptadecane (2). To a solution of **S3** (2.0 g, 4 mmol) in anhydrous THF (15 mL), di-*tert*-butyl dicarbonate (2.52 mL, 11 mmol) was added followed by addition of diisopropylamine (0.67 mL, 4.8 mmol). The solution was stirred at room temperature for 15 h, concentrated by rotary evaporation. The residue was purified by flash chromatography using a gradient of methanol (0-5% over 4 h) in dichloromethane to give **2** as colorless oil (2.1 g, 87%). ^{1}H

NMR (400 MHz, $CDCl_3$): δ 1.44 (s, 9H), 3.28-3.32 (m, 2H), 3.48 (t, 2H, J = 5.2 Hz), 3.49-3.68 (m, 20H), 4.50 (s, 2H), 5.11 (s, 1H), 7.10 (d, 2H, J = 8 Hz), 7.66 (d, 2 H, J = 8 Hz); ^{13}C NMR (100 MHz, $CDCl_3$): δ 28.4, 40.3, 68.9, 69.5, 70.1, 70.5-70.6, 72.4, 129.5, 129.8, 137.4, 138.0, 155.9. HRMS (APCI) (M+H): found m/z 598.1863, calcd for $C_{24}H_{40+1}INO_8$ 598.1867.

Synthesis of 20-azido-3n$_{18}^3$-hexaoxaicosan-1-oyl chloride (S7a) and 56-azido-3n$_{54}^3$-octadecaoxahexapentacontan-1-oyl chloride (S7b).

These two compounds were synthesized following a route as described in Scheme S2 and Scheme S3.

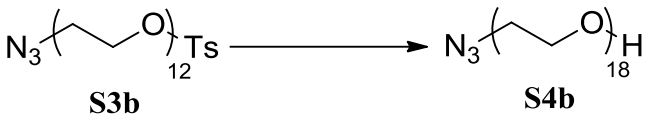

Scheme 4.2.3. Synthesis of S4b.

53-azido-3n$_{51}^3$-heptadecaoxatripentacontan-1-ol (S4b). Compound **S4b** was synthesized following a route described in Scheme 4.2.3. The starting material **S3b** was synthesized following a procedure we previously reported. [147]

To a solution of hexaethylene glycol (6.72 g, 23.8 mmol) in anhydrous THF (40 mL), Sodium hydride (0.74g, 30.8 mmol) was added and stirred at 0 °C for 1 h. Compound **S3b** (3.5 g, 7.5 mmol) in anhydrous THF (20 mL) was added to the mixture and allowed to warm to room temperature, stirred for another 15 h. Methanol (5 mL) was added dropwise to stop the reaction. The mixture was concentrated by rotary evaporation,

purified in a silica gel column by flash chromatography using a gradient of methanol (0-3.5% over 4 h) in dichloromethane. Compound **S4b** was obtained as a colorless liquid (2.9 g, 72%). ^{1}H NMR (400 MHz, CDCl3): δ 2.69 (s, 1 H, broad), 3.36 (t, 2 H, J = 5.2 Hz), 3.53- 3.68 (m, 70 H). ^{13}C NMR (100 MHz, $CDCl_3$): δ 69.5, 70.1, 70.5-70.6, 72.4. HRMS (APCI) (M+H): found m/z 836.5330, calcd for $C_{36}H_{73+1}N_3O_{18}$ 836.5332.

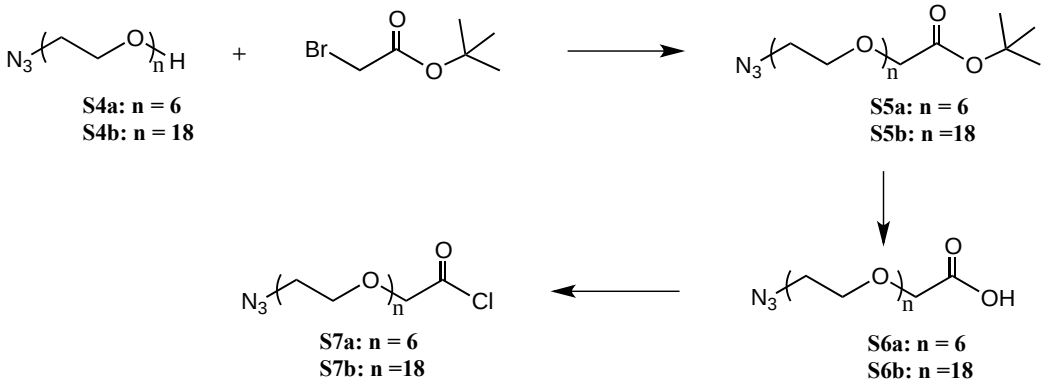

Scheme 4.2.4. Synthesis of S7a and S7b.

***Tert*-butyl 20-azido-3n$_{18}^{3}$-hexaoxaicosan-1-oate (S5a).** To a solution of compound **S4a** (2 g, 6.5 mmol) in anhydrous THF (10 mL), potassium *tert*-butoxide (0.54 g, 7.8 mmol) was added followed by addition of *tert*-butyl bromoacetate (0.65 mL, 8.8 mmol). The mixture was stirred at room temperature for 5 h, and concentrated by rotary evaporation. The residue was purified by flash chromatography using a gradient of methanol (0-3.3% over 4 h) in dichloromethane to give **S5a** as colorless oil (1.2 g, 52%). ^{1}H NMR (400 MHz, $CDCl_3$): δ 1.43 (m, 9H), 3.36 (t, 2 H, J = 5.2 Hz), 3.53-3.68 (m, 22H), 3.90 (s, 2H). ^{13}C NMR (100 MHz, $CDCl_3$): δ 28.03, 50.6, 68.9, 69.5, 70.0, 70.5-70.6, 72.4, 164.5. HRMS (APCI) (M+H): found m/z 422.3463, calcd for $C_{18}H_{35+1}N_3O_8$ 422.3465.

***Tert*-butyl 56-azido-3n$_{54}^3$-octadecaoxahexapentacontan-1-oate (S5b).** To a solution of compound **S4b** (2 g, 2.3 mmol) in anhydrous THF (10 mL), potassium *tert*-butoxide (0.34 g, 3.1 mmol) was added followed by addition of *tert*-butyl bromoacetate (0.45 mL, 3.1 mmol). The mixture was stirred at room temperature for 5 h, and concentrated by rotary evaporation. The residue was purified by flash chromatography using a gradient of methanol (0-3.3% over 4 h) in dichloromethane to give **S5b** as colorless oil (1.3 g, 57%). ^{1}H NMR (400 MHz, $CDCl_3$): δ 1.43 (m, 9H), 3.36 (t, 2 H, J = 5.2 Hz), 3.54-3.68 (m, 70H), 3.91 (s, 2H). ^{13}C NMR (100 MHz, $CDCl_3$): δ 28.4, 50.6, 69.0, 69.5, 70.0, 70.5-70.6, 72.4, 164.5. HRMS (APCI) (M+H): found m/z 950.6191, calcd for $C_{42}H_{83+1}N_3O_{20}$ 950.6192.

20-azido-3n$_{18}^3$-hexaoxaicosan-1-oic acid (S6a). Compound **S5a** (1.0 g, 2.4 mmol) was dissolved in 10 mL of trifluoroacetic acid and stirred for 4 h at room temperature, and concentrated by rotary evaporation. The residue was purified by flash chromatography using a gradient of methanol (0-6% over 3 h) in dichloromethane to give **S6a** as colorless oil (0.62 g, 73%). ^{1}H NMR (400 MHz, $CDCl_3$): δ 3.37 (t, 2 H, J = 5.2 Hz), 3.53-3.69 (m, 22H), 3.93 (s, 2H). ^{13}C NMR (100 MHz, $CDCl_3$): δ 50.6, 69.1, 69.5, 70.0, 70.5-70.6, 72.4, 166.8. HRMS (APCI) (M+H): found m/z 366.2754, calcd for $C_{14}H_{27+1}N_3O_8$ 366.2759.

56-Azido-3n$_{54}^3$-octadecaoxahexapentacontan-1-oic acid (S6b). Compound **S5b** (1.0 g, 1 mmol) was dissolved in 10 mL of trifluoroacetic acid and stirred for 4 h at room temperature, and concentrated by rotary evaporation. The residue was purified by flash chromatography using a gradient of methanol (0-6% over 3 h) in dichloromethane to give

S6b as colorless oil (0.65 g, 69%). ^{1}H NMR (400 MHz, $CDCl_3$): δ 3.37 (t, 2 H, J = 5.2 Hz), 3.54-3.69 (m, 70H), 3.92 (s, 2H). ^{13}C NMR (100 MHz, $CDCl_3$): δ 50.6, 68.9, 69.5, 70.0, 70.5-70.6, 72.4, 166.7. HRMS (APCI) (M+H): found m/z 894.5636, calcd for $C_{38}H_{75+1}N_3O_{20}$ 894.5637

Synthesis of 20-azido-3n$_{18}^{3}$-hexaoxaicosan-1-oyl chloride (S7a). Before use, **S6a** (0.5 g, 1.2 mmol) was dissolved in thionyl chloride (2 mL, 2.7 mmol), stirred for 6 h at room temperature, and concentrated by rotary evaporation to furnish **S7a** as yellowish oil.

56-azido-3n$_{54}^{3}$-octadecaoxahexapentacontan-1-oyl chloride (S7b). Before use, **S6b** (0.5 g, 0.55 mmol) was dissolved in thionyl chloride (2 mL, 2.7 mmol), stirred for 6 h at room temperature, concentrated by rotary evaporation to furnish **S7b** as yellowish oil.

Synthesis of 6a and 6b.

3,5-Bis{4-[19-*tert*-butoxycarbonylamino-(3n$_{18}^{3}$-1) hexaoxanonadecyl]phenylethynyl}aniline (3). To a solution of compound **2** (2.6 g, 4.4 mmol) in THF (20 mL), 3,5-diethynylaniline **1** (0.3 g, 2.1 mmol), bis(triphenylphosphine)palladium(II)dichloride (0.074 g, 0.1 mmol) and copper(I) iodide (0.040 g, 0.2 mmol) were added. The mixture was stirred at room temperature for 5 h, filtered to remove the precipitate, concentrated by rotary evaporation. The residue was purified by flash column chromatography on silica gel using a gradient of methanol (0-2.8% over 4 h) in dichloromethane as an eluent to give **3** as a colorless oil (1.72 g, 75%). ^{1}H NMR (400 MHz, $CDCl_3$): δ 1.43 (s, 18H), 3.27-3.32 (m, 4H), 3.52 (t, 4H, J = 5.2 Hz), 3.58-3.69 (m, 44 H), 4.56 (s, 4H), 5.13 (s, 2H), 6.81 (s, 2H), 7.10 (s, 1H), 7.32 (d, 4H, J =

8 Hz), 7.47 (d, 4H, J = 8 Hz); ^{13}C NMR (100 MHz, $CDCl_3$): δ 28.3, 40.3, 69.5, 70.1, 70.3-70.6, 72.7, 88.9, 90.0, 117.7, 122.2, 124.0, 124.9, 127.4, 131.5, 138.6, 146.5, 155.9; HRMS (APCI) (M+H): found m/z 1080.6002, calcd for $C_{58}H_{85+1}N_3O_{16}$ 1080.6001.

N-(3,5-Bis{4-[19-*tert*-butoxycarbonylamino-(3n$_{18}^3$-1)-hexaoxanonadecyl]phenylethynyl}aniline)-20-azido-3n$_{18}^3$-icosan-1-amide (4a). Compound **S7a** (see S2 in Supporting Information for its synthesis) dissolved in anhydrous dichloromethane (1 mL) was added to a solution of compound **3** (1.4 g, 1.27 mmol) in anhydrous dichloromethane (10 mL) and pyridine (98 μL, 1.2 mmol). The solution was stirred for 12 h at room temperature, concentrated by rotary evaporation. The residue was purified by flash column chromatography on silica gel using a gradient of methanol (0-4% over 4 h) in dichloromethane as an eluent to give **4a** as a colorless oil (1.1 g, 59%). ^{1}H NMR (400 MHz, $CDCl_3$): δ 1.43 (s, 18H), 3.21-3.25 (m, 4H), 3.34 (t, 6H, J = 5.2 Hz), 3.51-3.78 (m, 62 H), 4.13 (s, 2H), 4.56 (s, 4H), 5.13 (s, 2H), 6.81 (s, 2H), 7.12 (s, 1H), 7.33 (d, 4H, J = 8 Hz), 7.47 (d, 4H, J = 8 Hz), 8.85 (s, 1H); ^{13}C NMR (100 MHz, $CDCl_3$): δ 28.3, 40.3, 50.6, 69.4, 69.7, 69.9, 70.0, 70.4-70.6, 72.7, 88.9, 90.0, 117.7, 122.3, 124.1, 124.9, 127.4, 131.6, 138.6, 146.5, 155.9, 168.8. MALDI-MS (M+H): found m/z 1427.65, calcd for $C_{72}H_{110+1}N_6O_{23}$ 1427.67.

N-(3,5-Bis{4-[19-amino-(3n$_{18}^3$-1)-hexaoxanonadecylphenyl]ethynyl}aniline)-20-Azido-3n$_{18}^3$-icosan-1-amide (5a). Compound **4a** (0.50 g, 0.35 mmol) was dissolved in a solution of TFA (0.3 mL, 3.3 mmol) and anhydrous dichloromethane (0.2 ml). The solution was stirred for 10 minutes at room temperature, and concentrated by rotary evaporation. The residue was purified by flash column chromatography using a gradient

of methanol (0-13% over 4 h) in dichloromethane as an eluent to give **5a** as colorless oil (0.30 g, 69%). ^{1}H NMR (400 MHz, $CDCl_3$): δ 2.5 (s, 4H), 3.20-3.25 (m, 4H), 3.34 (t, 6H, J = 5.2 Hz), 3.50-3.77 (m, 62 H), 4.13 (s, 2H), 4.56 (s, 4H), 6.80 (s, 2H), 7.11 (s, 1H), 7.32 (d, 4H, J = 8 Hz), 7.47 (d, 4H, J = 8 Hz), 8.89 (s, 1H); ^{13}C NMR (100 MHz, $CDCl_3$): δ 40.3, 50.6, 69.4, 69.7, 69.9, 70.0, 70.4-70.6, 72.7, 88.9, 90.0, 117.7, 122.3, 124.1, 124.9, 127.4, 131.6, 138.6, 146.5, 168.8; MALDI-MS (M+H): found m/z 1227.40, calcd for $C_{62}H_{94+1}N_6O_{19}$ 1227.44.

N-(3,5-Bis{4-[19-biotinylated-amino-(3n$_{18}^{3}$-1)-hexaoxanonadecyl]phenylethynyl}aniline))-20-Azido-3n$_{18}^{3}$-icosan-1-amide (6a). A solution of **5a** (0.20 g, 0.16 mmol), NHS-Biotin (0.116 g, 0.34 mmol), and triethylamine (0.047 mL, 0.34 mmol) in anhydrous DMF (2 mL) was stirred at room temperature for 2.5 h, and concentrated by rotary evaporation. The residue was purified by flash column chromatography on silica gel using a gradient of methanol (0-5% over 4 h) in dichloromethane as an eluent to give **6a** as a colorless oil (0.17 g, 62%). ^{1}H NMR (400 MHz, $CDCl_3$): δ 1.30-1.80 (m, 12H), 2.21 (t, 4H, J = 7.1 Hz), 2.72 (d, 2H, J = 12.5 Hz), 2.86 (dd, 2H, J = 4.8 Hz, J = 12.5 Hz), 3.13-3.17 (m, 2H), 3.21-3.26 (m, 4H), 3.33 (t, 6H, J = 5.2 Hz), 3.52-3.78 (m, 62 H), 4.13 (s, 2H), 4.31-4.35 (m, 2H), 4.49-4.53 (m, 2H), 4.58 (s, 4H), 5.75 (s, 2H), 6.45 (s, 2H), 6.50 (s, 2H), 6.81 (s, 2H), 7.10 (s, 1H), 7.32 (d, 4H, J = 8 Hz), 7.47 (d, 4H, J = 8 Hz), 8.91 (s, 1H); ^{13}C NMR (100 MHz, $CDCl_3$): δ 25.5, 28.0, 28.1, 35.8, 39.1, 40.3, 50.6, 55.5, 60.1, 61.7, 69.3, 69.7, 69.9, 70.0, 70.4-70.6, 72.7, 88.9, 90.0, 117.7, 122.3, 124.1, 124.8, 127.4, 131.6, 138.6, 146.5, 163.9, 168.7, 173.5; MALDI-MS (M+H): found m/z 1679.76, calcd for $C_{82}H_{122+1}N_{10}O_{23}S_2$ 1679.81.

N-(3,5-Bis{4-[19-*tert*-butoxycarbonylamino-(3n$_{18}^3$-1)-hexaoxanonadecyl]phenylethynyl}aniline)-56-azido-3n$_{54}^3$-octadecaoxahexapentacontan-1-amide (4b). Compound **S7b** (see S2 in Supporting Information for its synthesis) dissolved in anhydrous dichloromethane (0.5 mL) was added to a solution of compound **3** (0.66 g, 0.6 mmol) in anhydrous dichloromethane (0.5 mL) and pyridine (98 μL, 1.2 mmol). The solution was stirred for 12 h at room temperature, and then concentrated by rotary evaporation. The residue was purified by flash column chromatography on silica gel using a gradient of methanol (0-4% over 4 h) in dichloromethane as an eluent to give 4b as a colorless oil (0.76 g, 69%). ^{1}H NMR (400 MHz, $CDCl_3$): δ 1.43 (s, 18H), 3.20-3.25 (m, 4H), 3.34 (t, 6H, J = 5.2 Hz), 3.52-3.78 (m, 110 H), 4.13 (s, 2H), 4.56 (s, 4H), 5.13 (s, 2H), 6.80 (s, 2H), 7.12 (s, 1H), 7.32 (d, 4H, J = 8 Hz), 7.47 (d, 4H, J = 8 Hz), 8.85 (s, 1H); ^{13}C NMR (100 MHz, $CDCl_3$): δ 28.3, 40.3, 50.6, 69.4, 69.7, 69.9, 70.0, 70.3-70.6, 72.7, 88.9, 90.0, 117.7, 122.3, 124.1, 124.9, 127.4, 131.6, 138.6, 146.5, 155.9, 168.9. MALDI-MS (M+H): found m/z 1957.36, calcd for $C_{96}H_{158+1}N_6O_{35}$ 1957.31.

N-(3,5-Bis{4-[19-amino-(3n$_{18}^3$-1)-hexaoxanonadecyl]phenylethynyl}aniline)-56-Azido-3n$_{54}^3$-octadecaoxahexapentacontan-1-amide (5b). Compound **4b** (0.7 g, 0.35 mmol) was dissolved in a solution of TFA (0.3 ml) and anhydrous dichloromethane (0.2 ml). The solution was stirred for 10 minutes at room temperature, and then concentrated by rotary evaporation. The residue was purified by flash column chromatography using a gradient of methanol (0-13% over 4 h) in dichloromethane as an eluent to give **5b** as colorless oil (0.44 g, 70%). ^{1}H NMR (400 MHz, $CDCl_3$): δ 2.5 (s, 4H), 3.20-3.25 (m,

4H), 3.34 (t, 6H, J = 5.2 Hz), 3.50-3.77 (m, 110 H), 4.13 (s, 2H), 4.56 (s, 4H), 6.81 (s, 2H), 7.11 (s, 1H), 7.32 (d, 4H, J = 8 Hz), 7.47 (d, 4H, J = 8 Hz), 8.89 (s, 1H); ^{13}C NMR (100 MHz, $CDCl_3$): δ 40.3, 50.6, 69.4, 69.7, 69.9, 70.0, 70.3-70.6, 72.7, 88.9, 90.0, 117.7, 122.3, 124.1, 124.9, 127.4, 131.6, 138.6, 146.5, 168.9; MALDI-MS (M+H): found m/z 1757.16, calcd for $C_{86}H_{142+1}N_6O_{31}$ 1757.07.

N-(3,5-Bis{4-[19-biotinylated-amino-(3n$_{18}^3$-1) hexaoxanonadecyl]phenylethynyl}aniline)-56-Azido-3n$_{54}^3$ octadecaoxahexapentacontan-1-amide (6b). To a solution of **5b** (0.2 g, 0.11 mmol), NHS-Biotin (0.116 g, 0.34 mmol), and triethylamine (0.047 mL, 0.34 mmol) in anhydrous DMF (2 mL) was stirred at room temperature for 2.5 h, and concentrated by rotary evaporation. The residue was purified by flash column chromatography on silica gel using a gradient of methanol (0-5% over 4 h) in dichloromethane as an eluent to give **6b** as a colorless oil (0.17 g, 67%). ^{1}H NMR (400 MHz, $CDCl_3$): δ 1.30-1.80 (m, 12H), 2.21 (t, 4H, J = 7.1 Hz), 2.72 (d, 2H, J = 12.5 Hz), 2.86 (dd, 2H, J = 4.8 Hz, J = 12.5 Hz), 3.13-3.17 (m, 2H), 3.21-3.26 (m, 4H), 3.33 (t, 6H, J = 5.2 Hz), 3.52-3.78 (m, 110 H), 4.13 (s, 2H), 4.30-4.35 (m, 2H), 4.49-4.52 (m, 2H), 4.58 (s, 4H), 5.75 (s, 2H), 6.45 (s, 2H), 6.50 (s, 2H), 6.81 (s, 2H), 7.09 (s, 1H), 7.32 (d, 4H, J = 8 Hz), 7.47 (d, 4H, J = 8 Hz), 8.90 (s, 1H); ^{13}C NMR (100 MHz, $CDCl_3$): δ 25.5, 28.0, 28.1, 35.8, 39.1, 40.3, 50.6, 55.5, 60.1, 61.7, 69.3, 69.7, 69.9, 70.0, 70.3-70.6, 72.7, 88.9, 90.0, 117.7, 122.3, 124.1, 124.8, 127.4, 131.6, 138.6, 146.5, 163.9, 168.8, 173.4; MALDI-MS (M+H): found m/z 2209.52, calcd for $C_{106}H_{170+1}N_{10}O_{35}S_2$ 2209.66.

4.2.4. Conclusions.

Departing from a benzene ring which is one of the most commonly used scaffolds to construct multivalent molecules,[134,148,149] we extended the structure with phenylethynyl groups to create a larger rigid structure, on which small sized antibody mimics can be constructed. The phenylacetylene chemistry used in this present study can be extended to synthesizing even more complicated and larger scaffolds.[150]

We have used the bis-biotin structure to study interactions with streptavidin and compared dissociation kinetics and stability with a monobiotin linker. It was observed that the Y-shaped bisbiotin ligand can: (1) form a 2:1 complex with streptavidin that was thermally more stable than the 4:1 complex composed of monobiotin ligand in solution; (2) form an intramolecular bivalent complex which is more stable than its intermolecular counterpart on the surface; (3) bind to streptavidin cooperatively. SPR study performed with the y-bisbiotin indicates that y-Bisbiotin greatly reduced the dissociation rate (k_{off}), resulting in a very stable complex with streptavidin. The increase in residence time ($1/k_{off}$) of a ligand interacting with its receptor is of importance in design of drugs. Besides binding affinity, the residence time—the period for which a drug remains bound to its target[151]—has been demonstrated for use as a parameter to determine the efficacy of a drug.[152,153]

4.3. Biochemical Construction of a Tripod Antibody to target Ebola Virus.

4.3.1 Introduction

Ebola virus (EBOV) causes severe hemorrhagic fever with up to 90% lethality, but no treatments have been approved for human use. Its 2014 outbreak warned us once more to develop effective pre- and post-exposure treatments with urgency. Presently, monoclonal

antibody (MAb) cocktails are appealing owing to their proven efficacy in nonhuman primates. ZMapp, one of the 3-MAb cocktails (containing MAbs c13C6, c2G4 and c4G7 produced in plants), has become a household name after it was used to treat two Americans who were infected while working in Liberia. However, Zmapp is not widely available to patients due to (1) one of the three MAbs expressed poorly and (2) an extraordinarily high treatment dosage (12 g per patient) is required. These highlight the urgency to optimize the MAb cocktails for greater potency, efficacy, and production. For therapeutic MAbs, the EBOV glycoprotein (GP) is their target. The GP forms trimeric spikes on the virion surface, in which each monomer is a disulfide-bonded complex of a receptor binding subunit (GP1) and a fusion subunit (GP2). Structural studies on how Zmapp MAbs bind to GP have revealed that the high-dosage requirement of Zmapp may be caused by their relative low affinity-binding to GP due to the architecture and distribution of spikes.[154,155] Other studies have shown that Mab variants that can bind bivalently to a single ENV trimeric spike of HIV-1 exhibit >100 fold increase in neutralization potencies due to their ability to perform high-avidity intra-spike crosslinking.[14] These show that multivalent interactions with class-I viral GP (including both HIV-1 and EBOV) increase the potency of MAbs and in turn reduce the administering dosage. Hence, we are developing an antibody mimic bearing trivalent antigen-binding sites, called tripod antibody (TripodAb) (**Fig.42**), as an immunotherapeutic agent against EBOV to enhance potency and producibility. The molecule is derived from a scaffold composed of a rigid tetrahedron core flanked with multiple hydrophilic chains. In the structure, three single chain variable fragments (scFv)

are linked to the scaffold to form a tripod base, which allows them to concomitantly interact with a trimeric GP spike that has a “chalice” configuration. Meanwhile, a human IgG1 Fc is installed on the top of the tetrahedron, exerting effector functions of a MAb, which has been shown to be critical for the potency of Zmapp MAbs. Unlike a natural antibody whose bivalent binding to antigens may be restricted due to antigen architecture or density, the antibody mimic we designed should allow the molecule to bind a GP spike multivalently and more tightly than MAbs in Zmapp, and leave Fc in the favorable position to exert effector functions. Strategies of using full MAbs to improve their production, binding-affinity and potency against EBOV have suffered from several setbacks: (1) optimization of Zmapp full MAb expression has been unsuccessful despite major efforts in both mammalian and plant systems; and (2) the architecture of a full IgG MAb is not favorable for at least two MAbs in Zmapp to bind GP spike bivalently while retaining effector function, leading to low-antigen affinity and potency. We also used non-peptide linkers with a precise length to chemically conjugate three scFVs (homo-tri-ScFvs or hetero-tri-ScFvs from the three Zmapp MAbs) with a human IgG1 Fc to form a tripodAb, rationally designed for high-avidity intra-spike multivalent interactions independent of spike architecture and distribution. We believe our synthetic antibody would be able to achieve a high level production of anti-EBOV MAb derivatives and their high-avidity binding to EBOV, enhancing the efficacy and availability of anti-EBOV immunotherapeutics. In addition to generating urgently needed therapeutic reagents for treating EBOV, this study provides a platform for optimizing MAbs efficacy

independent of antigen architecture and density, which should be broadly applicable to treatment of other viral disease.

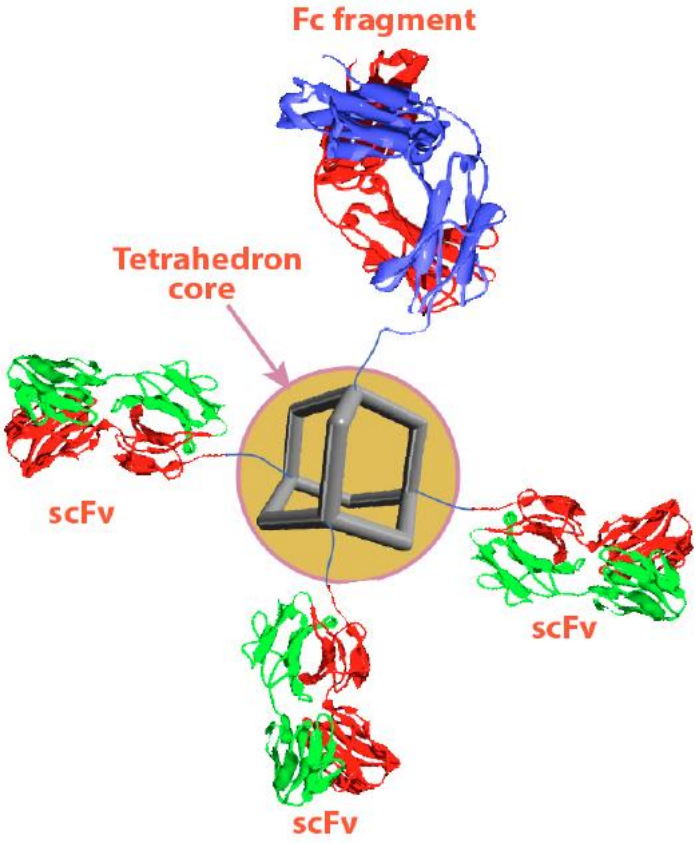

Figure 47. Tripod antibody (TripodAb) as an immunotherapeutic agent against EBOV. ScFv: single-chain variable fragment, they are optimally spaced to ensure intraspike cross-linking. Fc: from the crystallizable fragment of human IgG1 to exert EBOV killing through antibody effector functions.

4.3.2. Results and discussion.

Four-arm linker. We have synthesized a tetravalent linking molecule (Ar4) with Bicyclo[6,1,0]non-4-yn-9-ylmethanol (BCN) at three ends and (*E*)-Cyclooct-4-enol (TCO) at the other end.

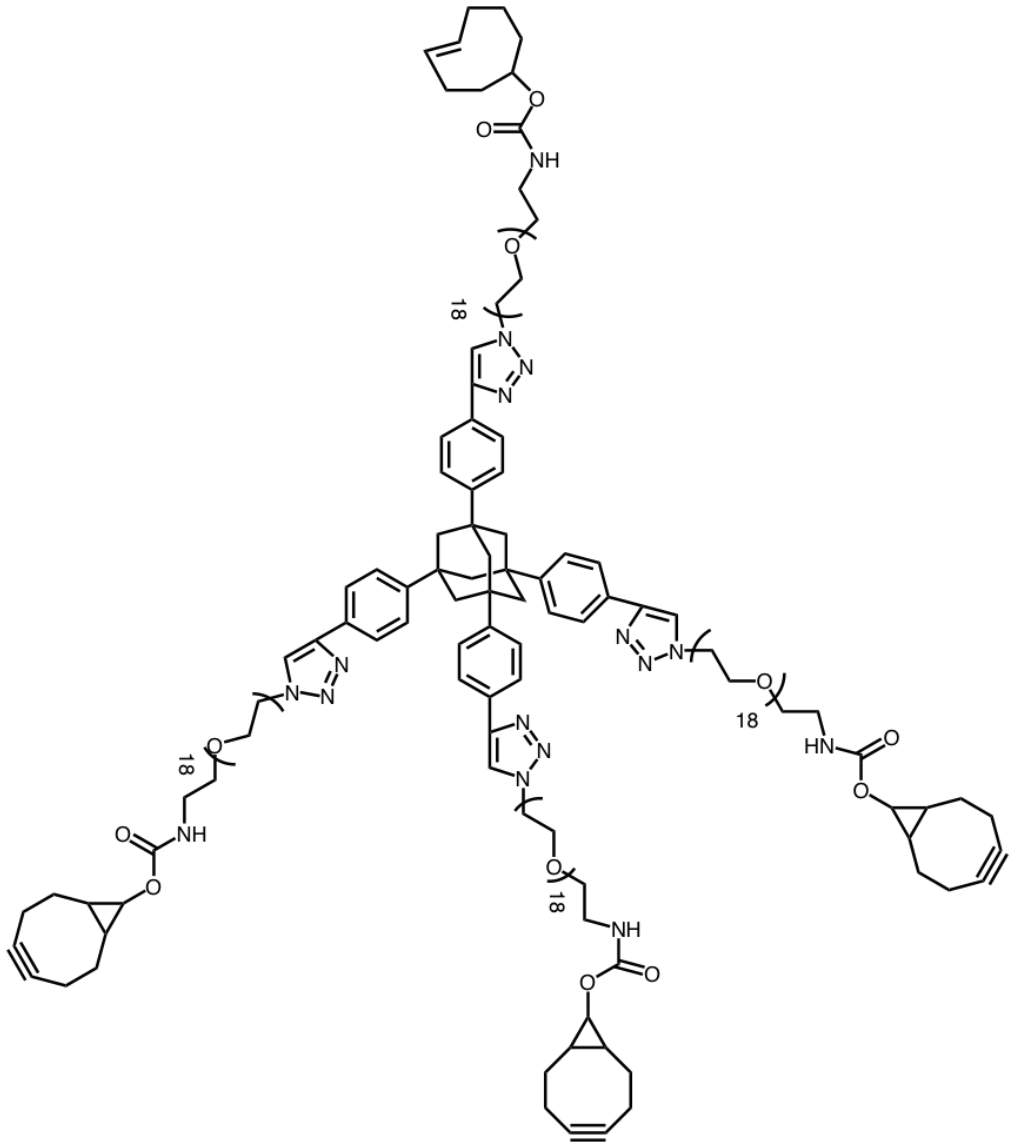

Figure48. Structure of 4-arm linker (Ar4)

The central part of the 4 arm linker consists of a C4 symmetric tetraamine molecule (3) that can be prepared from 1,3,5,7-tetrakis(4-ethynylphenyl)adamantane (1) in two steps by copper catalyzed click chemistry with compound 2 followed by hydrazinolysis.

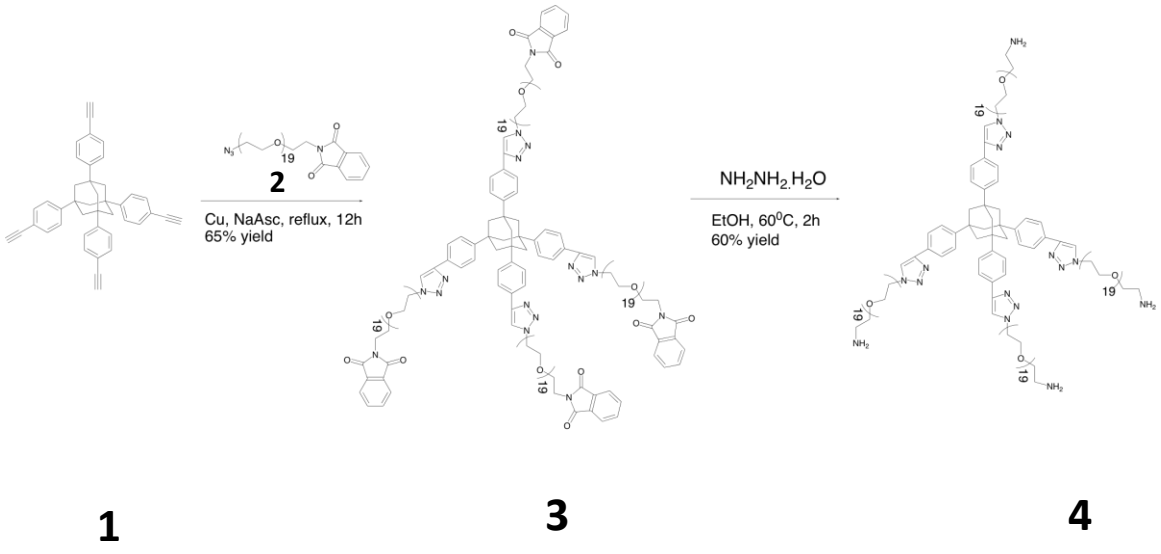

Scheme 4.3.1. Synthesis of compound 4

Following this compound 4 can be sequentially reacted with TCO-NHS and BCN-NHS to obtain compound 6.

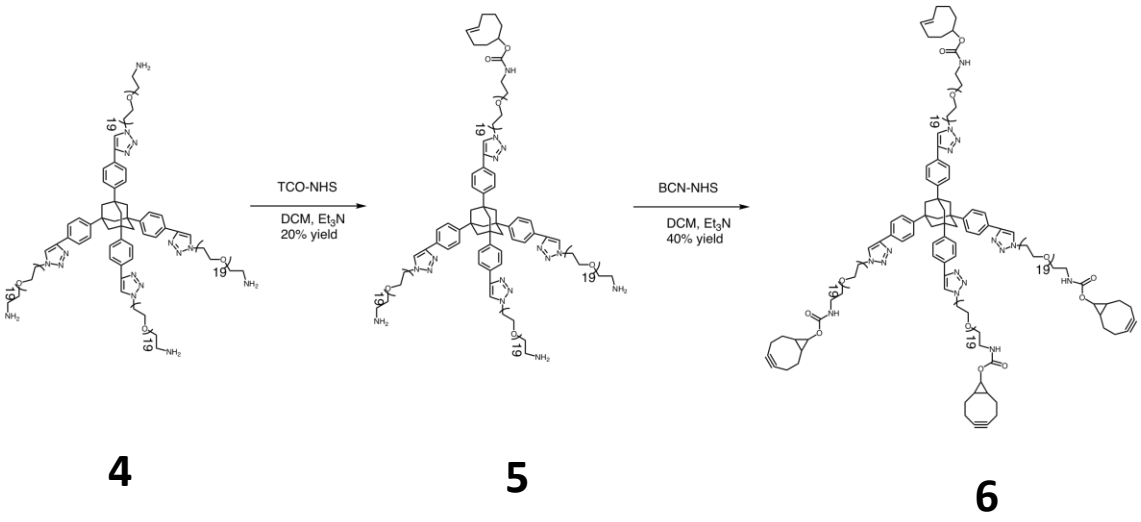

Scheme 4.3.2. Synthesis of compound 6.

We used c6D8, a protein that binds to mucin-like glycoprotein domains of ebola viruses as the single chain variable fragment for our synthetic antibody. The c6D8 protein was expressed in plants with a LPETGEE sequence at the C-terminus so that it can be reacted with a nucleophile by sortase A enzyme mediated ligation. We chose GGGAz (Az = Azidoalanine) as the nucleophiles to site-specifically functionalize the c6D8 protein with an azide group so that the protein may be attached to Ar4 by uncatalyzed click chemistry reaction between BCN and the azide moiety. By monitoring the amount of catalyst used for the reaction we observed that 500 ng of sortase A provided the best yield for reaction of 20 µg of c6D8 protein. The conversion was monitored by performing a ligation reaction followed by mixing the reaction mixture with DBCO functionalized Cy5. The amount of ligation is monitored by gel electrophoresis followed by fluorescence imaging of the gel to measure the intensity of the bands.

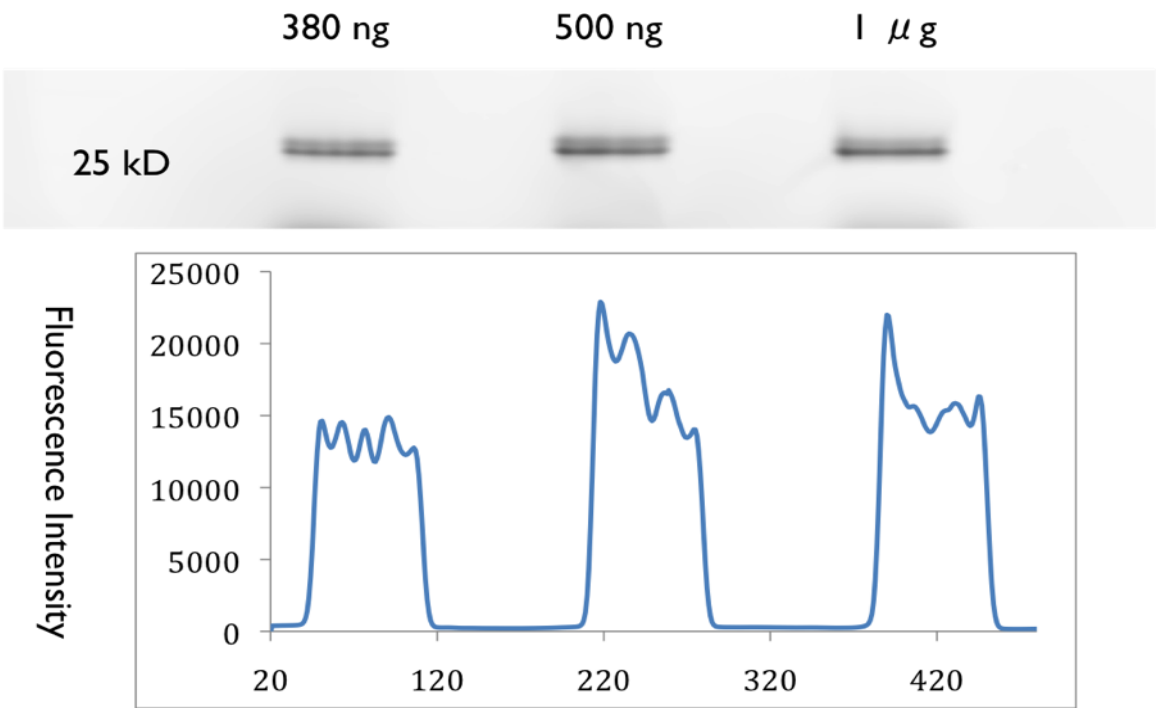

Figure 49. Fluorescence gel of sortase A mediated ligation of c6D8 protein.

Monitoring of the reaction at different time intervals for ligation of 20 μg of c6D8 protein using 500 ng of sortase A indicated the reaction reached completion after 15 h.

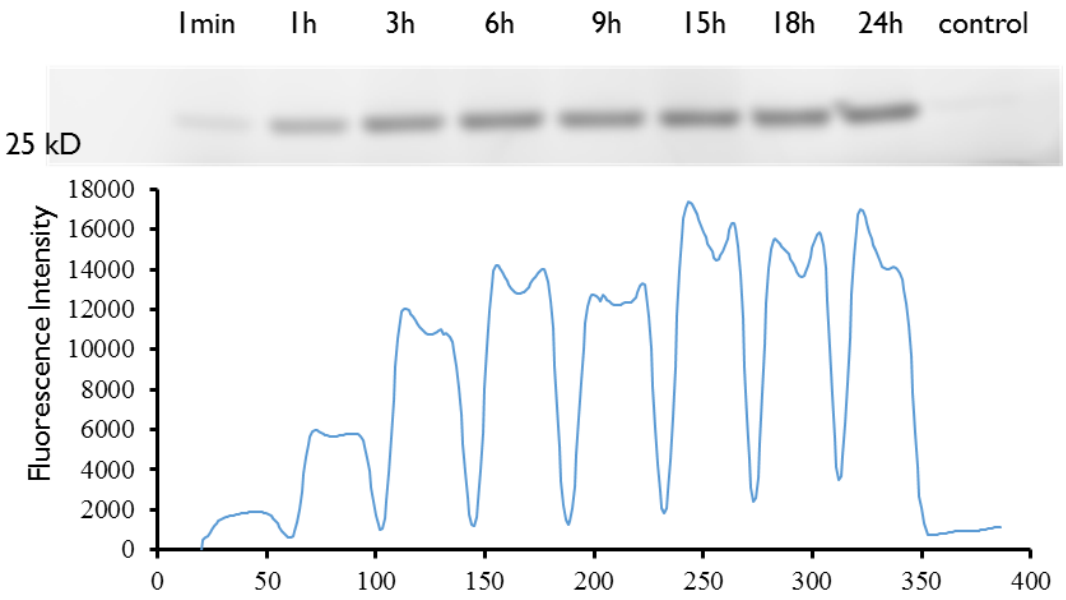

Figure 50. Time course for sortase A mediated reaction.

We are currently working on reaction between the azide functionalized c6D8 with Ar4.

4.3.3 Experimental section.

General Information

All reagents and solvents were purchased from commercial suppliers (Sigma-Aldrich, Alfa Aesar, Fluka, TCI America) and used as received unless otherwise noted. Cy5-DBCO was purchase from Click Chemistry Tools. *Staphylococcus aureus* sortase A pentamutant was purchased from BPS Bioscience. All peptides used in the study were custom synthesized from CPC Scientific. Centrifugal filter units were purchased from EMD Millipore. All experiments requiring anhydrous conditions were performed in

flame-dried glassware under nitrogen atmosphere. Reactions were monitored by thin layer chromatography (TLC) using silica gel precoated on glass plates (EMD Millipore). ^{1}H NMR and ^{13}C NMR spectra were recorded on Varian INOVA 400 (400 MHz) spectrometer at 25 °C. Chemical shifts (δ) are given in parts per million (ppm) and referenced to the residual solvent peak ($CDCl_3$, δH = 7.26 ppm; CD_3OD, δH = 3.31 ppm; DMSO-d6, δH = 2.50 ppm). Coupling constants (J) are expressed in hertz (Hz) and the values are rounded to the nearest 0.1 Hz. Splitting patterns are reported as follows: br, broad; s, singlet; d, doublet; dd, doublet of doublets; t, triplet; dt, doublet of triplets; q, quartet and m, multiplet. High-resolution mass spectra (HRMS) were acquired at the Arizona State University CLAS High Resolution Mass Spectrometry Facility. MALDI-MS was performed using a Bruker MALDI-MS instrument at ASU. Flash chromatography was performed in an automated flash chromatography system (CombiFlash Rf, Teledyne Isco, Inc.) with silica gel columns (60−120 mesh). RP-HPLC analysis and separation were performed with a Zorbax 300SB-C18 column (5 µm, 9.4x250 mm) in an Agilent 1100 HPLC equipped with UV monitor and fraction collector.

Synthesis of compound 1. Compound 1 was synthesized in four steps starting from 1-bromoadamantane in four synthetic steps following literature protocol.[156]

Synthesis of compound 2. The synthesis of compound 2 starting from *O*-(2-Azidoethyl)nonadecaethylene glycol (compound 2a) is shown in scheme 4.3.3

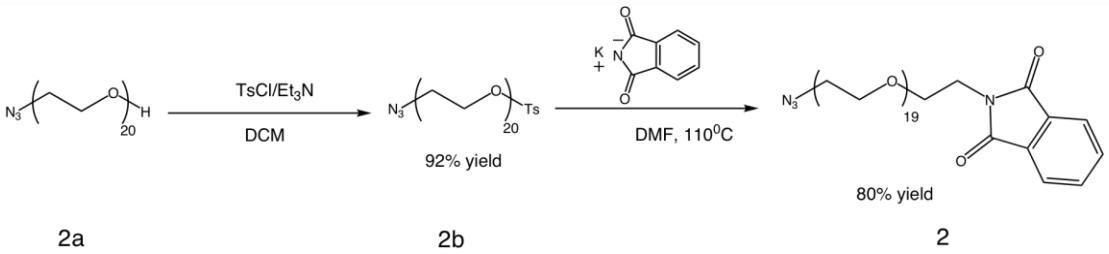

Scheme 4.3.3. Synthesis of compound 2.

Synthesis of compound 2b. Tosyl chloride (156 mg, 0.81 mmol) is added to solution of compound 2a (500 mg, 0.54 mmol) and triethylamine (0.5 mL, 3.59 mmol) in anhydrous dichloromethane (5 mL) under nitrogen. The reaction mixture was stirred at room temperature for 12 h, and then the solvent was removed by rotary evaporation. The residue was purified by silica gel column chromatography using a gradient of 4% methanol in dichloromethane over 1 h, giving compound **2b** as a colorless liquid (537 mg, 92% yield). ^{1}H NMR (400 MHz, CDCl3): δ 2.34 (s, 3H); 3.27 (t, 2 H, J = 4.8 Hz); 3.46-3.58 (m, 76 H); 4.04 (t, 2 H, J = 4.8 Hz); 7.23 (d, 2H, J = 8 Hz); 7.67 (d, 2 H, J = 8 Hz). ^{13}C NMR (100MHz, CDCl3): δ 144.67, 132.94, 129.74, 127.86, 70.72-70.46, 69.93, 69.18, 68.55, 50.57, 21.54.

MALDI-MS. m/z : found 1100.79; calcd. for C47H87N3O22SNa 1101.17

Synthesis of compound 2. Potassium phthalimide (133.4 mg, 0.72 mmol) is added to solution of compound 2b (500 mg, 0.46 mmol) in 5 mL anhydrous DMF under nitrogen. The reaction mixture is then heated at 110°C for 15 h following which the solvent was removed by rotary evaporation. The residue was purified by silica gel

column chromatography using a gradient of 4% methanol in dichloromethane over 1 h, giving compound 2 as a colorless liquid (390 mg, 80% yield). ^{1}H NMR (400 MHz, CDCl3): δ 3.32 (t, 2 H, J = 4.8 Hz); 3.51-3.69 (m, 76 H); 3.83 (t, 2 H, J = 5.6 Hz); 7.66 (dd, 2H, J = 5.6, 2.8 Hz); 7.78 (dd, 2 H, J = 5.6, 2.8 Hz). ^{13}C NMR (100MHz, CDCl3): δ 168.15, 133.87, 133.08, 123.15, 70.63-70.51, 67.83, 50.61, 37.19. MALDI-MS. m/z : found 1075.60; calcd. for C48H84N4O21Na 1076.09.

Synthesis of compound 3. Compound 1 (34 mg, 0.064 mmol) is added to a solution of compound 2 (300 mg, 0.28 mmol) in 2.5 mL tert-butanol and 2.5 mL water under nitrogen. This is followed by the addition of Copper sulfate pentahydrate (7.5 mg, 0.03 mmol) and Sodium Ascorbate (12 mg, 0.06 mmol). The reaction mixture is heated at 90°C for 8 h following which the reaction mixture is filtered and the solvent is removed by rotary evaporation. The solid residue is redissolved in a 1:1 mixture of water and acetonitrile following which the compound is purified by semiprep RP-HPLC using a 300SB-C18 column. The product was purified using RP HPLC with an eluting system composed of (A) 0.1% TFA in DI water and (B) 0.09% TFA in 80:20 acetonitrile: water. The retention time of the product in RP HPLC was 27.6 min with a mobile phase started at 70% eluent A and 30% eluent B, linearly increasing to 70% B in 30 min. The purified product was concentrated by rotary evaporation to obtain a colorless oil (241 mg, 65% yield). ^{1}H NMR (400 MHz, CDCl3): δ 2.21 (s, 12 H); 3.53-3.91 (m, 312 H); 4.56 (t, 8 H, J = 4.8 Hz); 7.75 (d, 8H, J = 8.4 Hz); 7.68 (dd, 8 H, J = 5.6, 3.2 Hz); 7.80 (dd, 8H, J = 5.6, 3.2 Hz); 7.81 (d, 8H, J = 8.4 Hz); 7.95 (s, 4H). ^{13}C NMR

(100MHz, CDCl3): δ 168.19, 149.09, 147.37, 133.89, 132.11, 128.78, 125.74, 125.49, 123.19, 120.83, 70.53, 70.05, 69.53, 67.86, 50.33, 47.17, 39.26, 37.21.

MALDI-MS. m/z : found 4774.4; calcd. for C234H368N16O84Na 4772.36.

Synthesis of compound 4. Compound 3 (200 mg, .042 mmol) is dissolved in anhydrous ethanol (5 mL) followed by the addition of hydrazine hydrate (36 µL, 0.75 mmol). The reaction mixture is heated for 2 h at 60°C following which the reaction mixture is filtered and the solvent is removed by rotary evaporation. The solid residue is redissolved in a 1:1 mixture of water and acetonitrile following which the compound is purified by semiprep RP-HPLC using a 300SB-C18 column. The product was purified using RP HPLC with an eluting system composed of (A) 0.1% TFA in DI water and (B) 0.09% TFA in 80:20 acetonitrile: water. The retention time of the product in RP HPLC was 22.5 min with a mobile phase started at 62% eluent A and 38% eluent B, linearly increasing to 45% B in 60 min. The purified product was concentrated by rotary evaporation to obtain a colorless oil (107 mg, 60% yield). ^{1}H NMR (400 MHz, CDCl3): δ 2.22 (s, 12 H); 3.11-3.15 (m, 8 H); 3.57-3.76 (m, 296 H); 3.92 (t, 8H, J= 4.8 Hz); 4.59 (t, 8 H, J = 4.8 Hz); 7.01 (s, 12 H); 7.57 (d, 8H, J = 8.4 Hz); 7.80 (d, 8H, J = 8.0 Hz); 8.08 (s, 4H). ^{13}C NMR (100MHz, CDCl3): δ 149.51, 146.86, 127.70, 126.00, 125.65, 121.59, 70.48-69.22, 66.75, 50.75, 47.08, 39.88, 39.30.

MALDI-MS. m/z (M+H): found 4230.67; calcd. for C202H360+1N16O76 4229.06.

Synthesis of compound 5. Compound 4 (40 mg, 0.009 mmol) is dissolved in anhydrous DCM under Nitrogen followed by the addition Triethylamine (0.1 mL, 0.7 mmol) and (*E*)-Cyclooct-4-enyl 2,5-dioxo-1-pyrrolidinyl carbonate (TCO-NHS) (3.6 mg, 0.014

mmol) following which the reaction is stirred and room temperature for 12 h. The solvent is then removed by rotary evaporation. The solid residue is redissolved in a 1:1 mixture of TEAA (0.1 M) and acetonitrile following which the compound is purified by semiprep RP-HPLC using a 300SB-C18 column. The product was purified using RP HPLC with an eluting system composed of (A) TEAA buffer (0.1 M) and (B) Acetonitrile. The retention time of the product in RP HPLC was 17.6 min with a mobile phase started at 70% eluent A and 30% eluent B, linearly increasing to 80% B in 60 min. The purified product was concentrated by rotary evaporation to obtain a colorless oil. (8 mg, 20% yield). ^{1}H NMR (400 MHz, CDCl3): δ 1.47-1.58 (m, 2H); 1.71-1.78 (m, 2H); 1.89-2.05 (m, 4H); 2.23 (s, 12H); 2.29-2.36 (m, 2H); 2.85-2.90 (m, 2H); 3.32-3.79 (m, 302H); 3.91 (t, 8H, J = 4.8 Hz); 4.30-4.32 (m, 1H); 4.58 (t, 8H, J = 4.8 Hz); 5.10-5.18 (m, 1H); 5.42-5.76 (m, H); 7.56 (d, 8H, J = 8.4 Hz); 7.83 (d, 8H, J = 8.4 Hz), 7.96 (s, 4H)

MALDI-MS. m/z (M+H): found 4284.7; calcd. for C211H372+1N16O78 4382.25.

Synthesis of compound 6. Compound 5 (8 mg, 0.0018 mmol) is dissolved in anhydrous DCM under Nitrogen followed by the addition Triethylamine (0.1 mL, 0.7 mmol) and (1*R*,8*S*,9*s*)-Bicyclo[6.1.0]non-4-yn-9-ylmethyl *N*-succinimidyl carbonate (BCN-NHS) (3.6 mg, 0.014 mmol) following which the reaction is stirred and room temperature for 12 h. The solvent is then removed by rotary evaporation. The solid residue is redissolved in a 1:1 mixture of TEAA (0.01 M) and acetonitrile following which the compound is purified by semiprep RP-HPLC using a 300SB-C18 column. The product was purified using RP HPLC with an eluting system composed of (A) TEAA buffer (0.01 M) and (B) Acetonitrile. The retention time of the product in RP HPLC was

33.2 min with a mobile phase started at 65% eluent A and 35% eluent B, linearly increasing to 80% B in 60 min. The purified product was concentrated by rotary evaporation to obtain a colorless oil. (3.5 mg, 40% yield). ^{1}H NMR (400 MHz, CDCl3): δ 0.82-0.98 (m, 9H); 1.28-1.42 (m, 6H); 1.47-1.58 (m, 2H); 1.68-1.78 (m,2 H); 1.89-2.05 (m, 4H); 2.23 (s, 12H); 2.17-2.67 (m, 12H); 2.27-2.38 (m, 8H); 2.83-2.90 (m, 8H); 3.33-3.82 (m, 296 H); 3.91 (t, 8H, J = 4.8 Hz); 4.13 (d, 6H, J= 8.4 Hz); 4.30-4.32 (m, 1H); 4.58 (t, 8H, J = 4.8 Hz); 5.10-5.18 (m, 1H); 5.20-5.32 (m, 3H) 5.42-5.76 (m, 2 H); 7.56 (d, 8H, J = 8.4 Hz); 7.83 (d, 8H, J = 8.4 Hz), 7.97 (s, 4H).

MALDI-MS. m/z: found 4949.10; calcd. for C244H408N16O84 4949.01.

Procedure for sortase mediated ligation. Sortase reaction was performed in 50 μL buffer solution containing 50 mM HEPES (pH=7.4), 150 mM NaCl, 5 mM $CaCl_2$, 0.5 mM GGGAz, 24 μM c6D8 protein, and 500 ng Sortase A pentamutant for 15 h at 30°C. Following this 5 μL of the reaction mixture is aliquoted with 5 μL of Cy5-DBCO (2 mM) for 2 h at room temperature following which the samples is loaded on a SDS-PAGE gel. Fluorescence image of the SDS-PAGE gel is obtained. The modified c6D8 protein is purified and buffer exchanged to PBS pH 7.4 using 10 kD Amicon ultracentrifugal filters.

4.3.4. Summary. We have synthesized a 4-arm scaffold in our quest to design a chemically synthesized antibody to target Ebola glycoproteins. We are have devised a sortase A mediated ligation chemistry to functionalize the protein site-selectively. We are currently working on attachment of the proteins to the four arm linker.

REFERENCES

(1) Choi, S.-K. *Synthetic Multivalent Molecules Concepts and Biomedical Applications*; Wiley-Interscience
2004.

(2) Mammen, M.; Chio, S.-K.; Whitesides, G. M. *Angew. Chem., Int. Ed.* **1998**, *37*, 2755.

(3) Levine, P. M.; Carberry, T. P.; Holub, J. M.; Kirshenbaum, K. *MedChemComm* **2013**, *4*, 493.

(4) Matrosovich, M.; Klenk, H.-D. *Rev. Med. Virol.* **2003**, *13*, 85.

(5) Matsubara, T.; Onishi, A.; Saito, T.; Shimada, A.; Inoue, H.; Taki, T.; Nagata, K.; Okahata, Y.; Sato, T. *J. Med. Chem.* **2010**, *53*, 4441.

(6) Waldmann, M.; Jirmann, R.; Hoelscher, K.; Wienke, M.; Niemeyer, F. C.; Rehders, D.; Meyer, B. *J. Am. Chem. Soc.* **2014**, *136*, 783.

(7) Rao, J.; Lahiri, J.; Isaacs, L.; Weis, R. M.; Whitesides, G. M. *Science* **1998**, *280*, 708.

(8) Mann, D. A.; Kanai, M.; Maly, D. J.; Kiessling, L. L. *J. Am. Chem. Soc.* **1998**, *120*, 10575.

(9) Gestwicki, J. E.; Strong, L. E.; Cairo, C. W.; Boehm, F. J.; Kiessling, L. L. *Chem. Biol.* **2002**, *9*, 163.

(10) Vauquelin, G.; Charlton, S. J. *Br. J. Pharmacol.* **2013**, *168*, 1771.

(11) Choi, S.-K. *Synthetic Multivalent Molecules: Concepts and Biomedical Applications*; John Wiley & Sons, Inc.: Hoboken, New Jersey, 2004.

(12) Mammen, M.; Choi, S.-K.; Whitesides, G. M. *Angew. Chem. Int. Ed.* **1998**, *37*, 2754.

(13) Cram, D. J.; Cram, J. M. *Container Molecules and Their Guests*; The Royal Society of Chemistry, 1994.

(14) Galimidi, R. P.; Klein, J. S.; Politzer, M. S.; Bai, S.; Seaman, M. S.; Nussenzweig, M. C.; West, A. P., Jr.; Bjorkman, P. J. *Cell (Cambridge, MA, U. S.)* **2015**, *160*, 433.

(15) Doppalapudi, V. R.; Huang, J.; Liu, D.; Jin, P.; Liu, B.; Li, L.; Desharnais, J.; Hagen, C.; Levin, N. J.; Shields, M. J.; Parish, M.; Murphy, R. E.; Del Rosario, J.; Oates, R. D.; Lai, J.-Y.; Matin, M. J.; Ainekulu, Z.; Bhat, A.; Bradshaw, C. W.; Woodnutt, G.; Lerner, R. A.; Lappe, R. W. *Proc. Natl. Acad. Sci. U. S. A.* **2010**, *107*, 22611.

(16) Tom, J. K.; Dotsey, E. Y.; Wong, H. Y.; Stutts, L.; Moore, T.; Davies, D. H.; Felgner, P. L.; Esser-Kahn, A. P. *ACS Cent. Sci.* **2015**, *1*, 439.

(17) McEnaney, P. J.; Parker, C. G.; Zhang, A. X.; Spiegel, D. A. *ACS Chem. Biol.* **2012**, *7*, 1139.

(18) McEnaney, P. J.; Fitzgerald, K. J.; Zhang, A. X.; Douglass, E. F., Jr.; Shan, W.; Balog, A.; Kolesnikova, M. D.; Spiegel, D. A. *J. Am. Chem. Soc.* **2014**, *136*, 18034.

(19) Begley, D. J. *Pharmacol. Ther.* **2004**, *104*, 29.

(20) de Boer, A. G.; Gaillard, P. J. *Annu. Rev. Pharmacol. Toxicol.* **2007**, *47*, 323.

(21) Pardridge, W. M. *Curr. Opin. Pharmacol.* **2006**, *6*, 494.

(22) Patel, M. M.; Goyal, B. R.; Bhadada, S. V.; Bhatt, J. S.; Amin, A. F. *CNS Drugs* **2009**, *23*, 35.

(23) Pardridge, W. M. *Expert Opin. Drug Delivery* **2015**, *12*, 207.

(24) Wu, D.; Yang, J.; Pardridge, W. M. *J. Clin. Invest.* **1997**, *100*, 1804.

(25) Boado, R. J.; Hui, E. K. W.; Lu, J. Z.; Sumbria, R. K.; Pardridge, W. M. *Bioconjugate Chem.* **2013**, *24*, 1741.

(26) Zlatanova, J.; Lindsay, S. M.; Leuba, S. H. *Prog. Biophys. Mol. Biol.* **2000**, *74*, 37.

(27) Binning, G., Quate, C. F., Gerber, Ch. *Phys. Rev. Lett.* **1986**, *56*.

(28) Binning, G.; Rohrer, H.; Gerber, C.; Weibel, E. *Phys. Rev. Lett.* **1982**, *49*, 57.

(29) Leite, F. L., Mattoso, L. H. C., Olibeira Jr., O. N., Herrmann Jr., P. S. P., ; Díaz, A. M.-V. a. J., Ed. 2007, p 747.

(30) Frisbie, C. D.; Rozsnyai, L. F.; Noy, A.; Wrighton, M. S.; Lieber, C. M. *Science (Washington, D. C.)* **1994**, *265*, 2071.

(31) Whited, A. M.; Park, P. S. H. *Biochim. Biophys. Acta, Biomembr.* **2014**, *1838*, 56.

(32) Agnihotri, A.; Soman, P.; Siedlecki, C. A. *Colloids Surf., B* **2009**, *71*, 138.

(33) Hussain, M. A.; Agnihotri, A.; Siedlecki, C. A. *Langmuir* **2005**, *21*, 6979.

(34) Litvinov, R. I.; Bennett, J. S.; Weisel, J. W.; Shuman, H. *Biophys. J.* **2005**, *89*, 2824.

(35) Touhami, A.; Hoffmann, B.; Vasella, A.; Denis, F. A.; Dufrene, Y. F. *Langmuir* **2003**, *19*, 1745.

(36) Wang, C.; Ehrhardt, C. J.; Yadavalli, V. K. *J. R. Soc. Interface* **2015**, *12*, 20141109/1.

(37) Jiang, Y.; Zhu, C.; Ling, L.; Wan, L.; Fang, X.; Bai, C. *Anal. Chem.* **2003**, *75*, 2112.

(38) Neundlinger, I.; Poturnayova, A.; Karpisova, I.; Rankl, C.; Hinterdorfer, P.; Snejdarkova, M.; Hianik, T.; Ebner, A. *Biophys. J.* **2011**, *101*, 1781.

(39) Harada, Y.; Kuroda, M.; Ishida, A. *Langmuir* **2000**, *16*, 708.

(40) Ouerghi, O.; Touhami, A.; Othmane, A.; Ben Ouada, H.; Martelet, C.; Fretigny, C.; Jaffrezic-Renault, N. *Sens. Actuators, B* **2002**, *84*, 167.

(41) Ros, R.; Schwesinger, F.; Anselmetti, D.; Kubon, M.; Schafer, R.; Pluckthun, A.; Tiefenauer, L. *Proc. Natl. Acad. Sci. U. S. A.* **1998**, *95*, 7402.

(42) Puntheeranurak, T.; Neundlinger, I.; Kinne, R. K. H.; Hinterdorfer, P. *Nat. Protoc.* **2011**, *6*, 1443.

(43) Senapati, S.; Lindsay, S. *Acc. Chem. Res.* **2016**, *49*, 503.

(44) Stroh, C. M.; Ebner, A.; Geretschlaeger, M.; Freudenthaler, G.; Kienberger, F.; Kamruzzahan, A. S. M.; Smith-Gill, S. J.; Gruber, H. J.; Hinterdorfer, P. *Biophys. J.* **2004**, *87*, 1981.

(45) Ebner, A.; Kienberger, F.; Kada, G.; Stroh, C. M.; Geretschlager, M.; Kamruzzahan, A. S. M.; Wildling, L.; Johnson, W. T.; Ashcroft, B.; Nelson, J.; Lindsay, S. M.; Gruber, H. J.; Hinterdorfer, P. *Chemphyschem* **2005**, *6*, 897.

(46) Bizzarri, A. R.; Cannistraro, S. *Chem. Soc. Rev.* **2010**, *39*, 734.

(47) Ebner, A.; Wildling, L.; Zhu, R.; Rankl, C.; Haselgruebler, T.; Hinterdorfer, P.; Gruber, H. J. *Top. Curr. Chem.* **2008**, *285*, 29.

(48) Hinterdorfer, P.; Kienberger, F.; Raab, A.; Gruber, H. J.; Baumgartner, W.; Kada, G.; Riener, C.; Wielert-Badt, S.; Borken, C.; Schindler, H. *Single Mol.* **2000**, *1*, 99.

(49) Ebner, A.; Hinterdorfer, P.; Gruber, H. J. *Ultramicroscopy* **2007**, *107*, 922.

(50) Limansky, A. P.; Shlyakhtenko, L. S.; Schaus, S.; Henderson, E.; Lyubchenko, Y. L. *Probe Microsc.* **2001**, *2*, 227.

(51) Guha Thakurta, S.; Subramanian, A. *Colloids Surf., A* **2012**, *414*, 384.

(52) Vandenberg, E. T.; Bertilsson, L.; Liedberg, B.; Uvdal, K.; Erlandsson, R.; Elwing, H.; Lundstroem, I. *J. Colloid Interface Sci.* **1991**, *147*, 103.

(53) Ebner, A.; Wildling, L.; Kamruzzahan, A. S. M.; Rankl, C.; Wruss, J.; Hahn, C. D.; Hoelzl, M.; Zhu, R.; Kienberger, F.; Blaas, D.; Hinterdorfer, P.; Gruber, H. J. *Bioconjugate Chem.* **2007**, *18*, 1176.

(54) Kamruzzahan, A. S. M.; Ebner, A.; Wildling, L.; Kienberger, F.; Riener, C. K.; Hahn, C. D.; Pollheimer, P. D.; Winklehner, P.; Hoelzl, M.; Lackner, B.; Schoerkl, D. M.; Hinterdorfer, P.; Gruber, H. J. *Bioconjugate Chem.* **2006**, *17*, 1473.

(55) Limanskii, A. *Biofizika* **2006**, *51*, 225.

(56) Riener, C. K.; Kienberger, F.; Hahn, C. D.; Buchinger, G. M.; Egwim, I. O. C.; Haselgrubler, T.; Ebner, A.; Romanin, C.; Klampfl, C.; Lackner, B.; Prinz, H.; Blaas, D.; Hinterdorfer, P.; Gruber, H. J. *Anal. Chim. Acta* **2003**, *497*, 101.

(57) Wildling, L.; Unterauer, B.; Zhu, R.; Rupprecht, A.; Haselgrubler, T.; Rankl, C.; Ebner, A.; Vater, D.; Pollheimer, P.; Pohl, E. E.; Hinterdorfer, P.; Gruber, H. J. *Bioconjugate Chem.* **2011**, *22*, 1239.

(58) Cuatrecasas, P.; Parikh, I. *Biochemistry* **1972**, *11*, 2291.

(59) Hermanson, G. T. *Bioconjugate Techniques*; second ed.; Elsevier:London, 2008.

(60) Senapati, S.; Manna, S.; Lindsay, S.; Zhang, P. *Langmuir* **2013**, *29*, 14622.

(61) Chen, G.; Ning, X.; Park, B.; Boons, G.-J.; Xu, B. *Langmuir* **2009**, *25*, 2860.

(62) Lyubchenko, Y. L.; Shlyakhtenko, L. S.; Ando, T. *Methods (Amsterdam, Neth.)* **2011**, *54*, 274.

(63) Lyubchenko, Y. L.; Shlyakhtenko, L. S. *Methods (Amsterdam, Neth.)* **2009**, *47*, 206.

(64) Lyubchenko, Y. L.; Shlyakhtenko, L. S.; Gall, A. A. *Methods Mol. Biol. (Totowa, NJ, U. S.)* **2009**, *543*, 337.

(65) Riener, C. K.; Stroh, C. M.; Ebner, A.; Klampfl, C.; Gall, A. A.; Romanin, C.; Lyubchenko, Y. L.; Hinterdorfer, P.; Gruber, H. J. *Anal. Chim. Acta* **2004**, *506*, 115.

(66) Shlyakhtenko, L. S.; Gall, A. A.; Filonov, A.; Cerovac, Z.; Lushnikov, A.; Lyubchenko, Y. L. *Ultramicroscopy* **2003**, *97*, 279.

(67) Agard, N. J.; Baskin, J. M.; Prescher, J. A.; Lo, A.; Bertozzi, C. R. *ACS Chem Biol* **2006**, *1*, 644.

(68) Mascini, M.; Palchetti, I.; Tombelli, S. *Angew. Chem., Int. Ed.* **2012**, *51*, 1316.

(69) Nimmo, C. M.; Shoichet, M. S. *Bioconjugate Chem.* **2011**, *22*, 2199.

(70) Morales-Sanfrutos, J.; Lopez-Jaramillo, J.; Ortega-Munoz, M.; Megia-Fernandez, A.; Perez-Balderas, F.; Hernandez-Mateo, F.; Santoyo-Gonzalez, F. *Org. Biomol. Chem.* **2010**, *8*, 667.

(71) Lopez-Jaramillo, F. J.; Hernandez-Mateo, F.; Santoyo-Gonzalez, F.; InTech: 2012, p 301.

(72) Agard, N. J.; Baskin, J. M.; Prescher, J. A.; Lo, A.; Bertozzi, C. R. *ACS Chem. Biol.* **2006**, *1*, 644.

(73) Loiseau, F. A.; Hii, K. K.; Hill, A. M. *J. Org. Chem.* **2004**, *69*, 639.

(74) Svedhem, S.; Hollander, C.-A.; Shi, J.; Konradsson, P.; Liedberg, B.; Svensson, S. C. T. *J. Org. Chem.* **2001**, *66*, 4494.

(75) Huang, Z.; Wang, R.; Sheng, S.; Zhou, R.; Cai, M. *React. Funct. Polym.* **2013**, *73*, 224.

(76) Stenzel, M. H. *ACS Macro Lett.* **2013**, *2*, 14.

(77) Sinclair, A. J.; del Amo, V.; Philp, D. *Org. Biomol. Chem.* **2009**, *7*, 3308.

(78) Alley, S. C.; Benjamin, D. R.; Jeffrey, S. C.; Okeley, N. M.; Meyer, D. L.; Sanderson, R. J.; Senter, P. D. *Bioconjugate Chem.* **2008**, *19*, 759.

(79) Lin, D.; Saleh, S.; Liebler, D. C. *Chem. Res. Toxicol.* **2008**, *21*, 2361.

(80) Bock, L. C.; Griffin, L. C.; Latham, J. A.; Vermaas, E. H.; Toole, J. J. *Nature (London)* **1992**, *355*, 564.

(81) Ruoslahti, E. *Annu. Rev. Cell Dev. Biol.* **1996**, *12*, 697.

(82) Schelte, P.; Boeckler, C.; Frisch, B.; Schuber, F. *Bioconjugate Chem.* **2000**, *11*, 118.

(83) Li, L.; Tsai, S.-W.; Anderson, A.-L.; Keire, D. A.; Raubitschek, A. A.; Shively, J. E. *Bioconjugate Chem.* **2002**, *13*, 110.

(84) Wang, H.; Bash, R.; Yodh, J. G.; Hager, G. L.; Lohr, D.; Lindsay, S. M. *Biophys. J.* **2002**, *83*, 3619.

(85) Lin, L.; Wang, H.; Liu, Y.; Yan, H.; Lindsay, S. *Biophys. J.* **2006**, *90*, 4236.

(86) Chang, S.; Sen, S.; Zhang, P.; Gyarfas, B.; Ashcroft, B.; Lefkowitz, S.; Peng, H.; Lindsay, S. *Nanotechnology* **2012**, *23*, 425202/1.

(87) Tuchband, M.; He, J.; Huang, S.; Lindsay, S. *Rev. Sci. Instrum.* **2012**, *83*, 015102/1.

(88) Liang, F.; Li, S.; Lindsay, S.; Zhang, P. *Chem. - Eur. J.* **2012**, *18*, 5998.

(89) Fuhrmann, A.; Getfert, S.; Fu, Q.; Reimann, P.; Lindsay, S.; Ros, R. *Biophys. J.* **2012**, *102*, 2381.

(90) Takeuchi, O.; Miyakoshi, T.; Taninaka, A.; Tanaka, K.; Cho, D.; Fujita, M.; Yasuda, S.; Jarvis, S. P.; Shigekawa, H. *J. Appl. Phys.* **2006**, *100*, 074315/1.

(91) Wang, H.; Bash, R.; Lohr, D. *Anal. Biochem.* **2007**, *361*, 273.

(92) Beal, D. M.; Jones, L. H. *Angew. Chem., Int. Ed.* **2012**, *51*, 6320.

(93) Viault, G.; Dautrey, S.; Maindron, N.; Hardouin, J.; Renard, P.-Y.; Romieu, A. *Org. Biomol. Chem.* **2013**, *11*, 2693.

(94) Chinchilla, R.; Najera, C. *Chem. Rev. (Washington, DC, U. S.)* **2007**, *107*, 874.

(95) Kienberger, F.; Ebner, A.; Gruber, H. J.; Hinterdorfer, P. *Acc. Chem. Res.* **2006**, *39*, 29.

(96) Martinez-Veracoechea, F. J.; Leunissen, M. E. *Soft Matter* **2013**, *9*, 3213.

(97) Potty, A. S. R.; Kourentzi, K.; Fang, H.; Jackson, G. W.; Zhang, X.; Legge, G. B.; Willson, R. C. *Biopolymers* **2009**, *91*, 145.

(98) Orava, E. W.; Jarvik, N.; Shek, Y. L.; Sidhu, S. S.; Gariepy, J. *ACS Chem. Biol.* **2013**, *8*, 170.

(99) Macaya, R. F.; Schultze, P.; Smith, F. W.; Roe, J. A.; Feigon, J. *Proc. Natl. Acad. Sci. U. S. A.* **1993**, *90*, 3745.

(100) Haubner, R.; Gratias, R.; Diefenbach, B.; Goodman, S. L.; Jonczyk, A.; Kessler, H. *J. Am. Chem. Soc.* **1996**, *118*, 7461.

(101) Berezovski, M.; Nutiu, R.; Li, Y.; Krylov, S. N. *Anal. Chem.* **2003**, *75*, 1382.

(102) Bochen, A.; Marelli, U. K.; Otto, E.; Pallarola, D.; Mas-Moruno, C.; Di Leva, F. S.; Boehm, H.; Spatz, J. P.; Novellino, E.; Kessler, H.; Marinelli, L. *J. Med. Chem.* **2013**, *56*, 1509.

(103) Lee, J. K.; Jung, Y. H.; Tok, J. B. H.; Bao, Z. *ACS Nano* **2011**, *5*, 2067.

(104) Xiong, H.; Leonard, P.; Seela, F. *Bioconjugate Chem.* **2012**, *23*, 856.

(105) Harrigan, R. J. 2008.

(106) Hubalek, Z.; Halouzka, J. *Emerg Infect Dis* **1999**, *5*, 643.

(107) Lai, H.; Engle, M.; Fuchs, A.; Keller, T.; Johnson, S.; Gorlatov, S.; Diamond, M. S.; Chen, Q. *Proc. Natl. Acad. Sci. U. S. A.* **2010**, *107*, 2419.

(108) Austin, S. K.; Dowd, K. A. *Viruses* **2014**, *6*, 1015.

(109) Nybakken, G. E.; Oliphant, T.; Johnson, S.; Burke, S.; Diamond, M. S.; Fremont, D. H. *Nature (London, U. K.)* **2005**, *437*, 764.

(110) Suen, W. W.; Prow, N. A.; Hall, R. A.; Bielefeldt-Ohmann, H. *Viruses* **2014**, *6*, 2796.

(111) Diamond, M. S.; Shrestha, B.; Mehlhop, E.; Sitati, E.; Engle, M. *Viral Immunol.* **2003**, *16*, 259.

(112) Kaufmann, B.; Nybakkent, G. E.; Chipman, P. R.; Zhang, W.; Diamond, M. S.; Fremont, D. H.; Kuhn, R. J.; Rossmann, M. G. *Proc. Natl. Acad. Sci. U. S. A.* **2006**, *103*, 12400.

(113) Sanchez, M. D.; Pierson, T. C.; DeGrace, M. M.; Mattei, L. M.; Hanna, S. L.; Del Piero, F.; Doms, R. W. *Virology* **2007**, *359*, 336.

(114) Sanchez, M. D.; Pierson, T. C.; McAllister, D.; Hanna, S. L.; Puffer, B. A.; Valentine, L. E.; Murtadha, M. M.; Hoxie, J. A.; Doms, R. W. *Virology* **2005**, *336*, 70.

(115) Throsby, M.; Geuijen, C.; Goudsmit, J.; Bakker, A. Q.; Korimbocus, J.; Kramer, R. A.; Clijsters-van der Horst, M.; de Jong, M.; Jongeneelen, M.; Thijsse, S.; Smit, R.; Visser, T. J.; Bijl, N.; Marissen, W. E.; Loeb, M.; Kelvin, D. J.; Preiser, W.; ter Meulen, J.; de Kruif, J. *J. Virol.* **2006**, *80*, 6982.

(116) Vogt, M. R.; Moesker, B.; Goudsmit, J.; Jongeneelen, M.; Austin, S. K.; Oliphant, T.; Nelson, S.; Pierson, T. C.; Wilschut, J.; Throsby, M.; Diamond, M. S. *J. Virol.* **2009**, *83*, 6494.

(117) Oliphant, T.; Engle, M.; Nybakken, G. E.; Doane, C.; Johnson, S.; Huang, L.; Gorlatov, S.; Mehlhop, E.; Marri, A.; Chung, K. M.; Ebel, G. D.; Kramer, L. D.; Fremont, D. H.; Diamond, M. S. *Nat. Med. (N. Y., NY, U. S.)* **2005**, *11*, 522.

(118) Demeule, M.; Regina, A.; Che, C.; Poirier, J.; Nguyen, T.; Gabathuler, R.; Castaigne, J.-P.; Beliveau, R. *J. Pharmacol. Exp. Ther.* **2008**, *324*, 1064.

(119) Ni, D.; Zhang, J.; Bu, W.; Xing, H.; Han, F.; Xiao, Q.; Yao, Z.; Chen, F.; He, Q.; Liu, J.; Zhang, S.; Fan, W.; Zhou, L.; Peng, W.; Shi, J. *ACS Nano* **2014**, *8*, 1231.

(120) Ren, J.; Shen, S.; Wang, D.; Xi, Z.; Guo, L.; Pang, Z.; Qian, Y.; Sun, X.; Jiang, X. *Biomaterials* **2012**, *33*, 3324.

(121) Wang, B.; Lv, L.; Wang, Z.; Zhao, Y.; Wu, L.; Fang, X.; Xu, Q.; Xin, H. *Biomaterials* **2014**, *35*, 5897.

(122) Xin, H.; Sha, X.; Jiang, X.; Chen, L.; Law, K.; Gu, J.; Chen, Y.; Wang, X.; Fang, X. *Biomaterials* **2012**, *33*, 1673.

(123) Yang, Z.-Z.; Li, J.-Q.; Wang, Z.-Z.; Dong, D.-W.; Qi, X.-R. *Biomaterials* **2014**, *35*, 5226.

(124) Manna, S.; Senapati, S.; Lindsay, S.; Zhang, P. *J. Am. Chem. Soc.* **2015**, *137*, 7415.

(125) Hong, V.; Presolski, S. I.; Ma, C.; Finn, M. G. *Angew. Chem., Int. Ed.* **2009**, *48*, 9879.

(126) Zuberbuehler, K.; Casi, G.; Bernardes, G. J. L.; Neri, D. *Chem. Commun. (Cambridge, U. K.)* **2012**, *48*, 7100.

(127) Nirschl, M.; Reuter, F.; Voros, J. *Biosensors* **2011**, *1*, 70.

(128) Scarano, S.; Scuffi, C.; Mascini, M.; Minunni, M. *Biosens. Bioelectron.* **2011**, *26*, 1380.

(129) Kim, C. H.; Axup, J. Y.; Dubrovska, A.; Kazane, S. A.; Hutchins, B. A.; Wold, E. D.; Smider, V. V.; Schultz, P. G. *J. Am. Chem. Soc.* **2012**, *134*, 9918.

(130) Imai, K.; Takaoka, A. *Nat. Rev. Cancer* **2006**, *6*, 714.

(131) Chan, A. C.; Carter, P. J. *Nat. Rev. Immunol.* **2010**, *10*, 301.

(132) Stanimirovic, D.; Kemmerich, K.; Haqqani, A. S.; Farrington, G. K. In *Advances in Pharmacology:Pharmacology of the Blood Brain Barrier: Targeting CNS Disorders*; Davis, T. P., Ed.; Elsevier Inc.: 2014; Vol. 71, p 301.

(133) London, N.; Raveh, B.; Schueler-Furman, O. *Curr. Opin. Chem. Biol.* **2013**, *17*, 952.

(134) McEnaney, P. J.; Fitzgerald, K. J.; Zhang, A. X.; Douglass, E. F., Jr.; Shan, W.; Balog, A.; Kolesnikova, M. D.; Spiegel, D. A. *J. Am. Chem. Soc.* **2014**, *136*, 18034.

(135) Mascotti, D. P.; Lohman, T. M. *Proc. Natl. Acad. Sci. U. S. A.* **1990**, *87*, 3142.

(136) Harries, D.; May, S.; Ben-Shaul, A. *Soft Matter* **2013**, *9*, 9268.

(137) Bruinsma, R. F. In *Physics of Bio-Molecules and Cells*; Flyvbjerg, H., Jülicher, F., Ormos, P., David, F., Eds.; Springer-Verlag: 2002, p 63.

(138) Le Trong, I.; Wang, Z.; Hyre, D. E.; Lybrand, T. P.; Stayton, P. S.; Stenkamp, R. E. *Acta Crystallogr. D Biol. Crystallogr.* **2011**, *67*, 813.

(139) WEBER, P.; OHLENDORP, D. H.; WENDOLOSIU, J. J.; SALEMME, F. R. *Science* **1989**, *243*, 85.

(140) Taylor, S. K.; Wang, J.; Kostic, N.; Stojanovic, M. N. *Angew. Chem. Int. Ed. Engl.* **2013**, *52*, 5509.

(141) Begum, R.; Matsuura, H. *J. Chem. Soc., Faraday T rans.* **1997**, *93*, 3839.

(142) Oesterhelt, F.; Rief, M.; Gaub, H. E. *New Journal of Physics* **1999**, *1*, 6.1.

(143) Gennes, P. G. d. *Macromolecules* **1980**, *13*, 1069.

(144) Chinchilla, R.; ́jera, C. N. *Chem. Rev.* **2007**, *107*, 874−922.

(145) Chinchilla, R.; Najera, C. *Chem. Soc. Rev.* **2011**, *40*, 5084.

(146) Pollock, J. B.; Cook, T. R.; Stang, P. J. *J. Am. Chem. Soc.* **2012**, *134*, 10607.

(147) Manna, S.; Senapati, S.; Lindsay, S.; Zhang, P. *Journal of the American Chemical Society* **2015**, *137*, 7415.

(148) Rao, J.; Lahiri, J.; Isaacs, L.; Weis, R. M.; Whitesides, G. M. *Science* **1998**, *280*, 708.

(149) Oohora, K.; Burazerovic, S.; Onoda, A.; Wilson, Y. M.; Ward, T. R.; Hayashi, T. *Angew. Chem. Int. Ed. Engl.* **2012**, *51*, 3818.

(150) Kawaguchi, T.; Walker, K. L.; Wilkins, C. L.; Moore, J. S. *J. Am. Chem. Soc.* **1995**, *117*, 2159.

(151) Copeland, R. A.; Pompliano, D. L.; Meek, T. D. *Nature Reviews Drug Discovery* **2006**, *5*, 731.

(152) Bradshaw, J. M.; McFarland, J. M.; Paavilainen, V. O.; Bisconte, A.; Tam, D.; Phan, V. T.; Romanov, S.; Finkle, D.; Shu, J.; Patel, V.; Ton, T.; Li, X.; Loughhead, D. G.; Nunn, P. A.; Karr, D. E.; Gerritsen, M. E.; Funk, J. O.; Owens, T. D.; Verner, E.; Brameld, K. A.; Hill, R. J.; Goldstein, D. M.; Taunton, J. *Nat. Chem. Biol.* **2015**, *11*, 525.

(153) Walkup, G. K.; You, Z.; Ross, P. L.; Allen, E. K.; Daryaee, F.; Hale, M. R.; O'Donnell, J.; Ehmann, D. E.; Schuck, V. J.; Buurman, E. T.; Choy, A. L.; Hajec, L.; Murphy-Benenato, K.; Marone, V.; Patey, S. A.; Grosser, L. A.; Johnstone, M.; Walker, S. G.; Tonge, P. J.; Fisher, S. L. *Nat. Chem. Biol.* **2015**, *11*, 416.

(154) Lee, J. E.; Fusco, M. L.; Hessell, A. J.; Oswald, W. B.; Burton, D. R.; Saphire, E. O. *Nature (London, U. K.)* **2008**, *454*, 177.

(155) Tran, E. E. H.; Simmons, J. A.; Bartesaghi, A.; Shoemaker, C. J.; Nelson, E.; White, J. M.; Subramaniam, S. *J. Virol.* **2014**, *88*, 10958.

(156) Plietzsch, O.; Schilling, C. I.; Tolev, M.; Nieger, M.; Richert, C.; Muller, T.; Brase, S. *Org. Biomol. Chem.* **2009**, *7*, 4734.

APPENDIX A

COPYRIGHT PERMISSIONS

PERMISSION/LICENSE IS GRANTED FOR YOUR ORDER AT NO CHARGE

Title: Application of Catalyst-Free Click Reactions in Attaching Affinity Molecules to Tips of Atomic Force Microscopy for Detection of Protein Biomarkers

Author: Subhadip Senapati, Saikat Manna, Stuart Lindsay, et al

Publication: Langmuir

Publisher: American Chemical Society

Date: Nov 1, 2013

This type of permission/license, instead of the standard Terms & Conditions, is sent to you because no fee is being charged for your order. Please note the following:

- Permission is granted for your request in both print and electronic formats, and translations.
- If figures and/or tables were requested, they may be adapted or used in part.
- Please print this page for your records and send a copy of it to your publisher/graduate school.
- Appropriate credit for the requested material should be given as follows: "Reprinted (adapted) with permission from (COMPLETE REFERENCE CITATION). Copyright (YEAR) American Chemical Society." Insert appropriate information in place of the capitalized words.
- One-time permission is granted only for the use specified in your request. No additional uses are granted (such as derivative works or other editions). For any other uses, please submit a new request.

Title: A Three-Arm Scaffold Carrying Affinity Molecules for Multiplex Recognition Imaging by Atomic Force Microscopy: The

Synthesis, Attachment to Silicon Tips, and Detection of Proteins
Author: Saikat Manna, Subhadip Senapati, Stuart Lindsay, et al
Publication: Journal of the American Chemical Society
Publisher: American Chemical Society
Date: Jun 1, 2015

PERMISSION/LICENSE IS GRANTED FOR YOUR ORDER AT NO CHARGE

This type of permission/license, instead of the standard Terms & Conditions, is sent to you because no fee is being charged for your order. Please note the following:

- Permission is granted for your request in both print and electronic formats, and translations.
- If figures and/or tables were requested, they may be adapted or used in part.
- Please print this page for your records and send a copy of it to your publisher/graduate school.
- Appropriate credit for the requested material should be given as follows: "Reprinted (adapted) with permission from (COMPLETE REFERENCE CITATION). Copyright (YEAR) American Chemical Society." Insert appropriate information in place of the capitalized words.
- One-time permission is granted only for the use specified in your request. No additional uses are granted (such as derivative works or other editions). For any other uses, please submit a new request.